5-21-2020

Development, Optimization and Clinical Evaluation Of Algorithms For Ultrasound Data Analysis Used In Selected Medical Applications.

Bartosz Slak
University of Windsor

www.manaraa.com

DEVELOPMENT, OPTIMIZATION AND CLINICAL EVALUATION OF
ALGORITHMS FOR ULTRASOUND DATA ANALYSIS USED IN SELECTED
MEDICAL APPLICATIONS.

by

Bartosz Slak

A Dissertation
Submitted to the Faculty of Graduate Studies
through the Department of Electrical and Computer Engineering
in Partial Fulfillment of the Requirements for
the Degree of Doctor of Philosophy
at the University of Windsor

Windsor, Ontario, Canada

© 2020 Bartosz Slak

DEVELOPMENT, OPTIMIZATION AND CLINICAL EVALUATION OF
ALGORITHMS FOR ULTRASOUND DATA ANALYSIS USED IN SELECTED
MEDICAL APPLICATIONS.

by

Bartosz Slak

APPROVED BY:

_____
N. Duric, External Examiner
Wayne State University School of Medicine

_____
W. Kedzierski
Department of Physics

_____
M. Ahmadi
Department of Electrical and Computer Engineering

_____
M. Khalid
Department of Electrical and Computer Engineering

_____
R. Gr. Maev, Advisor
Department of Electrical and Computer Engineering

April 9, 2020

DECLARATION OF CO-AUTHORSHIP / PREVIOUS

PUBLICATION

I. Co-Authorship

I hereby declare that this thesis incorporates material that is a result of joint research, as follows:

- o Chapter 5 and 6 include clinical-based prototype testing work performed by the author with the assistance of Dr. Laurent Bozec and Dr. Francesco D'Aiuto from the University College London, Eastman Dental Institute, London, UK
- o Chapter 6 includes clinical-based prototype testing work performed by the author with the assistance of Dr. Ali Tassi from Western University, London, Ontario, Canada
- o Chapter 2 includes selected equipment provided by Dr. Alex Denisov from Tessonics Inc., Windsor, Ontario, Canada.

In all cases, the key ideas, primary contributions, experimental designs, data analysis, interpretation, and writing were performed by the author, and the contribution of the rest of the co-authors for the publications included in chapters 1, 5 and 6 is primarily through provision of equipment, reviewing and editing manuscripts.

I am aware of the University of Windsor Senate Policy on Authorship and I certify that I have properly acknowledged the contribution of other researchers to my thesis and have obtained written permission from each of the co-author(s) to include the above material(s) in my thesis. I certify that, with the above qualification, this thesis, and the research to which it refers, is the product of my own work.

II. Previous Publication

This thesis includes materials from 4 original papers that have been previously published/submitted for publication in peer-reviewed journals, as follows:

Thesis Chapter	Publication title/full citation	Publication status*
Chapter 1,6	**B. Slak,** E. Strumban, R. Maev "Ultrasonic device for dental implant navigation" A patent in the United States (US9986968B2) June 5, 2018	*"Granted"*
Chapter 5	**B. Slak**, J. Lim, R. Rotundo, J. Buti, L. Bozec, R.G. Maev, F. D'Aiuto, "Non-invasive Ultrasound Device for Gingival Thickness Assessments. A Validation Study." *Journal of Periodontal Research*	*"Submitted"*
Chapter 6	R.A. Vacarescu, **B. Slak**, A. Maeva, and R.G. Maev, "Portable High-Frequency Device for Cosmetic and Clinical Fingernail Assessment," in *Canadian Conference on Electrical and Computer Engineering*, 2017	*"Published"*
	R.A. Vacarescu, **B. Slak**, A. Maeva, C. Hamm, N. Lewoc, A.T. Daabous, and others, "Investigation of a Correlation between Taxane-Based Chemotherapy and the Ultrasonic Time-of-Flight of Human Fingernails" *Skin Research and Technology*, 24 (2018)	*"Published"*
Chapter 6	**B. Slak**, R. Alkhuwaitem, S. Siddiqui, D. Mills, G. Davis, S. Parekh, R. Maev, L. Bozec,	*"Presented"*

	"A Multi-modality Detection and Volumetric Assessment of Dental Caries" *International Association for Dental Research,* 2018	
	J. Pattem, M. Davrandi, S. Aguayo, **B. Slak**, R. Maev, E. Allan, D. Spratt, and L. Bozec "Real-time Mechano-biology of (re)hydrated Oral Biofilms" *Journal of Dental Research, 2020*	*"Submitted"*

I certify that I have obtained written permission from the copyright owners to include the above-published materials in my thesis. I certify that the above material describes work completed during my registration as graduate student at the University of Windsor.

III. General

I declare that, to the best of my knowledge, my thesis does not infringe upon anyone's copyright nor violate any proprietary rights and that any ideas, techniques, quotations, or any other material from the work of other people included in my thesis, published or otherwise, are fully acknowledged in accordance with the standard referencing practices. Furthermore, to the extent that I have included copyrighted material that surpasses the bounds of fair dealing within the meaning of the Canada Copyright Act, I certify that I have obtained written permission from the copyright owners to include such materials in my thesis.I declare that this is a true copy of my thesis, including any final revisions, as approved by my thesis committee and the Graduate Studies office and that this thesis has not been submitted for a higher degree to any other University or Institution.

ABSTRACT

The assessment of soft and hard tissues is critical when selecting appropriate protocols for restorative and regenerative therapy in the field of dental surgery. The chosen treatment methodology will have significant ramifications on healing time, success rate and overall long-time oral health. Currently used diagnostic methods are limited to visual and invasive assessments; they are often user-dependent, inaccurate and result in misinterpretation. As such, the clinical need has been identified for objective tissue characterization, and the proposed novel ultrasound-based approach was designed to address the identified need. The device prototype consists of a miniaturized probe with a specifically designed ultrasonic transducer, electronics responsible for signal generation and acquisition, as well as an optimized signal processing algorithm required for data analysis. An algorithm where signals are being processed and features extracted in real-time has been implemented and studied. An in-depth algorithm performance study has been presented on synthetic signals. Further, in-vitro laboratory experiments were performed using the developed device with the algorithm implemented in software on animal-based samples. Results validated the capabilities of the new system to reproduce gingival assessment rapidly and effectively. The developed device has met clinical usability requirements for effectiveness and performance.

DEDICATION

I dedicate this thesis to my fiancé.

ACKNOWLEDGMENTS

TABLE OF CONTENTS

LIST OF TABLES

LIST OF FIGURES

LIST OF APPENDICES

Appendix 1 Ultrasound Dental System - User Manual

Appendix 2 Patent: Ultrasonic Device for Dental Implant Navigation

LIST OF ABBREVIATIONS/SYMBOLS

ADC – analog to digital

ALARA – as low as reasonably achievable

AU – arbitrary units

ANOVA – analysis of variance

AR – autoregressive

CBCT – cone-beam computed tomography

CT – computed tomography

DEJ – dentin-enamel junction

DOF – depth of field

DSP – digital signal processing

FIR – finite impulse response

FPGA – field-programmable gate array

FWHM – full width at half maximum

GT – gingival thickness

HF – high frequency

ICC – interclass correlation coefficient

ICDAS – intranational caries detection and assessment system

LASSO – least absolute shrinkage and selection operator

LCC – Lin's concordance coefficient

MI – mechanical index

MJ – mucogingival junction

MM – minimization majorization

MRI – magnetic resonance imaging

MSE – mean square error

NDE – non-destructive evaluation

OCT – optical coherent tomography

PSF – point spread function

PSNR – peak signal to noise ratio

PVDF – polyvinylidene fluoride

RF – radio frequency

SAM – scanning acoustic microscope

SNR – signal to noise ratio

TDE – time delay evaluation

TGC – time gain compensation

TGP – trans gingival probing

TI – thermal index

TOF – time of flight

US – ultrasound

XMT – x-ray microtomography

CHAPTER 1.

INTRODUCTION

The introductory chapter presents importance and motivation for research studies in the framework of electrical engineering, performance optimization and clinical usability of a recently developed medical device. Specifically, it deliberates the application of a high-frequency ultrasound system for diagnostics of selected medical assessments. Subsequently, alternative imaging modalities are briefly discussed to further present the benefits and limitations of ultrasound technology and clinical need for quantitative measurements. An introduction to the historical accomplishments of ultrasound technology in the high-frequency regime is provided with a concentration on medical applications.

The chapter is concluded with the scope and challenges related to the research question as well as a short summary of the dissertation contribution, organization, and the content of the consequent chapters.

1.1. Motivation

The scientific work described in this dissertation is motivated by the need for technological progress and innovation in the area of dental diagnostics where thin layers of soft tissues are of high importance and require characterization. Gingival thickness (biotype) has a significant impact on the outcome of dental restorative and regenerative therapy for a broad segment of patients. The assessment of periodontal biotype is critical when selecting appropriate protocols in the field of dental surgery. The chosen methodology will have significant ramifications on the restoration of the soft and hard oral tissues, healing time, success rate and overall oral post-surgery health. Currently used gingival biotype determination methods are limited to visual and invasive assessment; they are often user-dependent, inaccurate and result in misinterpretation. Other invasive methods such as mechanical trans-gingival penetration (bone sounding), transparency or radiography techniques are presently available, but all have proven to be inadequate in dental clinical practice. As such, the clinical need has been identified for an objective assessment of gingival biotype, and a novel compact device to address this has been proposed.

The use of ultrasound in dentistry has been an area of research for a few decades starting in the late 1950s. The progress has been made in directions involving hard (teeth and bone) and soft (gums, mucosa) tissues. The ultrasound technology benefits such as non-invasiveness, low cost, reliability, time efficiency were identified to meet the users' expectations and simultaneously be capable of addressing the clinical unmet needs. The problem was to identify and develop new methods and techniques to overcome the limitations of ultrasound technology in the proposed dental application and bring it closer to clinical practice. The digital signal processing (DSP) techniques offer a spectrum of methods to support and improve the operation of ultrasound-based systems and can be utilized to meet rigorous time constraints of clinical practice. The methodology proposed in this dissertation is crafted for the investigated application due to access to prior knowledge about the anatomical properties and the expected signal response (sparsity). The knowledge generated in the presented research was recognized

in dental ultrasound literature; conclusions, recommendations, and feedback in the published studies. The clinical interest was validated by numerous collaborations with specialists in the field, locally and internationally [1], [2].

1.2. Medical Imaging Modalities

There are several imaging modalities known and commonly used in medicine such as X-rays, computed tomography (CT), magnetic resonance imaging (MRI) and optical-based technologies, and just a couple were adopted to dentistry.

Conventional radiography (periapical and panoramic), as well as CT, is currently the imaging standard for dental surgeries. Unfortunately, they generate ionizing radiation, which is additive, may be harmful to patients and for that reason ALARA rule (As Low as Reasonably Achievable) has to be restrictively applied. The rule also applies to cone-beam computed tomography (CBCT), which is safer than regular CT, but it compromises resolution and scanning volume size. The CBCT has been gaining interest in dental practices, but it is still limited, and when available, quite expensive.

In general, the current dental diagnostic methodologies are focused on the imaging of the hard tissue and are mostly based on invasive methods. Shortcomings in terms of artifacts, accessibility, resolution, and object projections effectively limit usability and spread into other diagnostic dental directions [3].

1.3. Benefits and Limitations of Ultrasound Imaging

The ultrasound technology has a number of characteristics that make this modality unique in many clinical situations where it provides informative results for specialists to support medical decisions. A list of the most important advantages and limitations is in Table 1.1.

Table 1.1 The comparison includes a list of selected benefits and limitations related to the diagnostic application of ultrasound.

Benefits	Limitations
• portability of ultrasound units	• not as much detail as in X-rays
• non-invasive, non-ionizing nature of ultrasound waves	• doesn't pass through bones and other hard tissues
• ability to produce a real-time image	• can be wrong in detecting physical abnormalities (artifacts)
• relatively inexpensive	• limited depth penetration
• the intrinsic contract that allows soft tissue imaging	• artifacts are quite common

1.4.   Clinical Importance of Quantitative Ultrasound Assessments

In general, the value of ultrasound diagnostics lies in the capability of providing additional information so that practitioners can answer specific clinical questions. The quality of assessment is a function of resolution and it is quite important to understand limiting factors and utilize knowledge and advancement in order to maximize ultrasound system performance. In ultrasound, resolution can be defined in three interdependent forms such as spatial, temporal resolution, and contrast. The special resolution can be divided into axial (along the propagation direction) and lateral (capability of differentiating objects located next to each other in the presence of ultrasound).

For many years the main research focus was on improving the special aspect of the resolution. In fact, contrast is equally important. It can be defined as intrinsic and extrinsic; intrinsic contrast consists of echoes with varying signal amplitudes based on the physical differences between acoustic impedance and the nature of the interaction between the sound waves and the medium speckle reflections. Contrast can be also

affected by technical aspects like compression, displays technology or even image viewing conditions. The optimal settings where the signal to noise ratio (SNR) is maximized are desired, although, intrinsic contrast is user-independent and several factors could be manipulated to improve signals used for composing images. The factors such as sonographic path known as an acoustic window, output power or frequency can be modified or improved [4]. Developments in the direction of ultrasound digital signal processing can significantly improve image creation and readability, and at the same time help facilitate and possibly automate quantitative assessments where conventional ultrasound imaging is mostly qualitative in nature [5].

The objective of the current studies is to apply ultrasound for assessments of relatively small objects and layers not exceeding 3-4 mm in thickness. The other areas where high-frequency ultrasound technology improvement can have a significant impact are ophthalmology and dermatology.

1.4.1. Ophthalmology

The high-frequency ultrasound is an important modality for accurate diagnosis in ophthalmology. It has capabilities to image the anterior part including the cornea, anterior chamber, iris, and the lens. Micro-ultrasound is also used for diagnostic imaging of corneal diseases, glaucoma, and eye tumors. Focused, single-element, mechanically scanned transducers are most common in ophthalmic applications. Custom-designed transducers have been used to generate a high-intensity focused beam that uses thermal effects for glaucoma, tumors, and other pathologies treatments [6]. Ophthalmological applications have been facing similar challenges as other applications where the resolution is at a higher importance than the depth of penetration [7].

1.4.2. Dermatology

Ultrasound has been used in dermatology and has achieved a superior resolution in the high-frequency range due to minimal requirements for the propagation depth. The application has been researched for a few decades now and has resulted in several developed ultrasound systems [8].

The parameters of skin tumors, skin thickness analysis, hydration, and elasticity can be accurately evaluated [9]. The ultrasound scanners for skin examination are gaining popularity as an integral part of procedures in aesthetic medicine. Devices are applied for non-surgical facelift procedures where the obtained skin image support decisions and surgical parameters. Current ultrasound developments allow imaging of most of the neoplastic lesions in the skin, both benign and malignant, quantitatively assessing changes and evaluating them in relation to adjacent tissues. Research in the direction of automatic determination of cancerous tumors and the margin assessment is highly promising and actively promoted in the recent literature [10].

1.4.3. Dentistry

The oral cavity with its accessory organs has an important role in the human digestive system and overall health condition. Physiologically, teeth provide a greater chewing ability. They allow us to masticate food thoroughly, increasing the surface area necessary to allow for the enzymes present in the saliva to emerge. Trauma or teeth loss due to accidents and aging impacts chewing decreases the quality of life introduces social insecurity and decreases esthetics due to bone loss, which can result in the collapsed lower part of the face. As a consequence of a lack of certain nutrition due to altered eating habits, various health problems occur, from the mild to the extreme. For instance, edentulism affects approximately 158 million people globally as of 2010 (2.3% of the population).

Ultrasound in dentistry has been researched for over half of a century. The first trials of imaging teeth were conducted in 1950 - 1960 and from there the application

has been expanding to a number of different possible assessments where ultrasound technology can bring value to clinical practice [11], [12].

Table 1.2 The selected dentistry branches and applications where ultrasound has been applied in published research studies.

Teeth scanning	Maxillofacial fractures
Demineralization and caries detection	Periodontal bony defects
Mandibular nerve detection	Muscle and gingival thickness
Teeth cracks	Temporomandibular
Soft tissue lesions and assessment	Implant dentistry

Overall, the use of ultrasound in dental applications could be divided into hard tissues (enamel, dentin, alveolar bone including trabecular and cortical structure, and roots) and soft tissues (gingiva, keratinized gingiva, mucosa, pulp chamber, and any other form of a periodontium structure). The areas of interest and branches of dentistry where ultrasound research has been advancing are detailed in Table 1.2. The concluded results are promising, the developments could support the decision-making process in dental procedures in the future. Nevertheless, more research and improvements are required, specifically for device optimization [13], [14].

1.5. Objectives, Research Framework, and Contributions

The objectives of the research work within this dissertation are multifold. The primary goal was to develop and then investigate an appropriate digital signal processing methodology for the radio frequency (RF) signal treatment to optimize data acquisition and useful information extraction, and effectively solve the clinical problem of thickness measurements for planning dental periodontology surgeries.

The secondary goal was to test and validate the optimal performance of the proposed algorithm on synthetic signals representing the transfer function of the object

and Point Spread Function (PSF) of the ultrasonic transducer used in the developed system approach (Figure 1.1).

The third important aspect was to prove the clinical applicability and potential of the proposed solution through a series of experimental trials on gingival and bone samples.
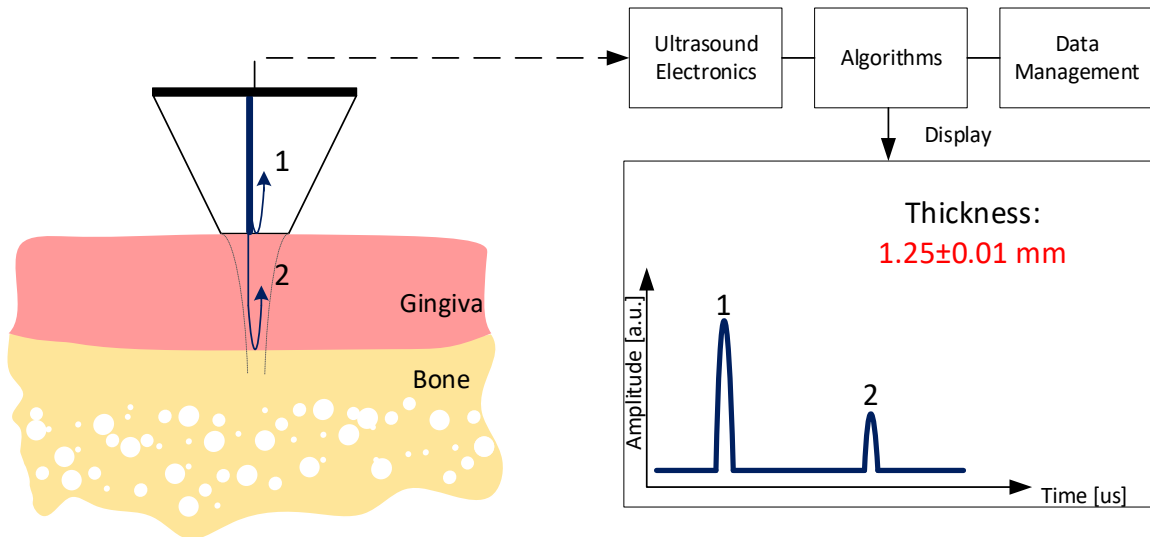
Figure 1.1 The diagram presents the fundamental operational principles for the proposed system. The reflection (1) is received from the gingiva surface, the reflection (2) is received from the interface between the gingiva and alveolar bone. The signal is acquired, digitized, analyzed, presented to the user in terms of numerical value and stored.

A variety of algorithms for processing of ultrasonic signals have been researched and proven to have potential in improving ultrasound imaging for layer structures [15]. Unfortunately, published data have shown limited studies that considered clinical implementation criteria. For that reason, the focus of this dissertation is to reflect the impact of the application and validate algorithm performance under medical constraints.

The research and development work conducted in the scope of the dissertation solves an important problem of diagnostic ultrasound system usability in the dental clinical setting through optimizing ultrasound signal processing. The main contribution is delivered in terms of the customized DSP approach that combines interdisciplinary

knowledge of wave propagation fundamentals with detailed anatomy consideration to eventually optimize system performance for the real-time operation. At the same time, the clinical user expectations are set to quickly, effectively and non-invasively assess oral tissues before planned surgeries for the purpose of long-term restoration success.

1.6. Dissertation Outline and Summary

The dissertation is divided into 7 chapters. The second chapter presents the summary of fundamentals from both the science and engineering perspective. The discussion starts with a medical ultrasound technology overview and related physics principles followed by the ultrasonic signal processing summary with examples relevant for this dissertation. The third chapter introduces the spare deconvolution approach, describes algorithm development and its implementation in detail. The fourth chapter presents insights about the testing methodology using synthetically generated and controlled signals including results obtained under several conditions. The fifth and sixth chapters present clinical data results and analysis of system performance. The last chapter summarizes the results and offers possible directions for future studies.

To sum up, the research work in the field of ultrasound is interdisciplinary and often conjugated with areas of knowledge such as electrical engineering and physics. For the following reason, the advancement depends on the development of DSP methods with system design considerations that could improve the overall system performance. The aim is to enhance and optimize a non-invasive, ultrasound-based gingival thickness measurement device recently developed through algorithms, validate its use against the gold standards.

CHAPTER 2.

INTRODUCTION TO ULTRASOUND PRINCIPLES AND SIGNAL PROCESSING TECHNIQUES

This chapter introduces an essential theory of ultrasound systems, data formation, and ultrasound data presentation. Next, a fundamental description of ultrasound wave propagation principles is given along with discussing phenomena that can affect signals and system execution. Further, the relevant digital signal processing techniques used for ultrasound-based measurements and image enhancement are provided and discussed in the context of tissue characterization in unconventional medical applications. The techniques are also described from the perspective of clinical applications and real-time usability.

The design criteria are considered and briefly described to further discuss hardware and software system implementation, design strategies and contributions.

2.1. Medical Ultrasound Diagnostic Systems – Overview

Ultrasound diagnostic systems used in the medical field generate energy in the form of mechanical displacement known as the acoustic wave or in general ultrasound. The waves propagate and interact with the organs and tissues along the beam path. The propagation is affected by physical phenomena such as reflection, attenuation, diffraction, interference, and others in more complex scenarios. Based on these interactions the reflected signal is acquired, processed, analyzed and transformed into information that can be presented in a form of a number, image, and 3D or 4D visualization.

The most popular parameter of ultrasound systems is the central operating frequency of a transducer. The majority of medical ultrasound imaging systems operate at frequencies ranging from 1 to 10 MHz and in some instances up to 15 MHz [16]. The frequency of ultrasonic transducers strongly influences the penetration depth and consequently the image resolution. Certain applications in the field of medicine such as ophthalmology or dermatology allow transducers to be positioned close to organs, consequently, do not require the penetrating ability and the frequencies can reach values up to 50 - 75 MHz [17].

Most of the medical specialties use ultrasound technology for diagnostics and/or therapy (heat delivery). In the medical diagnostic domain, the technique known as the pulse-echo method is widely utilized. The ultrasonic transducer driven by an electric spike generates a short-time wave that travels and penetrates tissues. The reflected wave is received by the same transducer and converted back into an electric signal. Further, the analog signal is pre-processed, digitized and then exposed to a sequence of processes for optimization, enhancement and information extraction.

Medical ultrasound systems are generally classified based on applications and diagnostic objectives (Table 2.1) [18].

Table 2.1 The list of common ultrasound imaging applications.

Abdominal ultrasound	to visualize abdominal tissues and organs
Bone sonometry	to assess bone fragility
Breast ultrasound	to visualize breast tissue
Doppler fetal heart rate monitors	to listen to the fetal heartbeat
Doppler ultrasound	to visualize blood flow through a blood vessel, organs, or other structures
Echocardiogram	to view the heart
Fetal ultrasound	to view the fetus in pregnancy
Ultrasound-guided biopsies	to collect a sample of tissue
Ophthalmic ultrasound	to visualize ocular structures
Ultrasound-guided needle placement	in blood vessels or other tissues of interest

The ultrasound systems can be also classified based on the technical scheme of operation (Table 2.2). The table summarizes several methods of presenting ultrasound data and operation modes that can be used in ultrasound diagnostics.

Table 2.2 The technical-based classification of ultrasound systems.

A-Mode (one-dimensional)

B-Mode (two-dimensional)

> Manual scanners
> Real-time scanners
> Mechanical scanners
> Electronic:
> > Linear array
> > Phased array

M-mode (motion) or TM mode (time motion)

C-mode (constant depth mode)

Doppler (velocity)

> Continuous-wave

Audible output
Analog-output
Spectrum-output
Doppler imagers
CW transverse scanners
Pulsed Doppler
Combined with B-mode (duplex)

The fundamental representation of ultrasound data (Figure 2.1 and 2.7) is known as an amplitude mode (A-scan or A-mode). The processed A-scans where the magnitude of the backscattered signal is presented in a grayscale format as a function of the spatial position of the scattering volume and signals are recorded from the known position (linear translation, rotational motion or electronic beam steering in azimuthal direction) is known as brightness mode (B-mode or B-scan). B-scans are the most common way of presenting ultrasound information in clinical practice and make up the largest class of instruments. A stack of B-scans collected in an elevation direction creates a 3D dataset, with visualizing the constant depth in the grayscale one can render an image that is known as C-scan. A less popular but equally important representation of ultrasonic imaging is so-called motion mode (M-scan) and continues wave Doppler where velocity and motion information could be provided. Many current systems are capable of projecting data overlap or combining different modes of operation (duplex scanners combining pulsed Doppler and B-scan, or M-mode combined with real-time B-scan).
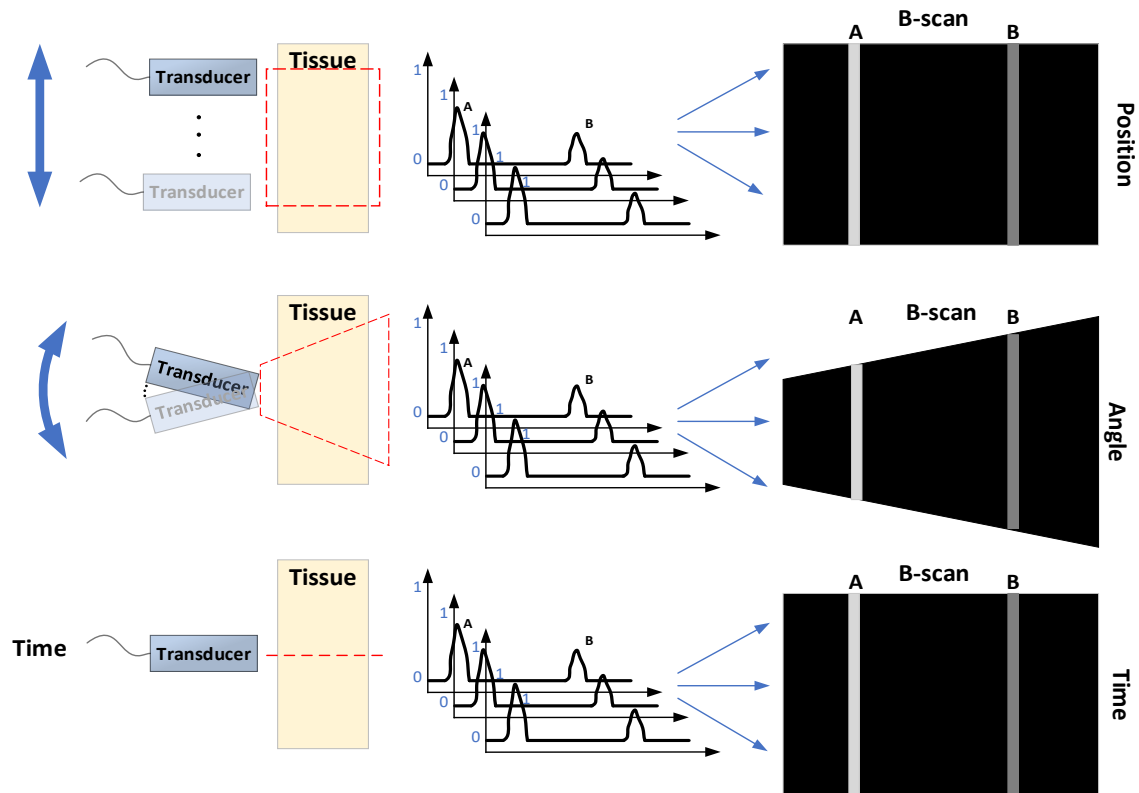
Figure 2.1 Three different ways of creating a standard image in ultrasound; (top) B-scan image based on lateral translation; (middle) B-scan image based on an oblique transducer movement; (bottom) M-scan imaging records dynamic changes in the medium as a function of time, the transducer stays still.

The common diagnostic medical ultrasound systems transmit ultrasound waves in the medium as a pulse train with parameters that depends on the specific application. After the waves are received back by the transducer in the form of echoes and converted to electrical signals, the analog front-end electronics processes the signal and prepares it for analog to digital conversion, usually in a range of 8-16 bits of resolution. The received signal is usually called the radio frequency (RF) ultrasound signal. There are several methods and schemes available for further digital system processing of ultrasound data. The selection criteria and suitability depending on processing power, system power consumption, and cost. It is quite challenging to find an optimal solution at low cost and for that reason improved and balanced mathematical signal operations could be of significant value. The areas of implementation could be generalized in groups of hardware and software. In the case of hardware implementation, there are

two main units: Field Programmable Gate Arrays (FPGA) and Application Specific Integrated Circuits (ASIC). Software processing is usually implemented in general-purpose processors or nowadays more commonly in graphics processors if the application requires high-speed parallel processing.

The benefit of using software implementation lies in simpler code modifications and debugging capabilities as compared to hardware. Personal computers have become a part of ultrasound systems for controlling and as user interface, and implementation of processing in software is quite natural. Unfortunately, most general-purpose operating systems cannot offer certain code to be executed within a specific time frame, so time-sensitive operations are executed within the external hardware. The hybrid models of system designs are popular and commonly used in research and in the low volume industrial applications.

Ultrasound technology is highly adjustable based on its utilization and application. Modifications can include hardware (transducer, pulse generator, data acquisition, and analog signal conditioning) as well as software (digital processing and information extraction).

2.2. Ultrasound Wave Propagation Principles

The proven safety of ultrasound technology in the medical field and benefits offered by the technology have been recognized and widely used. Certain properties of acoustic waves such as the speed of sound, impedance, absorption, scattering, and attenuation are used for providing information about the structure of biological tissues. In practice, these properties contribute to the quite complicated process of medical ultrasound image formation. The knowledge about the variation of these characteristics is important for understanding and optimizing the use of ultrasound technology.

2.2.1. Speckle, Scattering, Reflection, and Refraction

The acoustic pulse at a continuous boundary between materials behaves so that a part of the acoustic pressure is traveling forward, and it is being transmitted through. The rest of the pressure wave is reflected back towards the transducer. The wave propagation at the boundary depends mainly on the acoustic impedance of both connected sides. The characteristic acoustic impedance Z is equal to the normalized specific acoustic impedance (in Rayleigh).

$$z = \frac{p}{v} \tag{2.1}$$

$$Z = \frac{z}{area} = \rho c \tag{2.2}$$

Where p is sound pressure expressed in Pa, v is the particle velocity, c is the longitudinal sound velocity in m/s and ρ the material density kg/m^2. The reflected wave travels back to the transducer (Figure 2.2) triggering an electric pulse to be later present in the corresponding A-scan. The coefficients that describe the reflection and transmission phenomena for acoustic pressure in a continues boundary are often presented as T_{12} and R_{12}, respectively and are written in the following form:

$$T_{12} = \frac{2Z_2}{Z_2 + Z_1} \tag{2.3}$$

$$R_{12} = \frac{Z_2 - Z_1}{Z_2 + Z_1} \tag{2.4}$$

Where Z is the acoustic impedance and subscripts indicate the direction of propagation or the order of the materials (Figure 2.2) [19]. These relations are true in the case when the transducer is perpendicular to the tissue surface. The materials at the interface between the tissue and the coupling medium have characteristic impedances Z_1 and Z_2, respectively and subsequent reception of the reflected acoustic pressures changes at the

degradation, and others and in the general case is not common to provide pressure units along with the A-scan signal representation boundaries will be proportional to the signal amplitude. The proportionality ratio will depend on multiple variables such as transducer design and sensitivity, wiring, maintenance, and others.
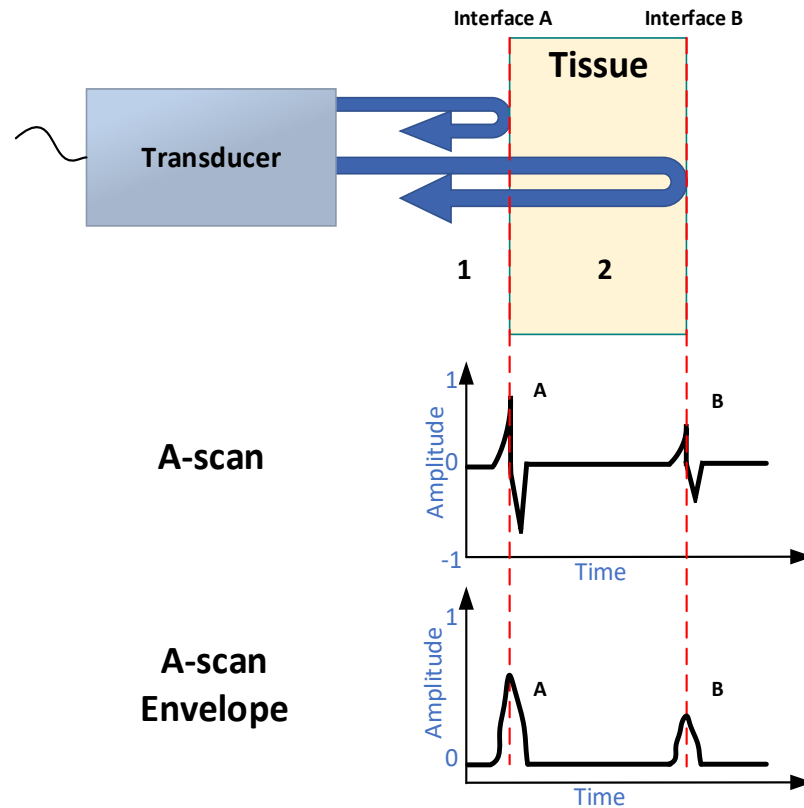
Figure 2.2 Ultrasound wave reflection principle and a fundamental method for representing ultrasound data. The consequent interfaces (acoustic impedance differences) A and B result in the signal amplitude change.

Quite often in research and non-clinical applications, the unit becomes an arbitrary unit since absolute amplitude readings are not as important as relative measurement values. A more complicated example of a layered structure is presented in Figure 2.3. The scattering at the multiple interfaces can create reverberations and possible interference of waves causing severe disturbance of reflections received from boundaries located axially deeper from the transducer. This is one of the problems addressed in Chapters 3 and 4. Additional problems can arise due to the nature of

medical applications where transducers are intended to be positioned and manipulated free-hand.
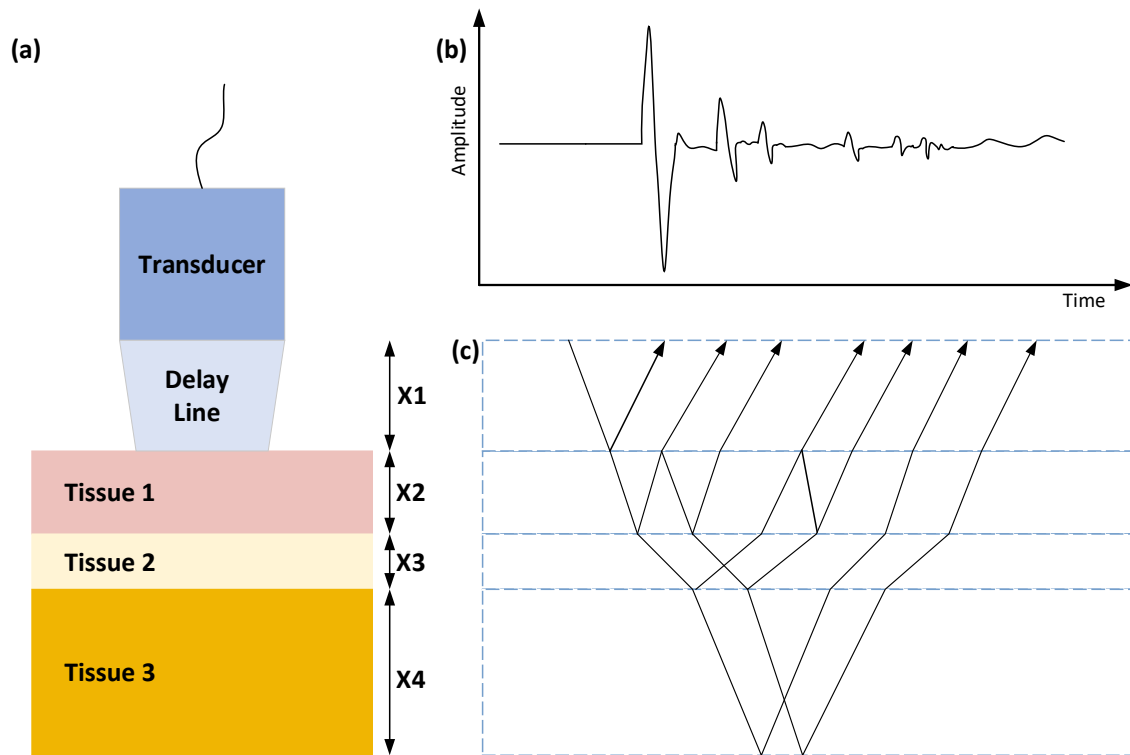
Figure 2.3 The incident wave and reflected wave patterns from the subsequent tissue layers. (a) Transducer with a delay line and tissue structure. (b) A-scan response from the object in (a). (c) The reflectivity pattern diagram represents the sourcing of multiple reflections in a multilayer structure.

Positioning the probe at an angle other than 90 degrees will cause wave refraction (change of direction of propagation described by the Snell's Law) and can additionally impact the SNR of the important pulses (Figure 2.4). So far, tissue homogeneity is assumed. In real applications, the internal structures of tissue include vessels, nerves, alternative cell layers and other biological structures that will contribute to the overall ultrasound response. Effectively, the desired signal will be compromised and convoluted with an unwanted interference signal (Figure 2.4).
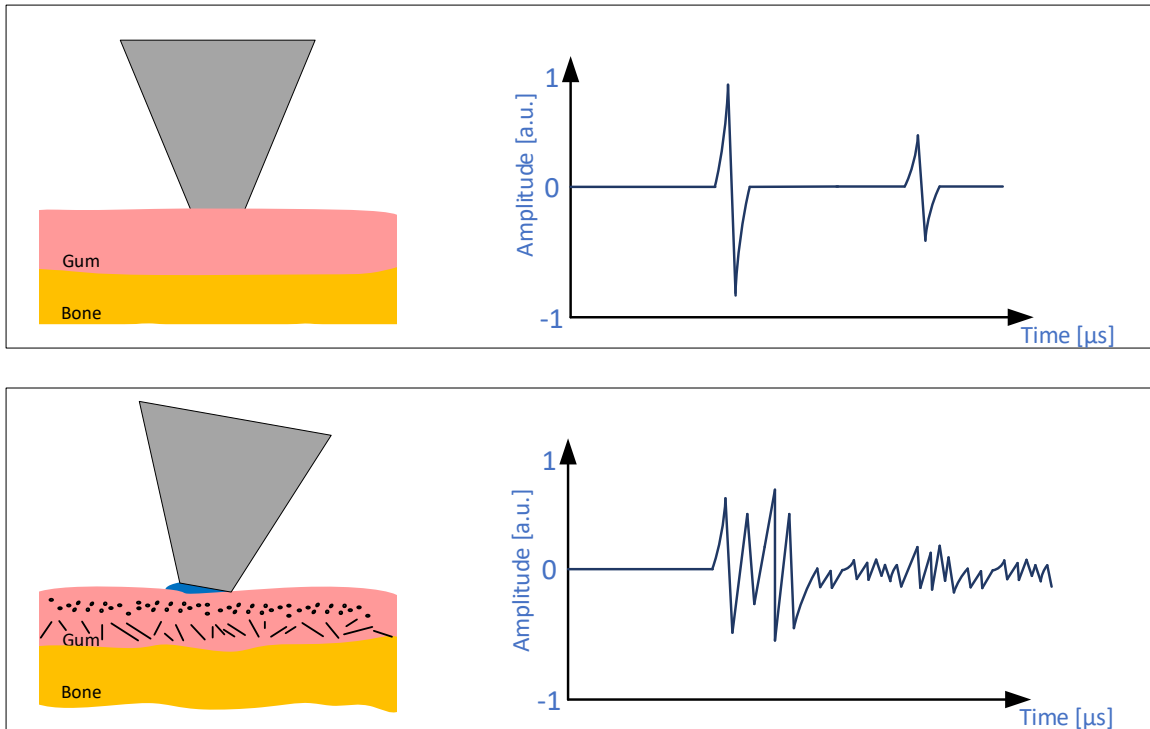
Figure 2.4 The diagram presents the problem of positioning the ultrasonic transducer delay line (the probe tip) on the surface of the sample; (top) the ideal case, often considered in research studies as a simplified model with limited variables; (bottom) an example highlighting common (heterogeneity, oblique angle, interference and refraction effects) contribution to the signal amplitude decay and noise.

2.2.2. Attenuation and Time Gain Compensation

In medical ultrasound-based diagnostic systems attenuation plays a prominent role. In general terms, it is the reduction of signal strength as a function of imaging depth. Attenuation is also a function of the frequency of ultrasound wave and in a fundamental form can be written as:

$$Attenuation = \alpha \left[\frac{db}{MHz\ cm} \right] \ l[cm]\ f[MHz] \tag{2.5}$$

The primary source of attenuation is the thermal absorption, secondary effects include focusing, and scattering. There are several directions of how attenuation can be effectively used as a characterization parameter, mainly for scatterer size and

backscattering coefficient estimations. It could be used as a tuning parameter in ultrasound therapy and in the time gain compensation (TGC) control [20]. Since the attenuation coefficient is not expected to fluctuate in the soft tissue of the study interest the value can be assumed and set as a constant and used in the TGC equation which takes the following form:

$$TGC(l) = e^{2\,\alpha\,l\,f} \tag{2.6}$$

The TGC gain is necessary in order to compensate for the predictable losses in the system. It is especially useful in simplified algorithms where thresholding methods are used to compute the time of flight.

2.2.3. Spatial and Lateral Resolution

The resolution of an ultrasound transducer is related directly to the central frequency and geometrical shape of the active surface (physically focused). The axial direction resolution can be approximated to:

$$R_{axial} \approx \frac{1}{2}\frac{c}{BW} \tag{2.7}$$

Where c is the speed of sound in the medium and BW is the bandwidth at -6 dB. The R_{axial} represents the ability to differentiate objects that are located along the imaging beam axis. It could be also expressed in terms of wave cycles in the time domain (for soft tissue: $0.77(nr.\,of\,cycles)/f$). In general, ultrasound imaging transducers are designed to have a minimum number of cycles per pulse but that could be also affected by excitation signal. For instance, a transducer operating at 50 MHz with BW at approx. 50 % and assuming the propagation in water, the axial resolution would be equal to ~30 µm.
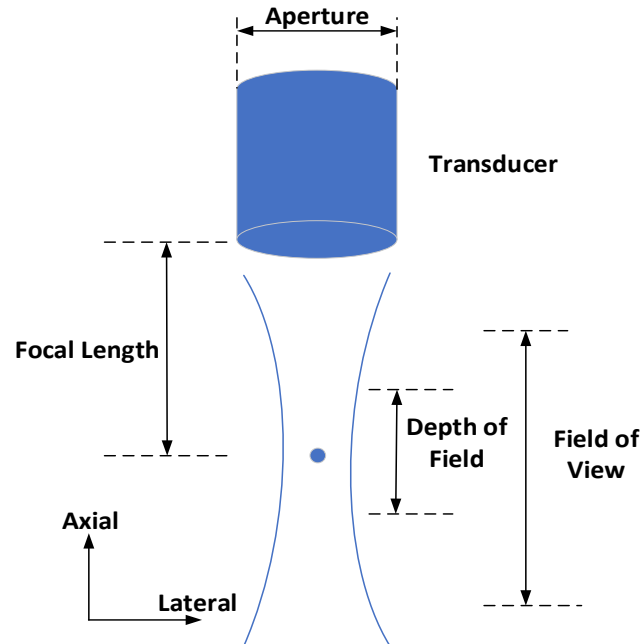
Figure 2.5 The focused transducer diagram and fundamental definitions related to the ultrasonic beam.

The lateral resolution is the minimum distance that is necessary in order to differentiate objects located side by side, perpendicular to the beam axis. The lateral resolution at the focal point is the beam width:

$$R_{lateral} \approx \lambda \frac{F_0}{D} = \lambda(f - number) \tag{2.8}$$

Where λ is the average wavelength, D is the diameter of the transducer F_0 is the focal length (the ratio is often expressed as $f - number$) [21]. The equation is only valid for a focused transducer in the focal zone or for unfocused but with an exemption of the near field. The resolution requirement of an ultrasound system has to be considered in the early phases of the development process due to multi-variable dependencies and impact on performance.

2.3. Ultrasound Signal Processing Methods for Tissue Characterization

In ultrasound, the information is usually hidden in RF signals. Most of the ultrasonic tissue characterization techniques are based on sampled RF data analysis involving spectral methods, features detection, filtering, enhancement, signal separation, and others. Mathematical calculations can be applied in 1D (A-scans), 2D (B-scans) or even on volumetric data. The ultimate goal of these operations is the identification and classification revealing tissue properties and enhancement of the readout in the form of images or measurements. A few relevant approaches to the research problems tackled in this dissertation have been selected and described. They are crucial for system performance improvement and finally satisfying the goal of improving detectability, accuracy and the assessment time in clinical settings.

The clinical assessment for a singular measurement location starts from activating data acquisition in software, typically the probe is at rest but ready to be put in contact with the patient. The signal response is being recorded and displayed in the form of an M-scan (Figure 2.6). Initially, due to lack of tissue contact with the probe tip, the wave is mostly reflected back creating echo (A) visible in Figure 2.7 (left and right). At the time t_1 the probe becomes in direct contact with soft tissue, it could be observed that reflection (A) converts into the reflection (D). The user is instructed to maneuver the probe angulation so perpendicular or close to the perpendicular position can be established (reflection B, at $t_1 - t_2$). The auditable feedback is provided to the user when reflection (C) is obtained at t_2. The algorithm terminates the operation at t_3 when a sufficient number of A-scans is obtained providing the calculated time delay deviation (thickness estimation deviation) not exceeding the empirical and clinically satisfactory limit. In order for the algorithm to perform well at the clinical level, it is necessary that the time period t_1 to t_3 is minimized. For that reason, a number of suitable signal processing techniques have been considered and engaged with the focus at methods for SNR enhancement.
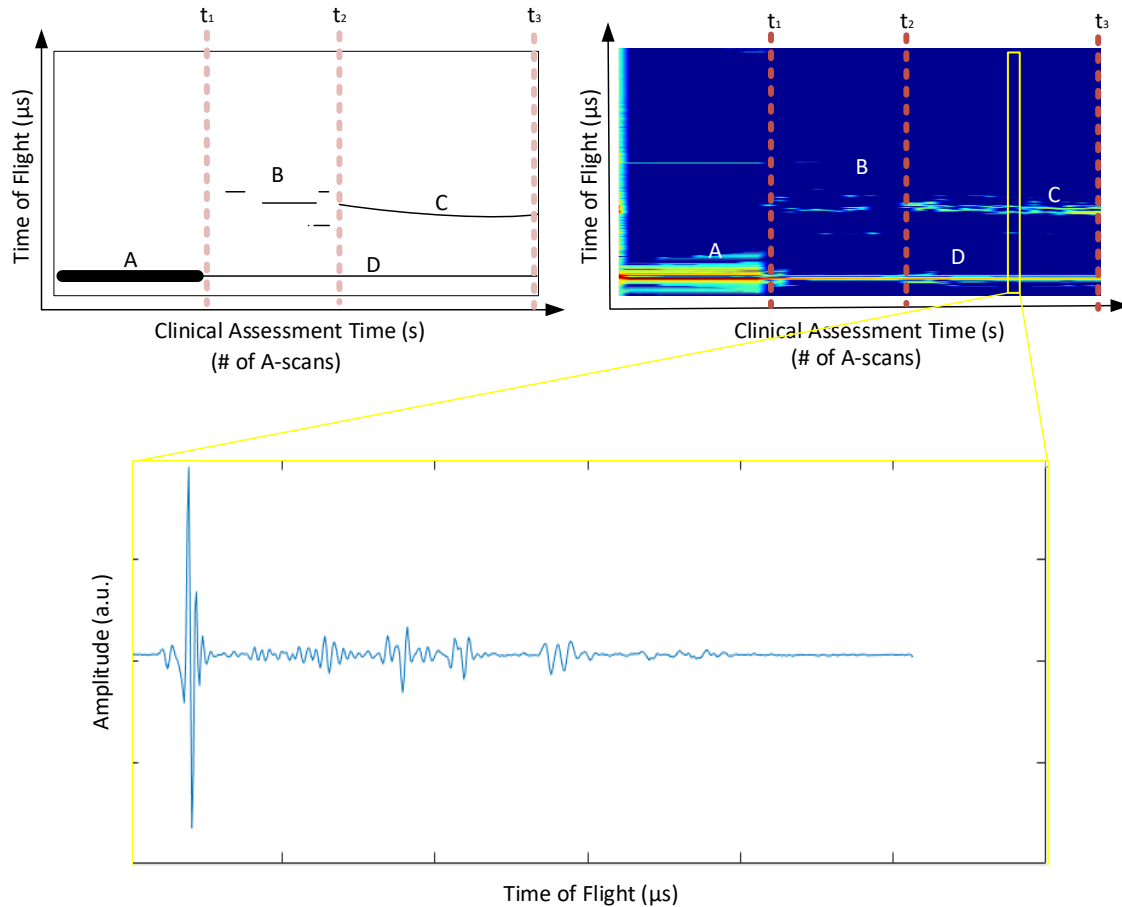
Figure 2.6 Schematic diagram (left) representing various reflections present in the clinically acquired M-scan (right). An example of clinically acquired A-scan (bottom).

Finally, the time delay between echoes of interest can be extracted and recalculated into the distance traveled based on the experimentally established average velocity of sound in the tissue of interest.

2.3.1. Time Delay Detection in RF Ultrasound Signals

The time-of-flight (TOF), known also as the time delay estimation (TDE) has been successfully used in biomedical and industrial applications for the purpose of thickness assessments, temperature estimations, equipment monitoring and other applications that could be a function of the wave velocity [22], [23]. A common practice

in ultrasound research is to identify pulses (interface signal reflections) based on its amplitude for the reflection spacing estimations (Figure 2.7). Multiple signal processing techniques have been described and investigated for the TOF quantification in the past [24], [25]. Techniques such as envelope peak detection, cross-correlation, amplitude thresholding, zero-crossing detection, maximum/minimum peak detection are amongst the most popular. Attention to the specimen characteristics must be made to investigate and incorporate possible phase changes, scattering contributions, reflector nonuniformity, angular alignment distortions caused by refraction and interference in order to operate a reliable TOF estimation. Many algorithms for automatic TOF selection have been coded and studied [26].
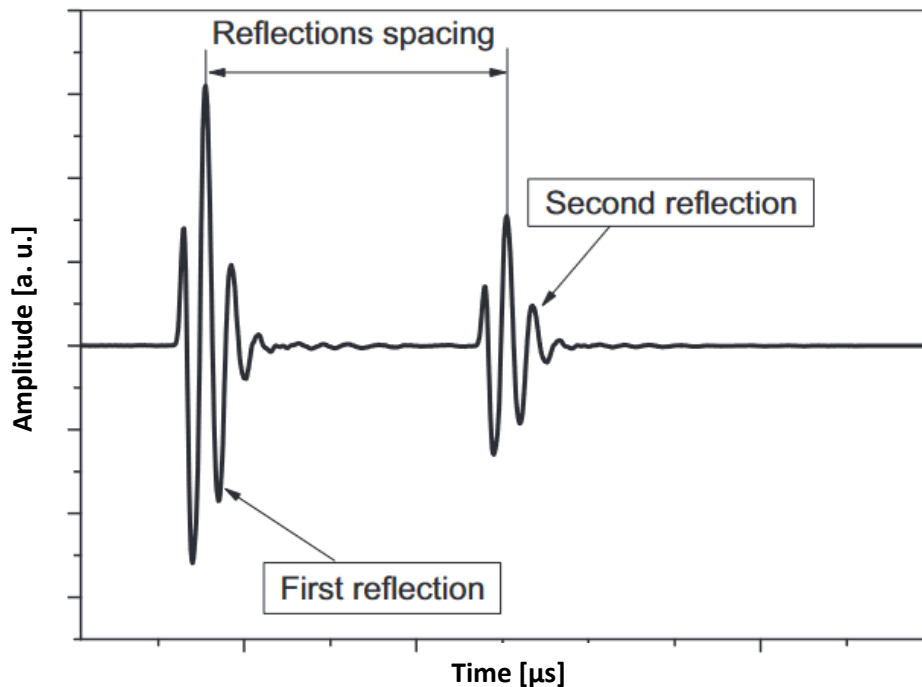
Figure 2.7 A schematic representation of an A-scan, reflections spacing is the time-delay or TOF between consecutive reflections first and second, respectively.

Some of the DSP methods for increasing effective TDE detection are supersampling or subsampling interpolation. The subsampling method (oversampling in reconstruction) is taking advantage of adding additional samples in between existing

ones, specifically in the region of interest so in the place of an expected maximum, minimum or zero-crossing. Various interpolation functions have been studied and the behavior of cosine interpolation function was concluded to produce smaller bias error than parabolic interpolation [27]. The upsampling method is performed during A-scan acquisition to increase the sampling rate by adding a time delay between consecutive analog to digital conversions of the same analog signal. This method is popular especially in the case of limited hardware resources.

2.3.2. Ultrasound Signal Enhancement Techniques

The ultrasound RF data often contain noise from several sources, signals form unexpected mode conversions and reflections. A good example of the unwanted signal is the granular pattern called speckle noise. The speckle noise is essentially an interference pattern coming from miniature scatterers embedded in the heterogeneous tissue structure. It is commonly called noise since it does not correlate well with physical objects. There are several effective methods known to reduce speckle noise and other electrically sourced unwanted signal components.

A. Time Averaging

The A-scan line averaging performs well and is one of the most common techniques used in ultrasound signal improvement due to its simplicity. Since the hardware used in the studies has the pulse repetition limited to $60\,Hz$ it was experimentally identified that 8x averaging is permitted for the signals. Higher averaging values caused the acquisition system to respond too slow to meet clinical criteria. Several factors can deteriorate the performance of the method such as jitter, sudden changes of medium properties and noise affecting the time of flight.

B. Filtering - Spectral Processing

The fundamental method for filtering out undesired A-scan content is band-pass filtering. Conventionally, in ultrasound technology transducers are described in frequency terms by specifying their central frequency and associated bandwidth. The operational frequency for the transducer designed for this study is 19.5 MHz with the bandwidth reaching 100 %. The following specifications set the desired passband to encompass frequency range 9 MHz to 31 MHz. The FIR bandpass filter transition bands are kept relatively broad, not exceeding 5 MHz, to allow lower order and quick filter computation. The filter is applied to every A-scan as it effectively eliminates frequencies that do not belong to the useful signal spectrum. Unfortunately, the filter does not interact with unwanted noise and response within the ultrasound signal. Alternative methods for eliminating signal components are proposed.

C. Signal Separation - Sparse Deconvolution

Sparse deconvolution is one of the approaches used to separate the received signal into a sparse (spike-like) train representing the impulse response of the object being investigated and residuals. This technique removes time spread introduced by the transducer response (point spread function) into the system [25]. It has been extensively investigated for the purpose of improving ultrasound readout for over 20 years now. The majority of the proposed algorithms were computationally too expensive to be freely adopted in the industry. However, over the years the cost of powerful computers decreased as well as more effective mathematical solvers were developed which resulted in increased interest in the signal deconvolution techniques. An early comparison study concluded a superior performance of Wiener filter for systems where timely performance is important [28]. Continuous improvements and iterations of the Wiener algorithm lead to hybrid approaches combining autoregressive spectral extrapolation or with L1-norm [29]. The methods have been successfully applied to geophysics, non-destructive evaluation of materials in industries like aerospace, automotive and pipelines [30], [31]. More advanced methods were proposed to

overcome common issues related to wave signals such as dispersion of selected frequencies or highly attenuated signals. The assumption that the wavelet is time-invariant, and the signals are stationary was not valid in these cases. The higher spectral order analysis method was proposed and exploited [32], deconvolution for ultrasound images based on automatic estimation of reference signals [33] or minimum entropy deconvolution with sparse and semi-sparse solutions [34], [35]. The mentioned methods could be very powerful at the expense of processing time, computational cost and overall complexity. The main objective of the current work in terms of signal deconvolution was to identify an approach that has a high hardware implementation potential, can operate at relatively low computational cost and high speed so it can function at quasi-real-time A-scan intervals. Most recent improvements and cost-effective implementations are available due to the availability of computational power and that has redirected research towards iterative deconvolution techniques.

2.4. Development of the High-Frequency Diagnostic System Prototypes

2.4.1. Hardware Components

The device consists of a miniaturized probe with a specifically designed ultrasonic transducer, electronics responsible for signal generation and acquisition, and a computer module (Figure 2.9) or a research-based version of the system with a high-speed USB interface (Figure 2.8).

In both cases, the enclosure has a built-in electronic board responsible for the ultrasound signal generation and acquisition. The board was custom-ordered and provided by the third-party supplier (Tessonics Inc., Windsor, Canada). Both research and a clinical prototype version of the system were designed, built and assembled in-house as a part of this work. The development work was necessary to conduct studies and evaluate produced algorithms.
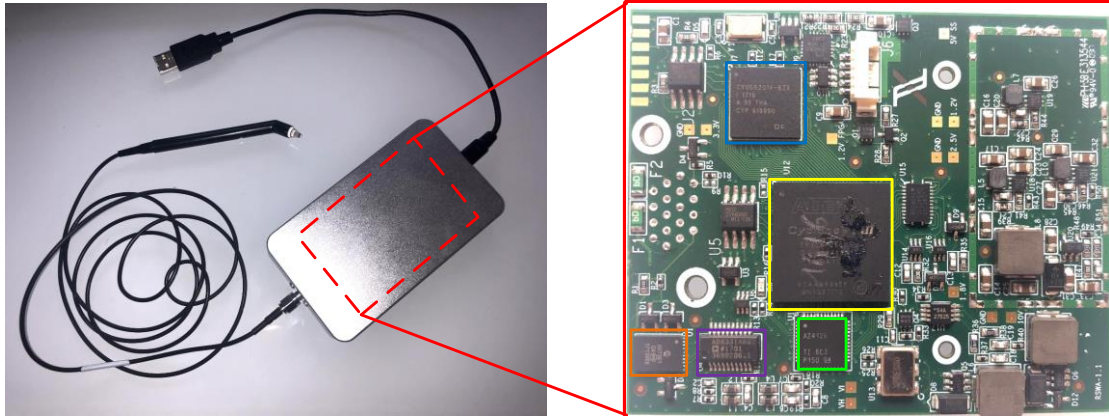
Figure 2.8 The system implementation for research (left) where the ultrasound electronics is placed in an enclosure connected to a computer through a universal serial bus (USB); (right) data acquisition and module with highlighted the most important components: (blue) USB 3.0 communication controller Cypress CYUSB2014-BZXI, (yellow) FPGA for data control by Altera Cyclone 3, (green) analog to digital converter 12bit/ 160 MSPS by TI AZ4126, (purple) ultra-low-noise preamplifier AD8331, (orange) an integrated pulse generator and T/R switch by Microchip HV7361.

Figure 2.9 The clinical system prototype hardware implementation, (left) the unit, (right) the probe tip - conical delay line with A = 12 mm and B = 1.5 mm.

The block diagram of the system (Figure 2.10) represents a simplified component structure of the ultrasound acquisition board. A host (PC) is connected through the universal serial bus (USB) communication controller (Cypress CYUSB2014-BZXI), the FPGA ((Altera Cyclone 3) is used as FIFO for data buffering and signal generation control. The functionality of the FPGA is planned to be extended for DSP processor and memory control (embedded development). The FPGA communicates with the analog to digital converter, 12-bit and 160 MSPS (Texas Instruments AZ4126) through

a parallel LVDS interface and SPI for configuration, and an integrated pulse generator and transmit and receive (T/R) switch (Microchip HV7361). Experimental studies and performance assessments presented in this dissertation were conducted on the research system connected to a computer (Intel Core i7- 7700HQ 2.8GHz, 16GB RAM). The unit board was fabricated and delivered by a 3rd party with an appropriate API and drivers that allow ultrasound data streaming.
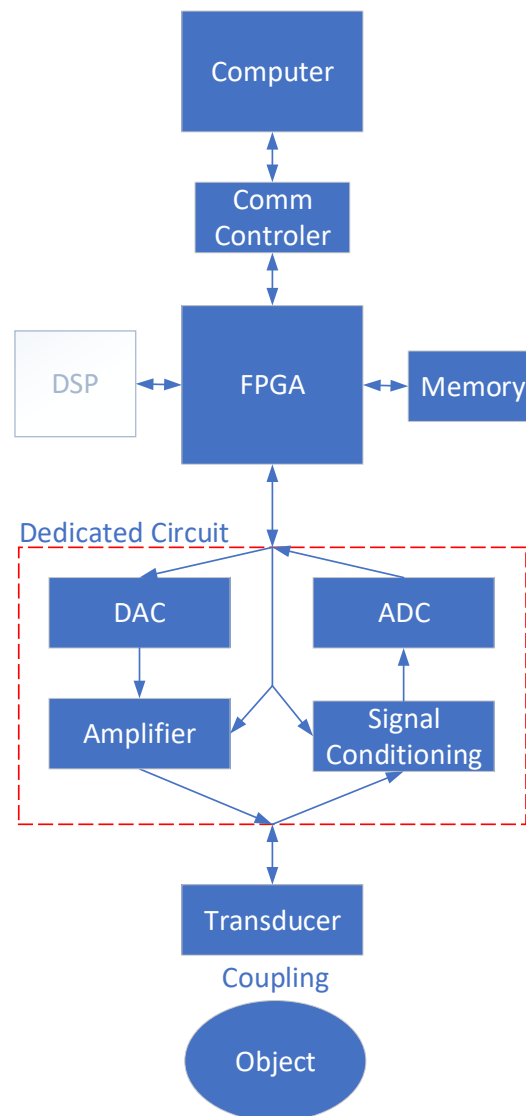
Figure 2.10 The diagram presents the flow of signals through a basic ultrasound system with a computer interface.

The hand-held probe (Figure 2.9) has a built-in 19.5 MHz spherically focused, single-element transducer with a focal distance controlled by the attachment of a polystyrene cone tip. The spherically focused transducer was selected for this application to enhance lateral resolution within the focal zone which in the application of interest would be located at the narrow end of the probe (B) in Figure 2.9. The central frequency was chosen to accommodate the required resolution and fit into the data streaming process. Both the research prototype (Figure 2.8) and the clinical device prototype include the same data streaming and processing pipelines. The reason for creating two units was to simulate further constrains on the functionality of the prototype in the clinical setting and eliminate unnecessary components that can complicate and compromise disinfection and cross-contamination prevention efforts.

2.4.2. Software Design

The developed system software is composed of several layers (Figure 2.11). The front- and back-end parts of the software were created in MATLAB v. R2017b (The MathWorks Inc., Natick, Massachusetts, USA) as a platform for implementation and algorithm testing. The contributed back-end algorithm for data analysis was connected to the ultrasound board dynamic link libraries for streaming data in real-time. A configuration file was also created to setup characteristics of the transmitted pulse and preamplifiers (peripherals that require configuration before the data stream initiation). This layer of configuration cannot be modified by the user due to safety requirements and it is not exposed. The created software structure is optimized and easily transferable to different programming environments; for that reason, the use of internal functions and toolboxes in the programming environment was minimized. The contributed script code could be further optimized in the C++ implementation.
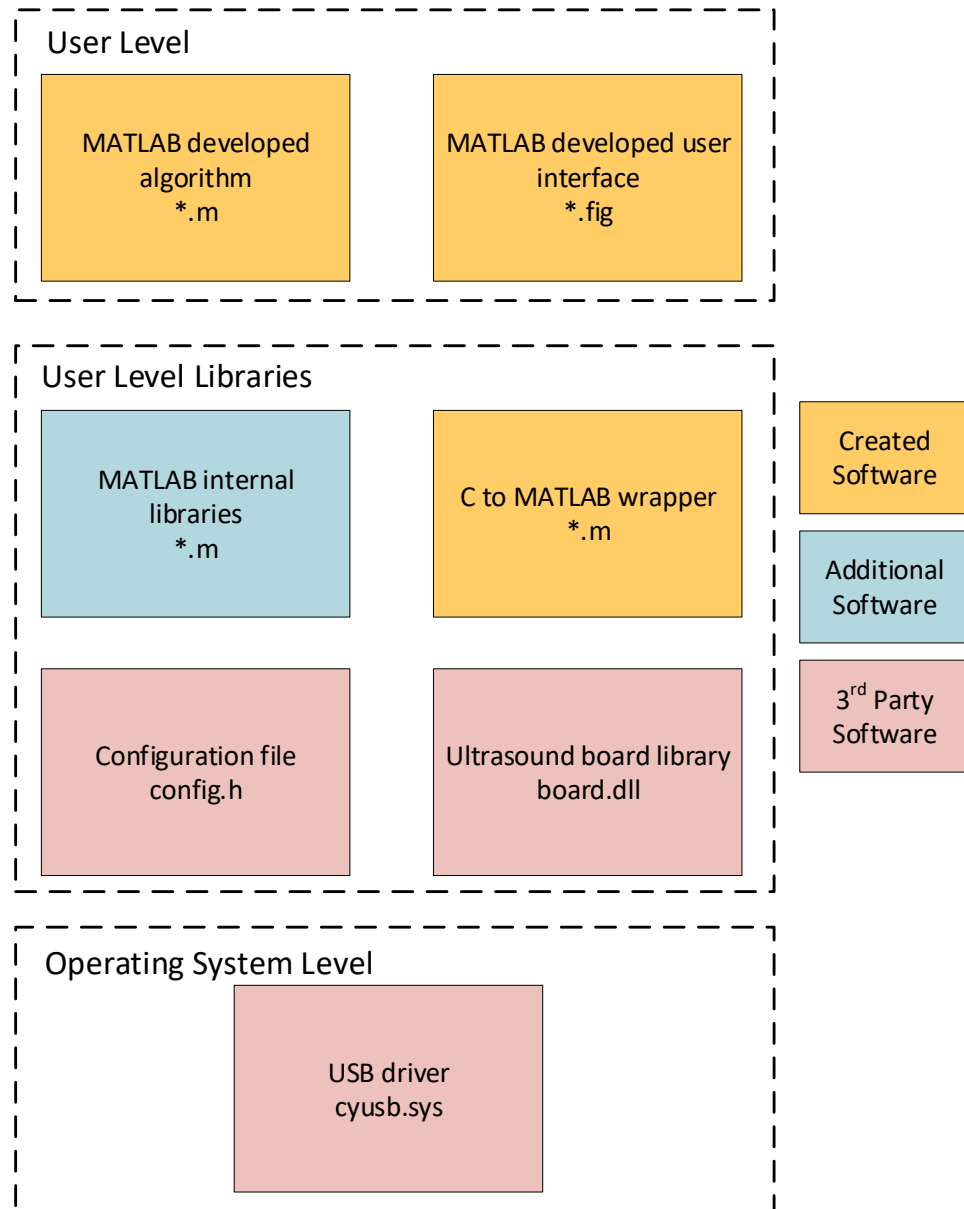
Figure 2.11 The software structure used in the proposed system highlights contributed parts to the overall device.

2.5.   Summary

The goal of this chapter was to introduce practical challenges and problems associated with the technicality of the assessment that was identified in applications where a quick and reliable assessment is necessary. The complicated anatomy, number

of locations that require diagnosis as well as the time available for diagnostics specify conditions for the proposed system performance. One of the tasks of this dissertation was to address the need by proposing algorithmic solutions and validating its performance. The rigorous clinical criteria set apart similar systems adopted for research in the past.

The system implementation solutions were described including software and hardware. Although the clinical prototype was not necessary at this stage of experimental work it provided valuable feedback, development requirements revision and constraints testing. The front- and back-end software was created in script-based programming language for flexibility, quick changes implementation and code optimization for other applications.

The utilization of digital signal processing for optimizing performance, enhancing the signal to noise ratio that simplifies feature extraction is essential and necessary to accelerate execution. It also allows shortening clinical time to spend on diagnostics and promotes ultrasound as a commercially viable method in this application.

CHAPTER 3.

SPARSE ULTRASOUND SIGNAL DECONVOLUTION

ALGORITHM DEVELOPMENT

The propagating ultrasound pulse-echo signal generated by the piezoelectric transducer deteriorates with depth, effectively the axial resolution of the A-scans decreases. The following chapter elaborates on the sparse deconvolution algorithm implemented in the proposed ultrasound diagnostic system. The inverse problem tackled by the developed algorithm is ill-posed/ill-conditioned due to noise content and requires an iterative method to address signal enhancement. The algorithm's task is to separate and enhance useful signals from scattering that do not contribute to the searched TOF estimation. The invariance assumption throughout the propagation path is valid in this case and the generalized inverse (pseudoinverse) techniques can be employed and evaluated. The following chapter includes an introduction to the deconvolution algorithm's achievements and motivation for development in the direction of signal processing for the purpose of medical diagnostics. The chapter also presents the mathematical background and explains details for the operation of the proposed solution adaptation.

3.1.   Inverse Problem of RF Signals

The diagnostic goal of the ultrasound-based medical imaging is to extract information about the tissue structures located along the pathway of the ultrasound beam based on the acquired echoes. In physics, those echoes would be the solutions of the wave equation given the impedance map of the medium [36], [37]. In a practical approach, it is well accepted that the received RF signal of a singular A-scan could be represented as:

$$y(t) = h(t) * x(t) + n(t) \text{ or} \tag{3.9}$$

$$Y(\omega) = H(\omega)X(\omega) + N(\omega) \tag{3.10}$$

where $x(t)$ is the medium response, and it is convolved with the ultrasound pulse $h(t)$ (known also as the PSF or the ultrasound system response) and $n(t)$ is additive noise [29], [38], [39]. Equation (3.9) can be also represented in the frequency domain (3.10). Traditional B-scan image is reconstructed based on the received degraded representation of the tissue response $y(t)$. It has been proven that deconvolution enhances SNR and consequently improves resolution [40]. It is expected that the deconvolution process would improve data interpretation and for further analysis. A tempting solution would be to perform straightforward inversion in the Fourier domain and through inverse Fourier transform get the deconvoluted signal back. In real signals analysis, the consequence of such calculation would be rather disappointing due to corruption caused by the additive noise, especially in the case of higher frequencies. This issue is known as *ill-conditioning* in the inverse problem theory. The easiest way to eliminate noise amplification would be to design a simple low-pass filter to remove unwanted frequencies. Unfortunaly, this solution would be far from optimal solution. More advanced methods have been developed to produce estimates of $h(t)$. A significantly better result could be achieved using the Wiener inverse filter. In the frequency domain the filter could be expressed as:

$$X(\omega) = \frac{Y(\omega)H^*(\omega)}{|H(\omega)|^2 + S_n(\omega)/S_x(\omega)} \qquad (3.11)$$

As provided by [41] where $S_x(\omega)$ and $S_n(\omega)$ represent power spectral densities. Due to the requirement of estimates for the distribution of noise and scattering the term $S_n(\omega)/S_x(\omega)$ could be replaced by so-called noise desensitizing factor 0.01 times the maximum value of $|H(\omega)|^2$. Unfortunately, it is not recommended for advanced practical solutions, simplification in the following form causes a non-optimal solution [41]. Nevertheless, several research studies have shown that the Wiener filter and its modifications could be effective and applicable in selected practical applications [42], [43].

3.2.   Sparse Signal Deconvolution Algorithm Development

The simplest definition of the deconvolution process is calculating components of input of a discrete-time system based on the provided output. It is usually assumed that the system is linear. In ultrasound, deconvolution is known for separating useful information from residuals (for example the point spread function, noise or both). For systems that are non-invertible or nearly non-invertible, the problem is more difficult. In practical applications, the output signal is always noisy. As it was already mentioned, the use of an exact inverse method can amplify the noise and result in distortions that could be destructive for the analysis process.

In selected industrial and medical applications, it is expected that the input signal is sparse (for example a delta functions train) or at least could be assumed to be close to sparse. Utilizing a priori knowledge about the object of investigation enhances the algorithm and increases the probability of receiving a realistic estimate of the input, even when the system output includes noise.
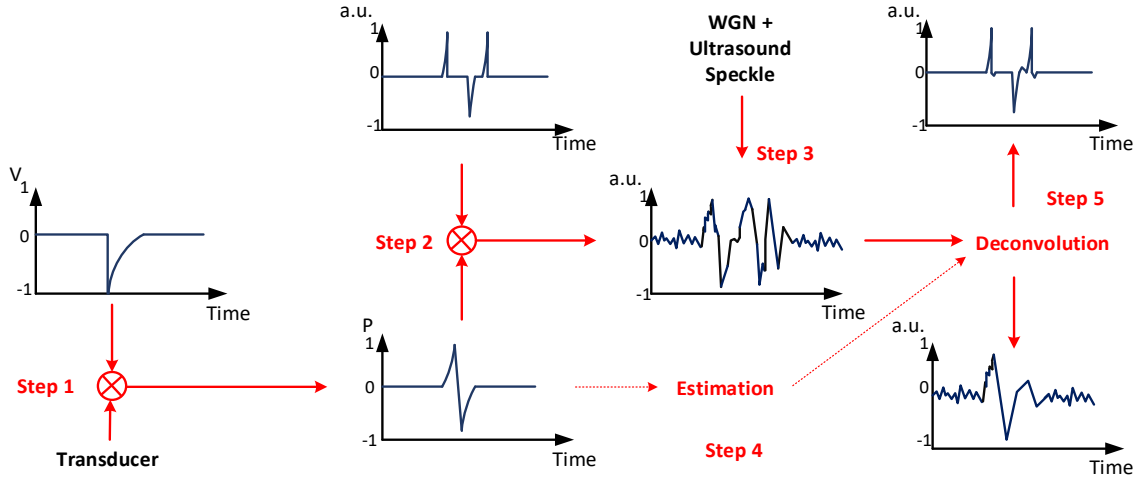
Figure 3.1 The diagram presents the following process: (Step 1) convolution of the transducer response with the initial electrical signal resulting in the PSF, (Step 2) convolution of the PSF with a specimen, (Step 3) addition of white Gaussian noise and specular noise, (Step 4) signal estimation based on the autoregressive model, (Step 5) deconvolution process based on the proposed algorithm.

The linear time-invariant system can be described by the recursive differential equation

$$y(n) = \sum_k b(k)\, x(n-k) - \sum_k a(k)\, y(n-k) \tag{3.12}$$

The following equation can be also written in matrix form as

$$\mathbf{A}y = \mathbf{B}x \tag{3.13}$$

With A and B being the following matrixes

$$\boldsymbol{A} = \begin{bmatrix} 1 & & & & \\ a_1 & 1 & & & \\ & \ddots & \ddots & & \\ & & a_1 & 1 & \\ & & & a_1 & 1 \end{bmatrix} \quad \mathbf{B} = \begin{bmatrix} b_0 & & & & \\ b_1 & b_0 & & & \\ & \ddots & \ddots & & \\ & & b_1 & b_0 & \\ & & & b_1 & b_0 \end{bmatrix} \tag{3.14}$$

The system could be also represented as

$$y = \mathbf{A}^{-1}\mathbf{B}\mathrm{x} \qquad (3.15)$$

And further simplified by substituting with the system transfer matrix. The actual data model for the system can be written as

w

$$y = \mathbf{H}\mathrm{x} + \mathrm{w} \qquad (3.16)$$

Using the knowledge of the system as the selection criterium, the sparse representation could be regularized with L1 norm ($\|x\|_1 = \sum_{n=0}^{N-1}|x(n)|$). It is one of the most natural among convex functionals to capture spares a priori information. In effect, the optimization formulation has the form

$$\arg \min_x \frac{1}{2}\|y - \mathbf{H}\mathrm{x}\|_2^2 + \lambda\|x\|_1 \qquad (3.17)$$

And it is known as the Least Absolute Shrinkage and Selection Operator (LASSO) [44]. It is a powerful method that could be utilized for tasks such as sparse deconvolution and feature extraction. Effectively, the algorithm minimizes the following cost function

$$f(x) = \sum_n |y - Hx|^2 + \lambda \sum_n |x(n)| \qquad (3.18)$$

Where the first part of the expression is the least square error and the second part is the explicit definition of the norm (p=1).

The LASSO method puts a constraint on the sum of the absolute values of the parameters and it applies a regularization process where it penalizes the coefficients of the regression variables causing shrinkage towards zero. In practice, parameter λ

(controls the strength of the penalty) is of great importance. In the case of ordinary signals corrupted by white Gaussian noise, certain assumptions can be made about the noise levels and the regularization parameter could be potentially estimated to form an optimal solution.

In the problem tackled in this dissertation, the electronic noise is considered an irrelevant variable. Scattering is considered to be the main problem interfering with the echo signal of the interest. With the parameter λ equal to zero the algorithm cost function is unregularized and becomes the regular least squares regression. With increasing the value of λ the shrinkage increases so fewer noise and scattering artifacts stay in the final estimation but in the cost of the signal attenuation. The trade-off in selecting (or estimating) parameter λ should be reached and individualized for particular characteristics of the research object. Another important benefit of using the LASSO method is the significant improvement in the extraction of the time of flight. The shrinkage causes an improvement in axial resolution for TOF estimation which is the overall substantial improvement in data acquisition to be achieved [45].

The optimization problem (Equation 3.13) cannot be solved directly since it is not differentiable ($\|x\|_1$ is defined as a sum of absolute values and the absolute value is not differentiable at zero), however, the cost function is convex and therefore the practice of iterative solvers can be easily applied. The selected solving algorithm is based on the majorization-minimization (MM) optimization method and exploits the availability of fast matrix-based algorithms for solving banded systems of linear equations [46]. The MM procedure consists of two steps. In the first majorization step, a surrogate function that locally approximates the objective function is selected with their difference minimized at the current point of the process. The surrogate function approaches the objective function up to a constant. Further, in the minimization step, the surrogate function is minimized, and the new local minimum becomes the initialization point for the next iteration (Figure 3.2).
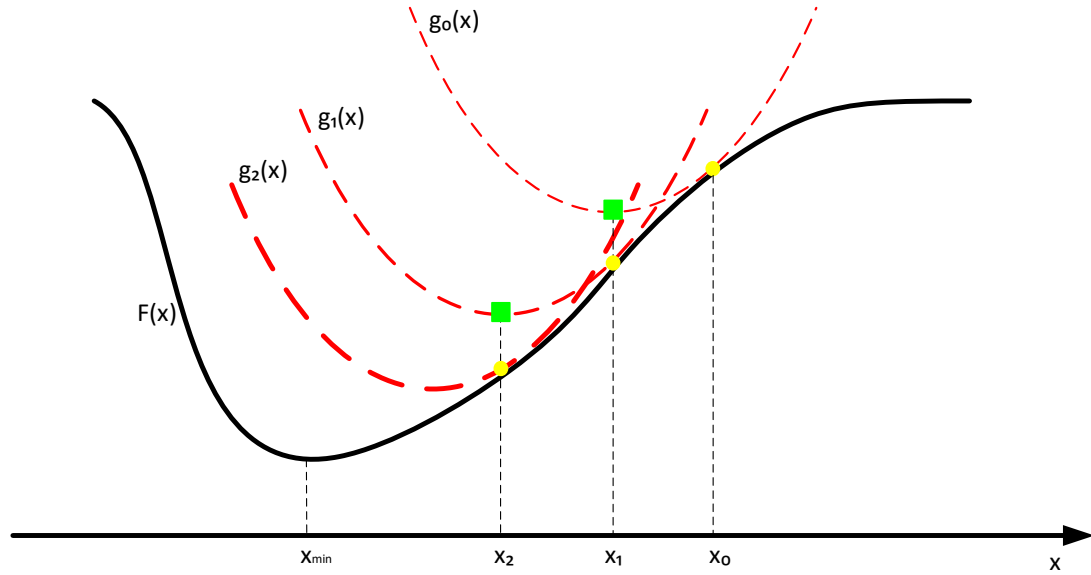
Figure 3.2 The diagram presents the majorization-minimization procedure where the cost function F(x) is being minimized by majorizer $g_k(x)$. The algorithm is initiated with x_0 and iteratively progressed.

The challenge of MM is to construct a surrogate function. The surrogate functions with the following features are desired: (a) Separability in variables (parallel computing), (b) Convexity and smoothness, (c) The existence of a closed-form minimizer. In general, terms, to minimize $F(x)$, the majorization-minimization approach solves a sequence of simpler optimization problems [47], [48]

$$x^{(k+1)} = \arg\min_{x} g_k(x) \qquad (3.19)$$

And the $g_k(x)$ must be a majorizer of $f(x)$ such that

$$g_k(x) \geq f(x), \text{ for all x} \qquad (3.20)$$

$$\text{and } g_k\left(x^{(k)}\right) \geq f\left(x^{(k)}\right), \qquad (3.21)$$

The surrogate function ($g_k(x)$) should be chosen so that it is easy to minimize fast. The update (3.19) produces a series of vectors $x^{(k)}$ (with k being an iteration counter) and it is converging towards the minimizer of $F(x)$. Consequently, minimizing the surrogate function is efficient and scalable, yielding a fast algorithm that is easy to implement [47].

1   Set k=1, Initialize $x_0 = y$ or $x_0 = H^T y$

2   Choose $g_k(x)$ so 3.16 and 3.17 are met.

3   Set x_{k+1} as the minimizer of $g_k(x)$ as in Equation 3.15

4   Set k=k+1 and go to step (2)

Finding an appropriate surrogate function (majorizer) that yields an algorithm with low computational complexity is not trivial. To achieve a fast convergence rate, a minimizer function that is somewhat similar and follows the shape of the objective function is desired. The trade-off between these two opposite requirements must be properly balanced for optimal performance. There have been methods described that present surrogate function construction techniques [49]. The design of the surrogate function was not an objective of this thesis and for that reason, the following approach was adopted [47]. A quadratic function was proposed that can be minimized by solving a system of linear equations

$$\frac{1}{2|t_k|} t^2 + \frac{1}{2} |t_k| \geq |t| \tag{3.22}$$

Replacing t with $x(n)$

$$\sum_n \frac{1}{2|v_k(n)|} x(n)^2 + \frac{1}{2} |v_k(n)| \geq \sum_n |x(n)| \tag{3.23}$$

The above equation can be also rewritten with using a compact matrix notation

$$\frac{1}{2} x^T \Theta x + \frac{1}{2} \|v\|_1 \geq \|x\|_1 \tag{3.24}$$

Where Θ is a matrix with $1/|v|$ on the diagonal. The left-hand side of the equation is a majorizer of the L1 norm of x. Based on that, the cost function (3.9) update could be now presented in the form after omitting the term that is not x dependent

$$x^{(k+1)} = \arg \min_x \left[\frac{1}{2} \|y - Hx\|_2^2 + \frac{1}{2} x^T \Theta_k x\right] \tag{3.25}$$

Where Θ_k is equal to $\frac{\lambda}{|x^k(n)|}$ Due to the use of quadratic equation linear algebra can be employed and the solution to (3.21) can be rewritten in a matrix form

$$x^{(k+1)} = (H^T H + \Theta_k)^{-1} H^T y \tag{3.26}$$

By applying mathematical manipulations (matrix inversion identities [46]) the issues related to solving the equation can be addressed and simplified to generate a set of banded matrixes that can be solved with applying fast solvers (LAPACK) built-in MATLAB. From the computational point of view, banded matrixes (non-zero entries located in the diagonal band) are desired [50]. Effectively, with expressing H in terms of A and B the update equations can be written as follows

$$g = B^T A^{-T} y \tag{3.27}$$

$$W_k = \Theta_k^{-1} = \frac{1}{\lambda} diag\left(|x^{(k)}|\right) \tag{3.28}$$

$$x^{(k+1)} = W_k[g - B^T(AA^T + BW_k B^T)^{-1} BW_k g] \tag{3.29}$$

As provided by [47]. The equations 3.23, 3.24 and 3.25 constitute the iterative computation part of the deconvolution algorithm.

Since the solution is not direct and parametrized, the regularization parameter λ controls the estimated results. With increasing the value (more regularization) it can yield estimates with less noise. The trade-off is in between distortion of the deconvoluted signal (attenuation) and the noise content. In this specific application, the parameter λ was selected empirically, the algorithm could be further improved by automatizing the selection by setting additional criteria for λ values.

3.3.   Autoregression Model (AR) for the System Response Estimation

Frequently in linear ultrasound systems, the input and output signals are either known or possible to acquire. The input signal can be analytically obtained based on the electrical pulse signal knowledge and transducer characteristics, recorded in a sperate experiment as a reference measurement or dynamically retrieved from the same output signal. The dynamic input signal estimation is the most effective due to adaptiveness to the current conditions. It can be pursued in the case where the signal or the geometrical structure of the sample allows to isolate an echo signal not affected by the propagation through the sample (for example reflected from the sample surface). Effectively, the autoregressive filter coefficients will be adaptively derived. The importance of selecting the right model order of the AR filter has been evaluated in the theoretical and experimental studies, a large filter can cause spurious spectral peaks and alternatively to small order could result in the prediction that is relatively poor and incomplete [51].

3.4.   The Summary of Algorithms and Conditions

The work presented in this chapter summarizes the theoretical aspects of the dissertation. The algorithm was implemented in the script-based programming

environment so the code could be further optimized and edited during clinical experimental work. The aim is to validate the overall performance and make necessary adjustments to the algorithm architecture so that the framework could be verified and validated for embedded implementation based on an efficient microprocessor, microcontroller or an extended FPGA design.

CHAPTER 4.

ALGORITHM EVALUATION BASED ON SYNTHETIC

ULTRASOUND SIGNALS

The goal of this chapter is to demonstrate the algorithm performance using synthetic signals mimicking the real ultrasound signal characteristics appropriate for the investigated applications. Traditionally, algorithm testing is performed in terms of quality (effectiveness) and latency [52]. In this chapter, the proposed algorithm will be tested using both approaches with an emphasis on the possible future clinical utilization of the system and acceptable latency versus systems cost. Similarly, as in the case of image assessments for example in other medical imaging modalities, a set of criterion parameters can be adopted for the proposed system. The multi-level assessment that represents technical features, as well as the wider perspective of possible clinical interactions, was adopted based on a hierarchical approach for image analysis [53]. The assessment of controlled signals with an added artificial variability was used to demonstrate the performance of the proposed algorithm and support further clinical evaluation.

4.1. Performance Studies

The technical performance is used to indicate the improvement of signals and images, speed of data extraction and visualization that can impact the clinical applicability of the proposed solution. The following metrics could be used in objective evaluation and determination of system capabilities. There are several international guidelines available for quality assessment including publications from the American Institute of Ultrasound in Medicine, the International Electrotechnical Committee, the International Organization for Standardization and others. Since there is not a unified formulation of the assessment methodology, the wildly accepted metrics include system sensitivity and echo signal detection capability, resolution and object visualization as general image characteristics. In the case of this thesis operation latency is of importance due to the real-time algorithm requirements as well as the overall time of a single data point assessment, trueness of the thickness estimation and accuracy.

4.2. Evaluation Parameters

4.2.1. Sensitivity - Signal to Noise Ratio

Sensitivity is quantified by either the signal to noise ratio (SNR) or signal penetration. In ultrasound, noise arises from the transducer, cabling, electronics, and the random nature of the background medium that give rise to speckle (for example body fluids). With an assumption that the noise is white over the system bandwidth and with taking into consideration, that signal strength is depth, focusing and attenuation dependent the SNR in a general form can be expressed as follows

$$SNR = \frac{Max\ Instant\ Received\ Signal\ Power}{Noise\ Power} = \frac{S}{N} \qquad (3.30)$$

Also, the popular signal power estimation used in ultrasound signals is represented as

$$S(t) = \left(\frac{1}{M} \sum_{m=1}^{M} x_m(t) \right)^2 \tag{3.31}$$

Where M is the number of measurements. The noise power is [54]

$$N(t) = \frac{1}{M} \sum_{m=1}^{M} \left(x_m(t) - \frac{1}{M} \sum_{m=1}^{M} x_m(t) \right)^2 \tag{3.32}$$

Based on the above equations the improvements in performance can be achieved twofold, either by the noise reduction associated with the reception process or by increasing of energy sent in the pulse form. There is a limit to signal amplitude regulated by safety considerations. The spatial peak pulse average (is the average flux over the time duration of the transmitted pulse) and the spatial peak time average (a time average over the entire pulse repetition period) should be less than the values specified by the regulatory body (for example Health Canada, Canada or Food and Drug Administration, USA). In addition, mechanical (MI) and thermal (TI) indexes could be controlled to prevent and minimize the risk of tissue damage [55]

$$MI = \frac{p_-(MPa)}{\sqrt{f(MHz)}}, \qquad TI = \frac{W_p}{W_{deg}} \tag{3.33}$$

The values for MI in diagnostic imaging range from 0.04 to 1.7. W_p attenuated output power and W_{deg} is the ultrasonic power required to raise the target tissue temperature by one degree Celsius.

Additionally, to evaluate noise reduction capabilities, the mean square error (MSE) and peak signal-to-noise ratio (PSNR) could be also used. The MSE measures

the quality change between the original and enhanced image (in the case of this study it would be the image reconstructed in the form of the time-motion scans with and without engaging deconvolution algorithm). The error calculation is widely used to quantify image quality; however, it does not correlate well with perceptual quality when used alone, therefore it should be used together with other quality indicators. The SNR compares the level of the desired signal to the level of background noise. The higher the ratio, the less obtrusive the background noise is and the better the overall performance. In general ultrasound applications, SNR is referring to a ratio from signal amplitude divided by noise amplitude commonly expressed in decibels. From this perspective, the noise would be coming from all sources including electronic noise. The electronically sourced SNR is a special case not specific to the medium, and the noise is electronically generated: thermal noise, flicker noise and other types of electronic noises. In ultrasound specifications, the signal to noise ratio is often given. This is the electronic signal to noise ratio, and it may be given referenced to the input of the amplifier circuit or the output, and sometimes given as a noise figure rather than a signal to noise ratio. It is a specific value related to components and quality (stability) of the system itself, lower noise numbers (i.e. higher signal to noise ratio) are generally better.

In this thesis, the SNR will refer to the signal to noise ratio as the ratio of the boundary echo amplitude to the amplitude of background scatterers. The background scatterers would be the tissue microstructures. In this case, the SNR depends on physical factors as seen in the formula where the S/N ratio depends on the ultrasonic speed in the metal, the density, the beam dimensions, etc. Note also that this defect S/N ratio is frequency dependent. Once again, lower noise numbers are generally better.

While the system user cannot minimize the electronic noise (except perhaps limiting the use of surrounding electronic devices), certain parameters of ultrasound system hardware might be modified and customized (beam dimensions, pulse characteristics, frequency) during the development process.

4.2.2.   Synthetic Signals – Pulse-Echo Wavelets

A decaying pulse representation of the signal that is produced by an ultrasonic transducer (ideally driven by a short time spike) has been proposed for the algorithm evaluation. The signal can be obtained from a simple mathematical representation. The wavelet of decaying oscillations defined by the difference equation has the following coefficient form:

$$b = [1 \ 1] \tag{4.34}$$

$$a = [1 \quad -r\cos\alpha \quad r^2] \tag{4.35}$$

As presented in [50]; r and α are constants. The coefficient form was proposed explicitly for the algorithm testing purpose. Based on that, the quality of the system transfer function estimation could be evaluated by removing the variability of estimating the point spread function (PSF). Several scenarios with noise presence have been tested and performance estimation results are provided.
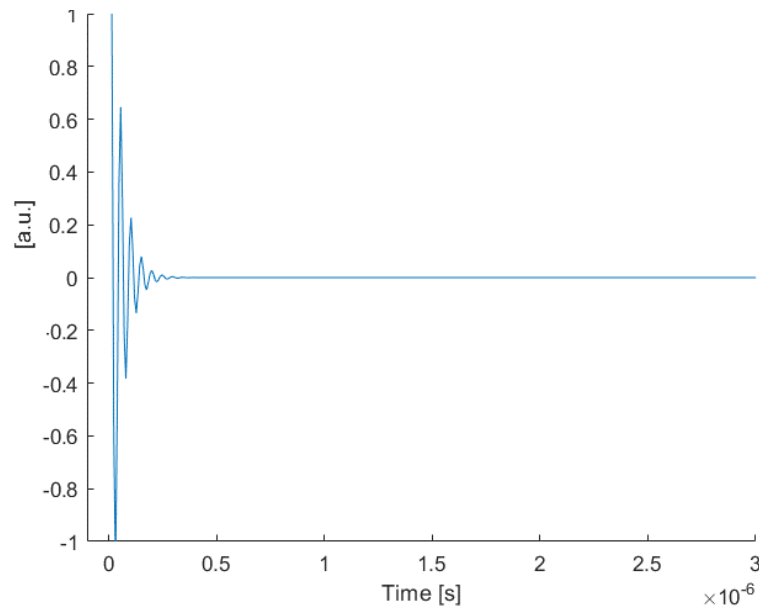
Figure 4.1 The simulated point spread function of the transducer presented with an alternative time scale.
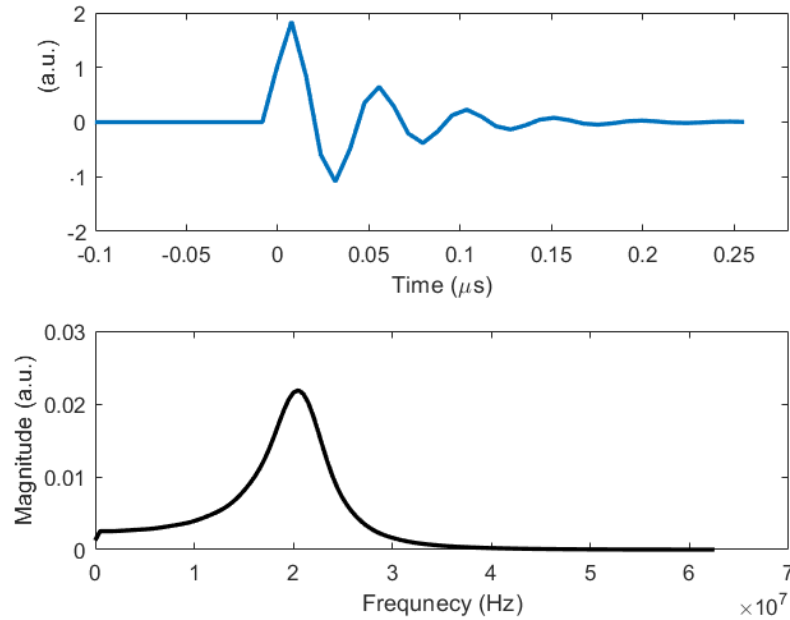
Figure 4.2 The decaying oscillation signal that simulates the PSF of a transducer at 20 MHz.

Further, the Gaussian-shaped signal was created as an additional model of the PSF. The model-specific set of well-controlled parameters such as bandwidth factor α and central frequency f_c was considered. By manipulating parameters, the signal can be brought to a close reproduction of a signal reflected from an ideal reflector.

$$\text{s(t(nT))} = \beta e^{-\alpha(t(nT)-\tau)^2}\cos(2\pi f_c(\text{t(nT)}-\tau)+\varphi);\qquad(4.36)$$
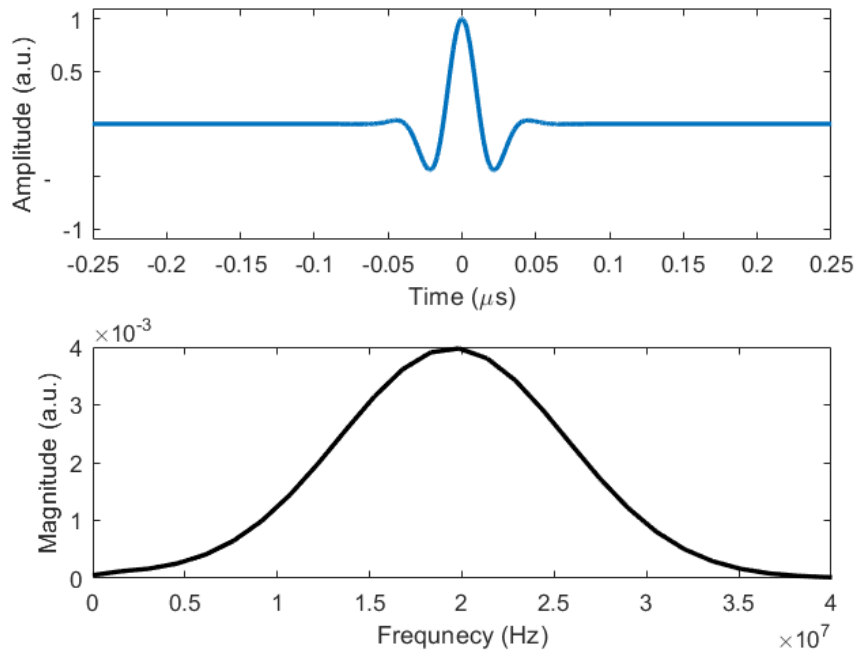
Figure 4.3 The graphical representation of a signal used for simulation. The bandwidth specified to be equal to 78 % to match the characteristics provided by the transducer manufacturer.

4.2.3.   The Transfer Function of the Simulated Object

It can be assumed that the ideal reflectors with varying transmission and reflection coefficients are distributed axially at 3 different locations (Figure 4.4). The expected signal is effectively a convolution of the previously described PSFs with the provided signal in order to simulate the wave reflection effect. The time delays, as well as amplitudes of the signals, are alternated to investigate the effect of deconvolution as a function of time and amplitude as parameters.
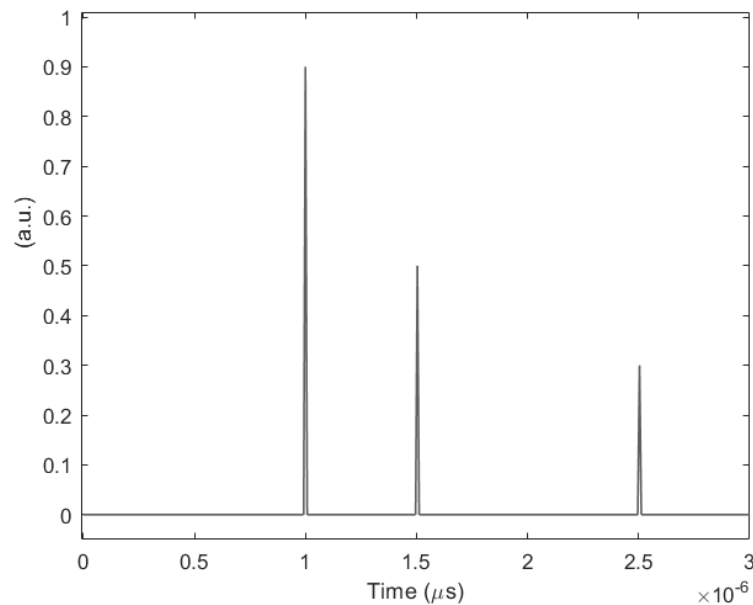
Figure 4.4 The diagram represents a signal simulating 3 ideal interfaces such that the individual peaks have 3 values of normalized amplitude and are separated in time.

4.3. Analysis and Results

The deconvolution method described and discussed in Chapter 3 has been implemented in the software environment for testing such that configuration parameters could be selected experimentally. A series of tests were designed to gain input information so the algorithm could be used in clinical studies described in Chapter 5.

4.3.1. Signal Estimation Results in Terms of the Autoregressive Model

The Burg's method was used for calculating the autoregressive model of the signal pulse convoluted with the transducer response (according to the diagram in Figure 3.1). This commonly used model of a linear system is the all-pole model, a filter representation with all zeroes located at the origin (in the z-plane). This method of power spectral density estimation works well to describe spectra of data that is sparse, where PSD is relatively large at certain frequencies. Data in many practical applications (such as ultrasound signals described in this dissertation) tend to have energy

accumulated around the resonant frequency and that makes AR models quite efficient estimators. Additionally, Burg's method is based on minimizing the forward and backward prediction and it leads to a system of linear equations that is computationally very efficient. This method estimates the PSD by first estimating the parameters (coefficients) of the linear system that hypothetically generates the signal. Burg's method tends to produce better results than classical nonparametric approaches, especially when the data length of the available signal is relatively short. Additionally, the Burgs method is characterized by important advantages such that it always produces a stable model and the method does not apply a window to data.

It can be seen in Figure 4.5 that the consequent effect of the number of coefficients used for signal estimation. To support further selection parameters such as elapsed time, variance and amplitude ratio have been collected and presented in Table 4.1. The parameters were normalized and presented in diagrams (Figure 4.6) to support an optimal criterion for the order selection.

n=10
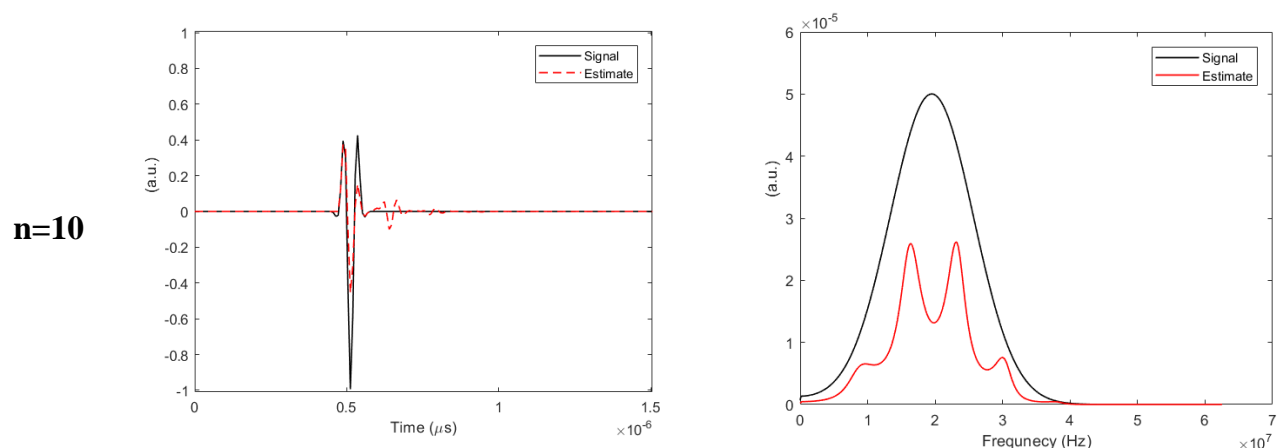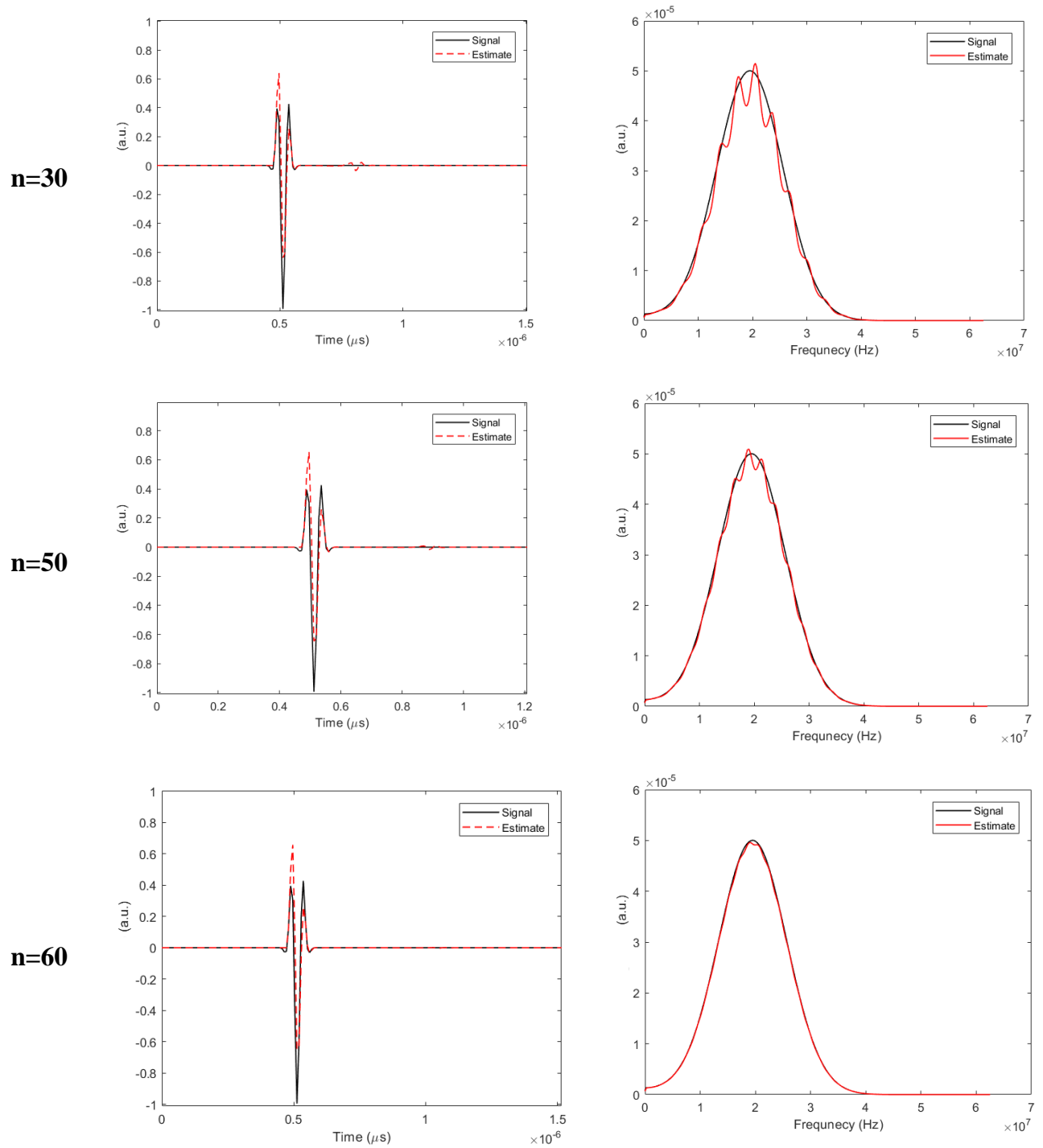
Figure 4.5 The diagrams in rows present original and estimated signals (black and red) as a function of an autoregressive filter order in time and frequency domain.

The red dotted line in Figure 4.5 represents the estimated signals. It can be seen that continuous improvement can be achieved.

Table 4.1 Results represent values of selected characteristics calculated to assess the Burgs method of approximation.

Filter Order	Elapsed Time [s]	Variance	Amplitude Y/X
10	0.000275	3.7766e-04	1.8588
30	0.000438	1.5947e-04	1.1707
50	0.000610	1.5289e-04	1.1074
60	0.001161	1.5274e-04	1.1019

Effectively, the results presented in Figure 4.5 and Table 4.1 were normalized to support an optimal filter order selection for the coefficients estimator. Figure 4.6 includes parameters discussed in Table 4.1 as a function of filter coefficients. Based on the diagram it is straightforward to observe that optimal condition surrounding n=30 where time necessary for computation is relatively low 0.4 ms and variance as well as the amplitude ratio reach values lower than 10 % of their values calculated for filter order equal 10. It is natural to conclude that selection can be further optimized and adjusted. An alternative progression to this selection would be an adaptive algorithm for the coefficient selection or forward estimation approach and possibly can be considered before perusing the embedded implementation.
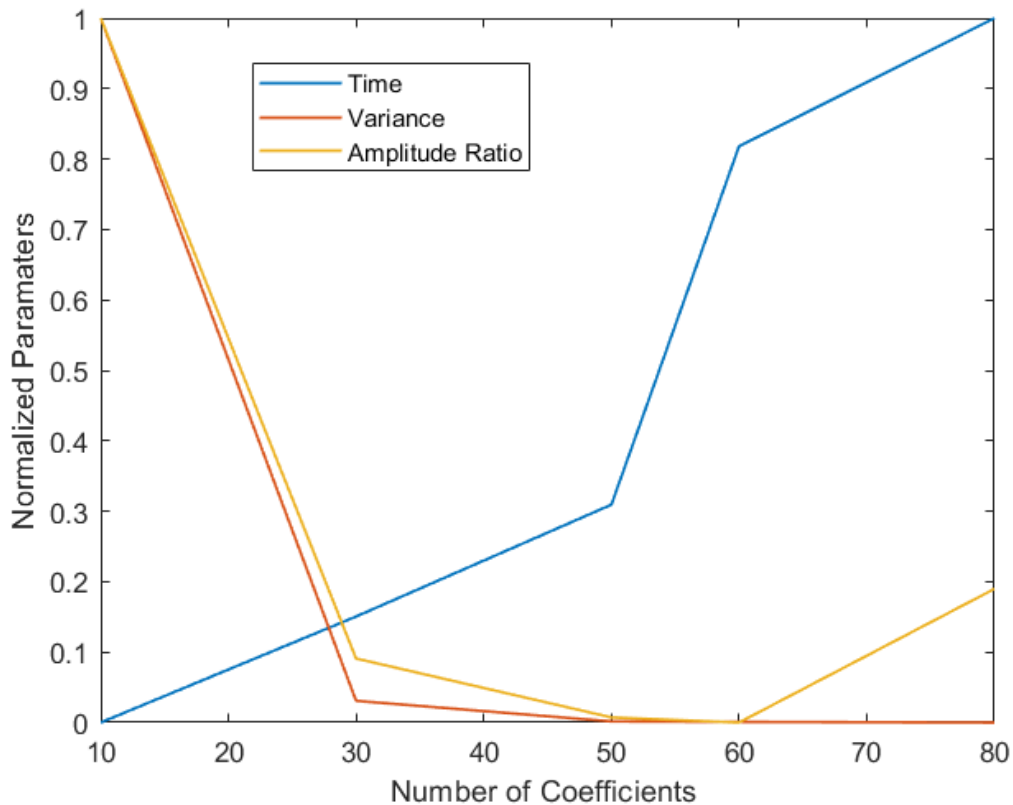
Figure 4.6 The diagram presents normalized parameters (time, variance and amplitude ratio) vs a number of filter coefficients.

4.3.1. Results in Terms of the Signal to Noise Ratio

A subsequent value of SNR was added to the simulated signals to investigate the robustness of the approach to additional noise content. It was proven that the synthetic signals used in the study were robust to realistic signal contamination. For further performance testing, SNR was evaluated until the algorithm failure. The results are presented in Figure 4.7 and show signals convoluted with the 3 simulated representations of reflectors with gradually added noise. The results on the right side represent the deconvolved reflectors. The effort has been made to minimize computation in the case of the future low-cost and possibly embedded implementation.

SNR=100 dB
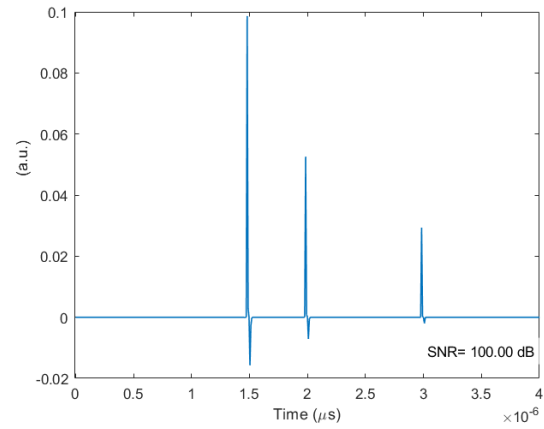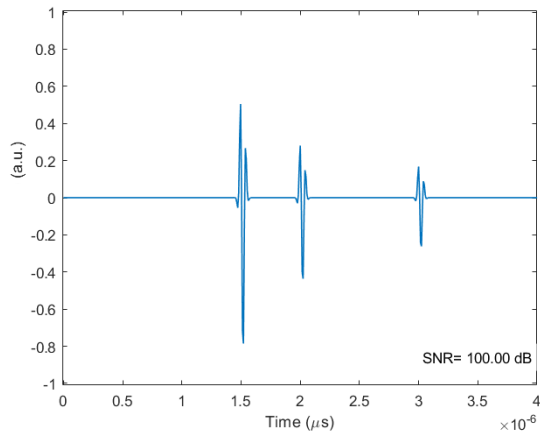
SNR=60 dB
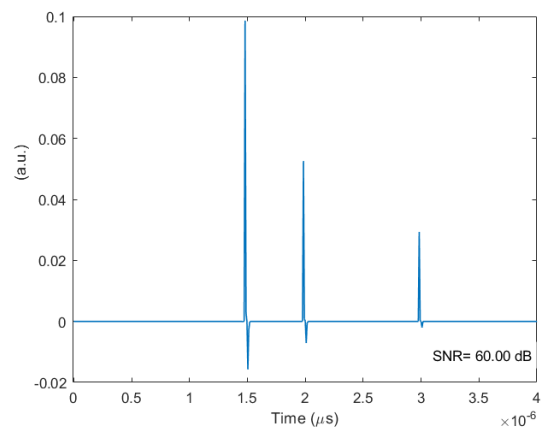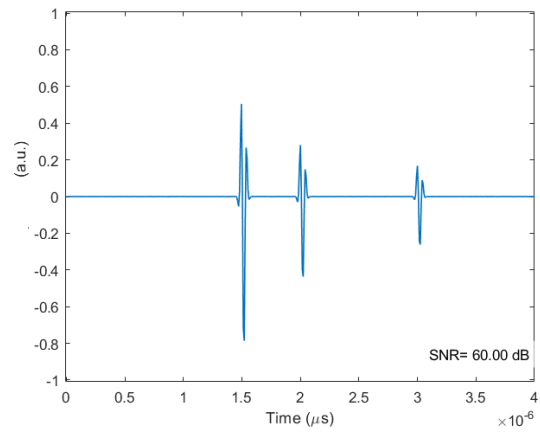
SNR=40 dB
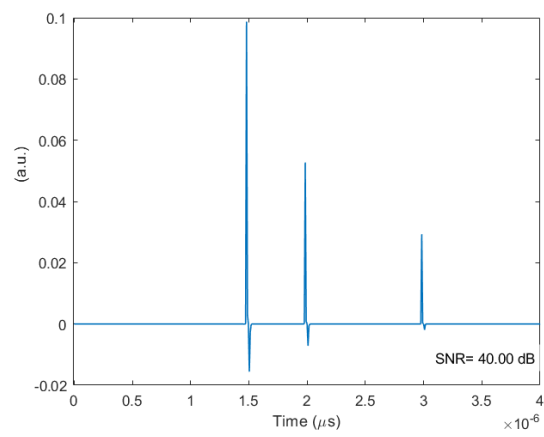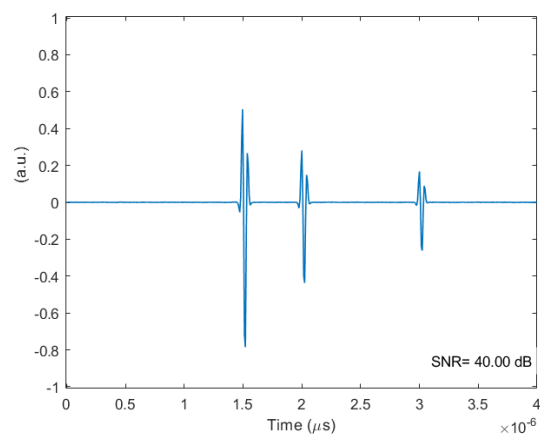
SNR=20 dB
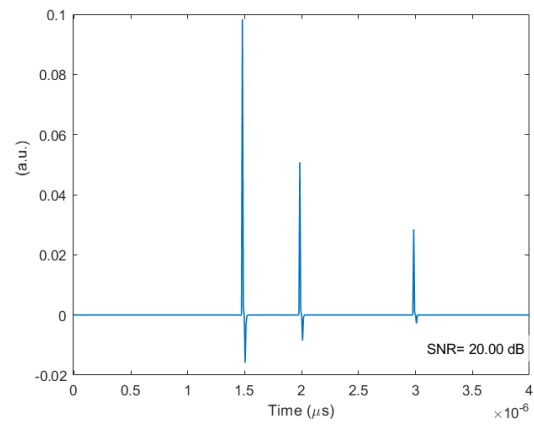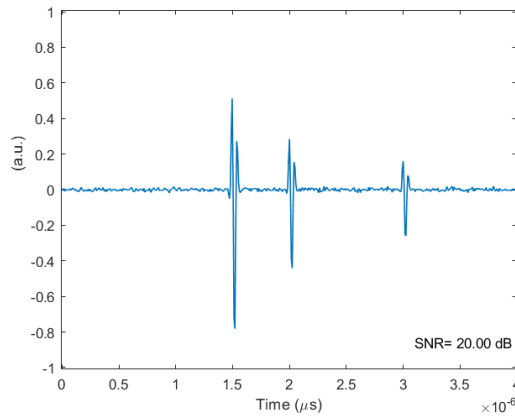
SNR=10 dB
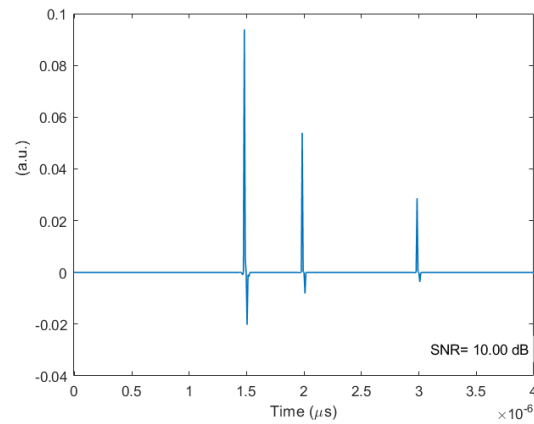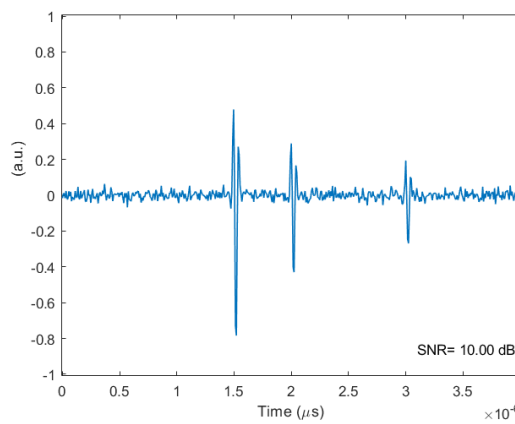
SNR=5 dB
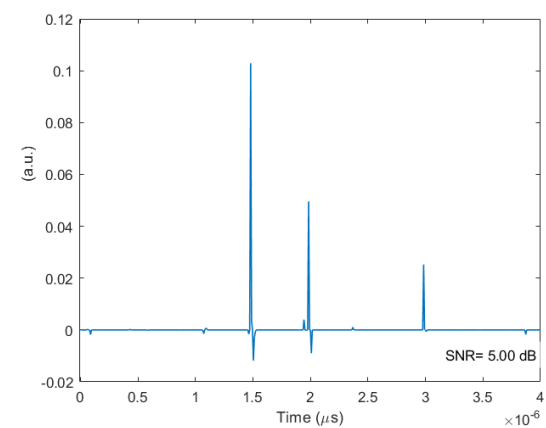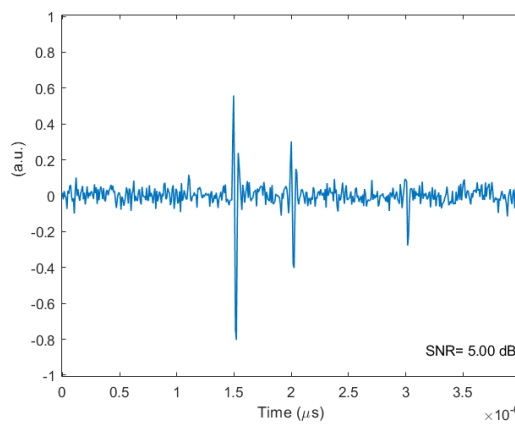
SNR=0 dB
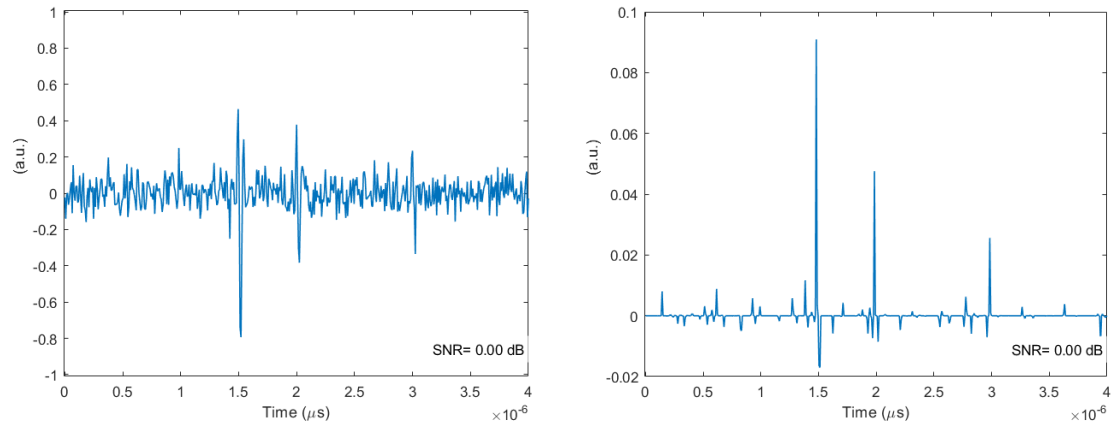
SNR=-5 dB
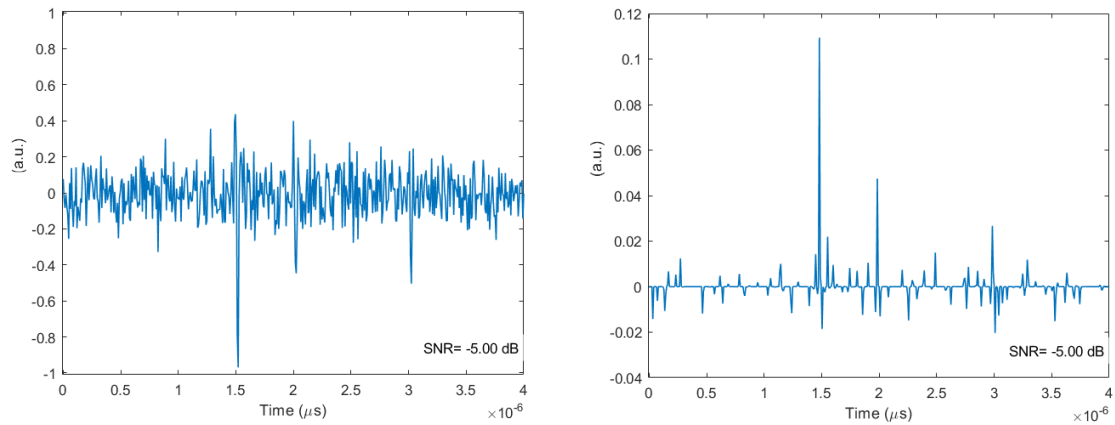
SNR=-10 dB
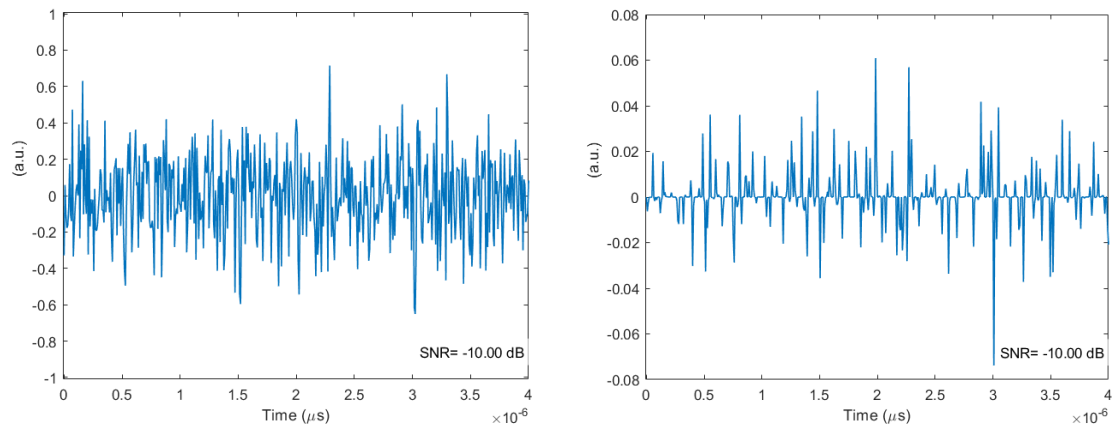
Figure 4.7 Results present added noise to signals consisted of the transducer PSD convoluted with the simulated object response in the left column. In the right column, the deconvolution results are captured after processing with the proposed algorithm.

It is possible to observe based on results in Figure 4.7 that the PSF can be effectively isolated from the signal of interest, even in a significant noise presence. The algorithm was tested quite comprehensively based on a range of SNRs to prove ordinary performance. Further tests were performed to characterize the algorithm behavior and select a unique set of input variables to optimize the clinical applicability of the algorithm in real-time studies so that the system could be efficiently used with biological specimens.

4.3.2. Results in Terms of the Regularization Parameter

Equation 3.13 (Chapter 3) includes the regularization parameter. The parameter helps to suppress deconvolution artifacts and estimation errors. The drawback of the non-optimized regularization parameter might be under- or over the suppressed signal. For that reason, the parameter has to be modified according to the application and signal characteristics. From the signals analyzed and presented in Figure 4.7 the signal that represents clinical-like characteristics was selected (A) and investigated with a range of values for regularization parameter lambda spanning from 0.5 to 10. The results and effectiveness of the parameter are summarized in Figure 4.8.

Initial Signal
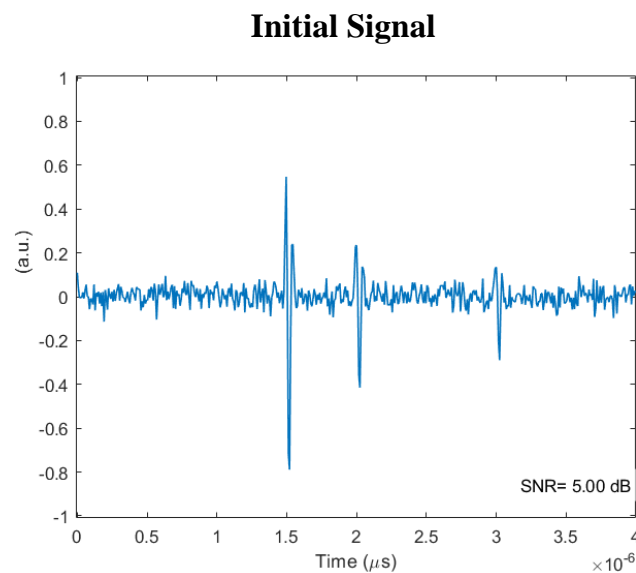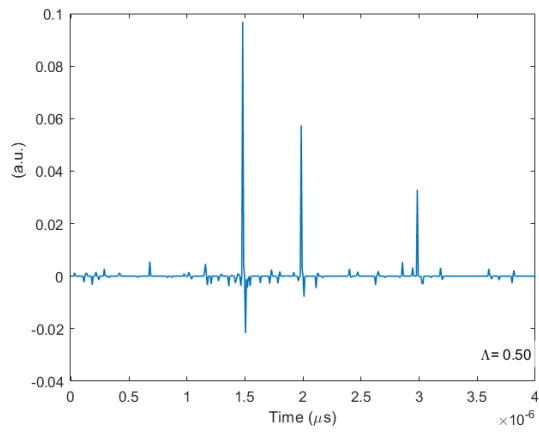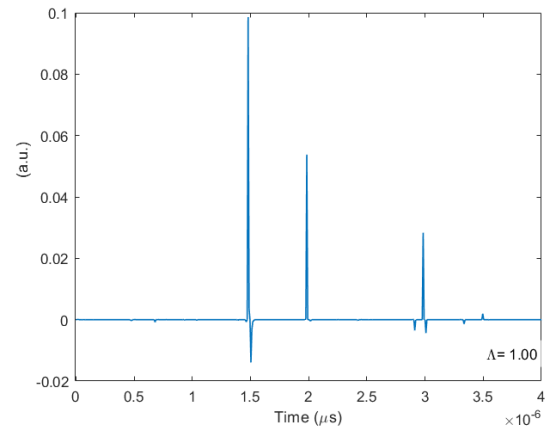
Lambda = 0.5

Lambda = 1

Lambda = 1.5
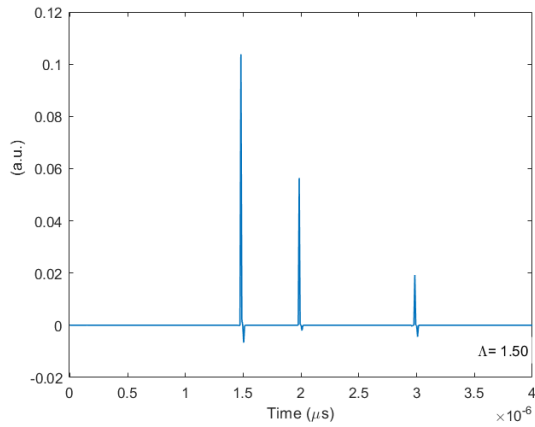
Lambda = 2
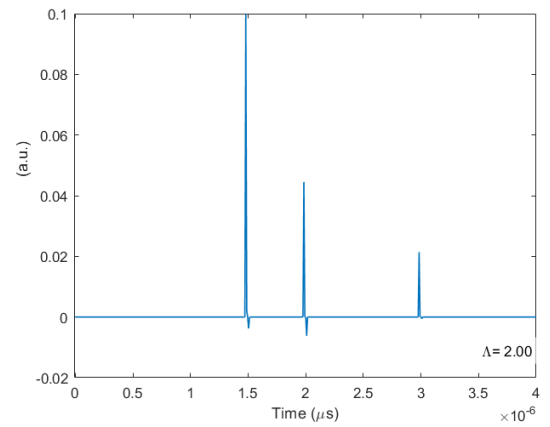
Lambda = 2.5
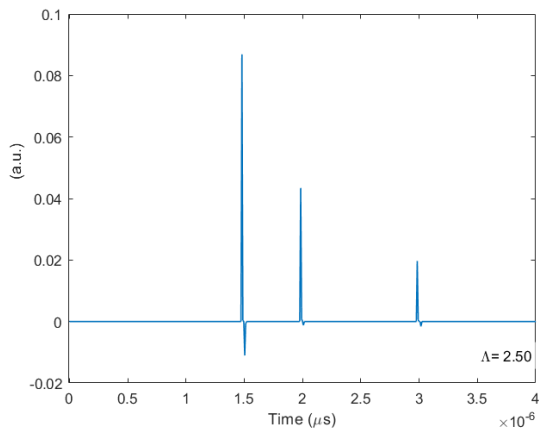
Lambda = 3
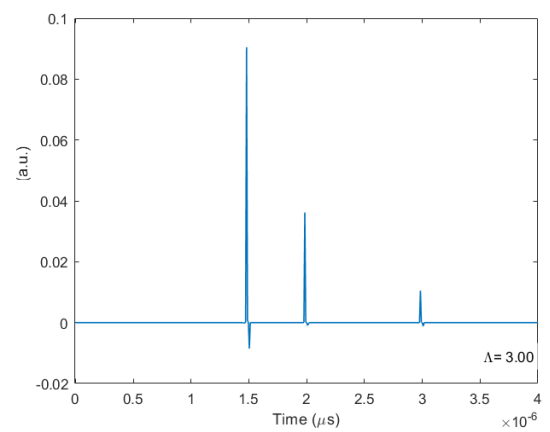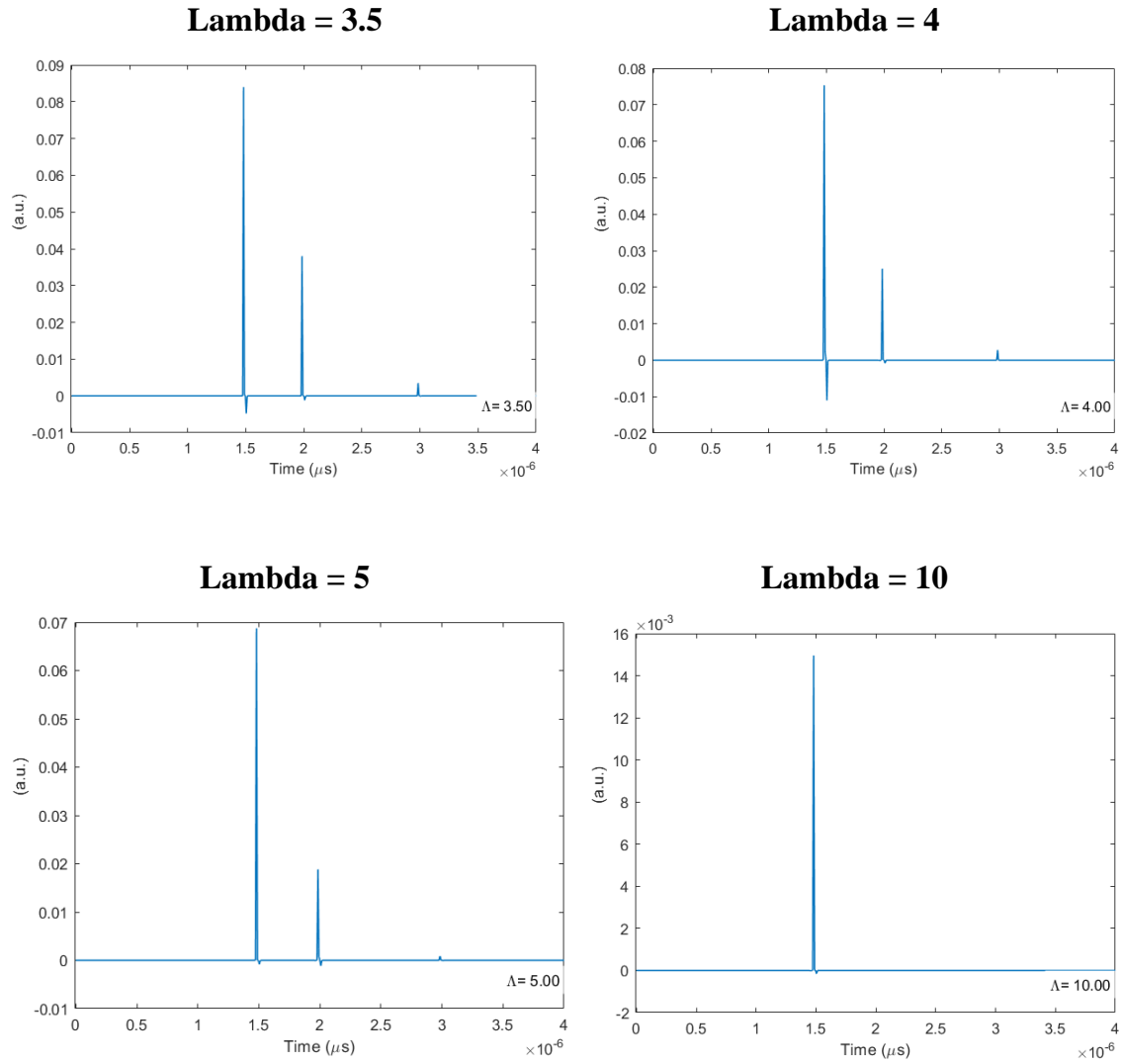
Figure 4.8 Results represent signals consisted of a function of different values as a function of the regularization parameter lambda.

The application-specific balance level of acceptable distortion versus attenuation has to be selected. Based on the results presented in Figure 4.8 the dependence on the regularization parameter can be concluded based on the initial signal (input) and several outputs. It can be seen that the recovery of the 3rd reflection (lowest amplitude reflection) was possible up to certain values of regularization. At λ=3 and above the amplitude decreased by more than 50 % based on the initial estimations with λ=1 and 2.

4.3.3. Results in Terms of Cost Function

The time-based algorithm performance was tested to investigate the time needed for the cost function minimization. The results presented in Figure 4.9 showed that a significant improvement can be achieved just after several iterations of the algorithm. The time required for the algorithm to reach a minimum was approximately 20 ms and could be further optimized by the measurement protocol adjustments so that the final time-of-flight calculation is performed with higher accuracy. In the top of Figure 4.9 is the example signal that represents the convolution of the PSF and added noise. This signal is considered the starting point of the following diagrams presenting deconvolution results as a function of the algorithm iterations. The red-dotted lines represent the initial position of the reflectors prior to the convolution. The right-hand column shows the cost function, it can be seen that the algorithm reaches the minimum just after a few iterations so the iteration number can be limited and optimized for the application. It could be also observed that the detection of local maximums was possible after only the second algorithm iteration (Figure 4.9).

Initial Signal:
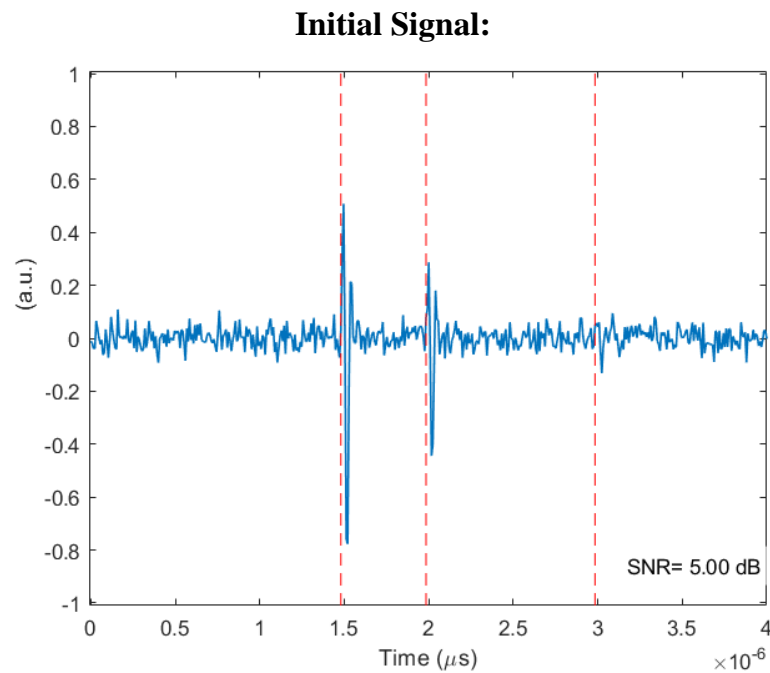
Execution Time = 0.009072 s, N=2
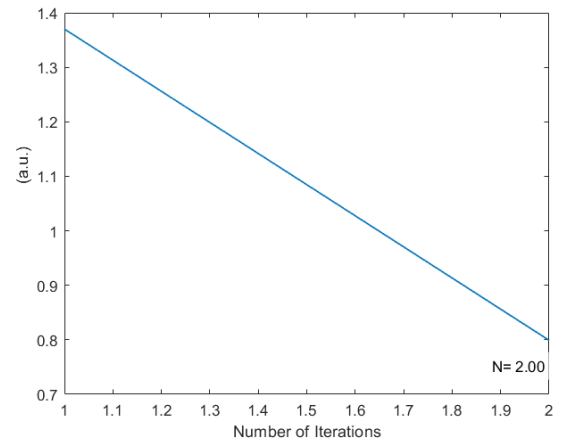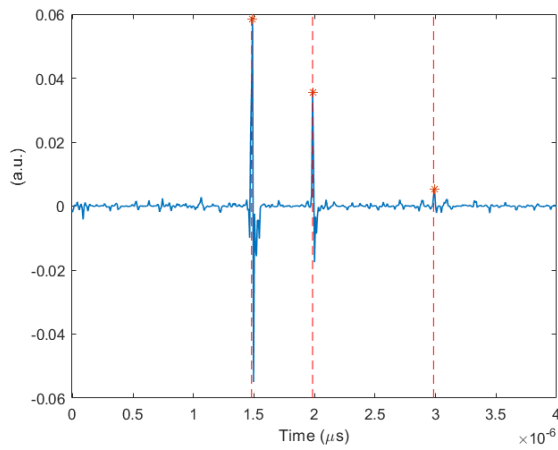
Execution Time = 0.012078 s, N=4
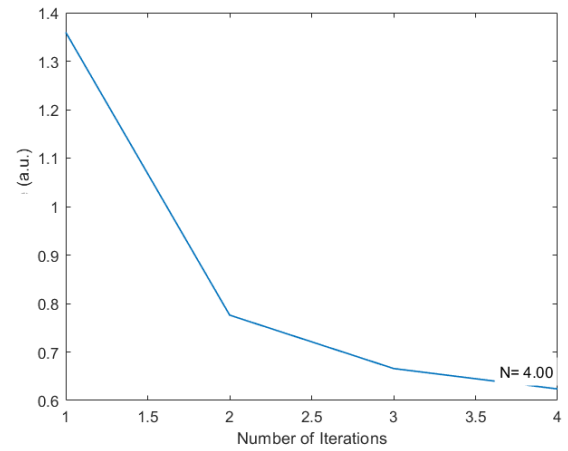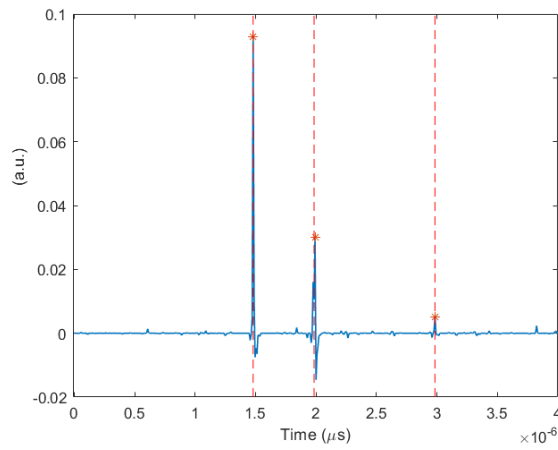
Execution Time = 0.019419 s, N=8

Execution Time = 0.021759 s, N=15

Execution Time = 0.045612 s, N=30
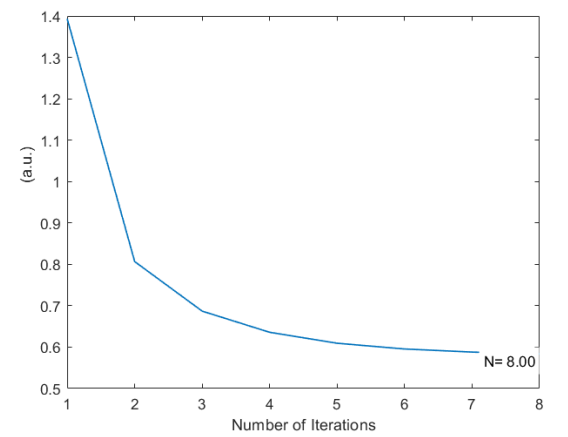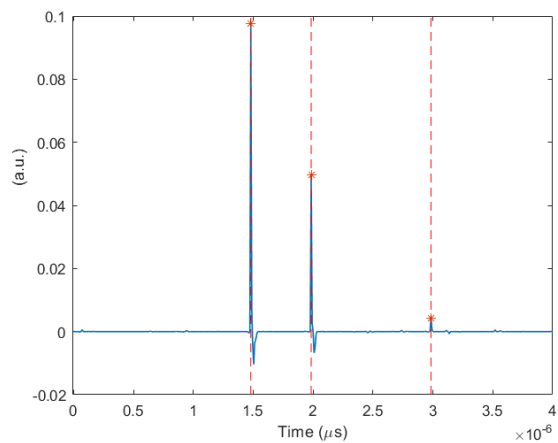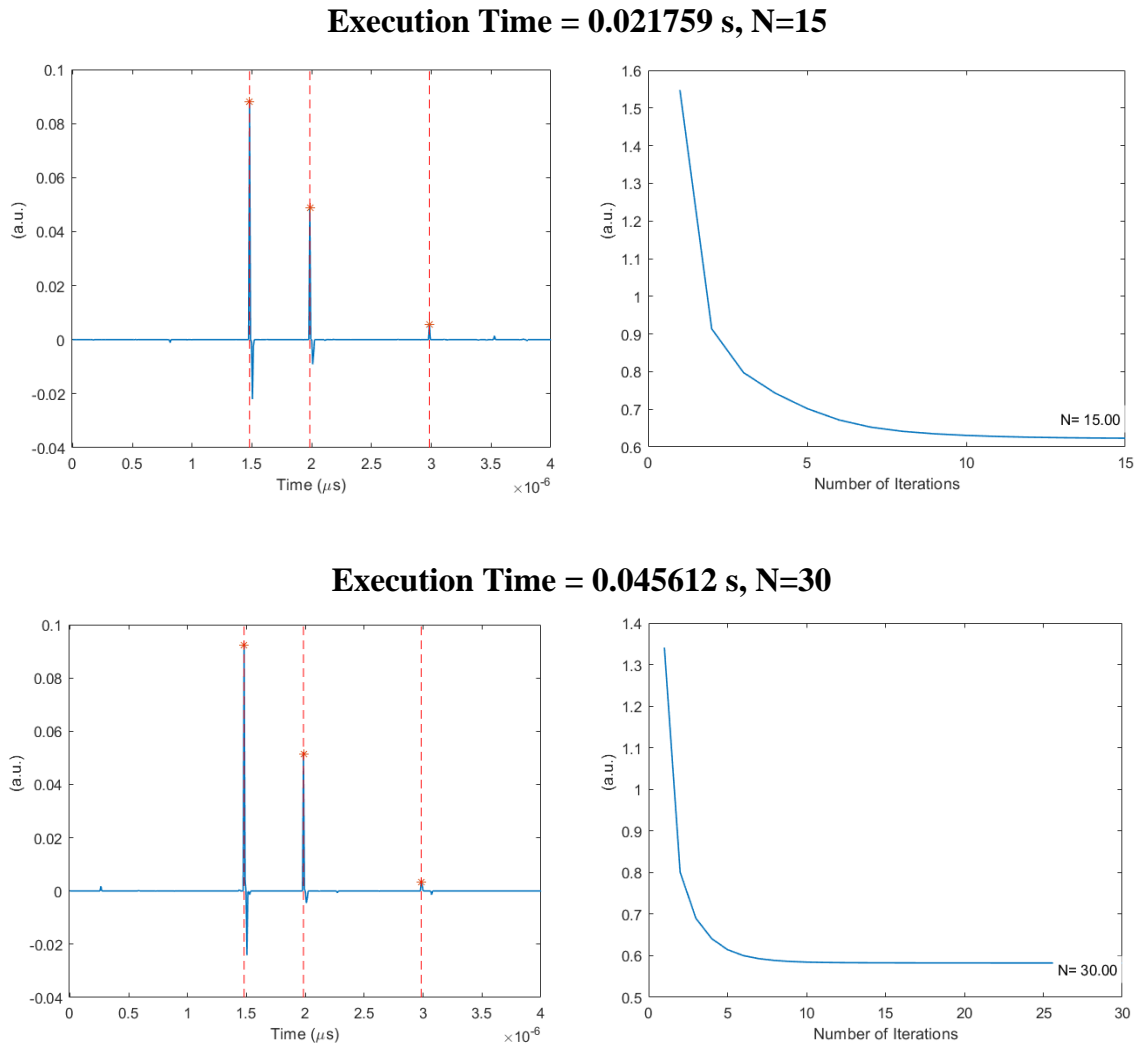
Figure 4.9 The diagrams present an impact of the number of iterations on signal maximums detectability for the time of flight extraction.
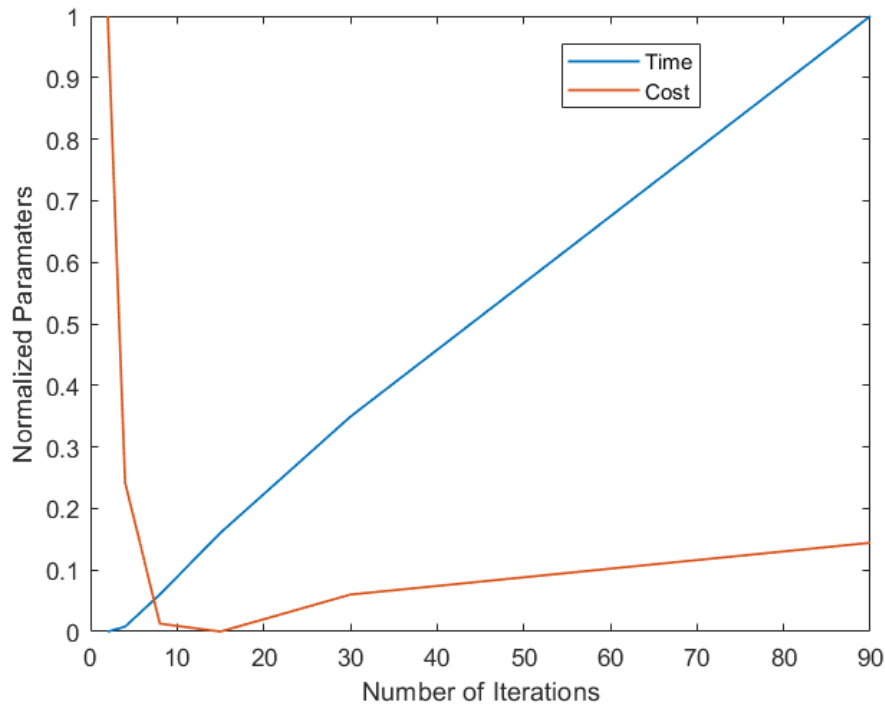
Figure 4.10 The diagram presents the normalized cost function and transient time versus the number of algorithm iterations.

Lastly, Figure 4.10 is a summary of the previous discussion showing the relation between the iterations of the algorithm and time. It can be observed from the figure that the overfitting effect can be minimized by proper control of the algorithm repetitions.

4.3.4. Time of Flight Calculation Results

The final test includes the time of flight calculations. The following Figure 4.11 presents an example of algorithm capabilities to enhance the signal and the time of flight estimation. The red dotted vertical lines in Figure 4.11 show the locations of the signals used for the reflector simulation before convolution with the PSF. In B it could be observed that the peak detection algorithm could not determine the location of the third reflection when in C with applying deconvolution scheme the echo can be identified. Diagram D presents a zoom-in view at the third peak where the star indicates a deconvolution peak detection result. The initial timestamp perfectly aligns with the

deconvolution time of flight results confirming accurate reconstruction of the initial time of flight.
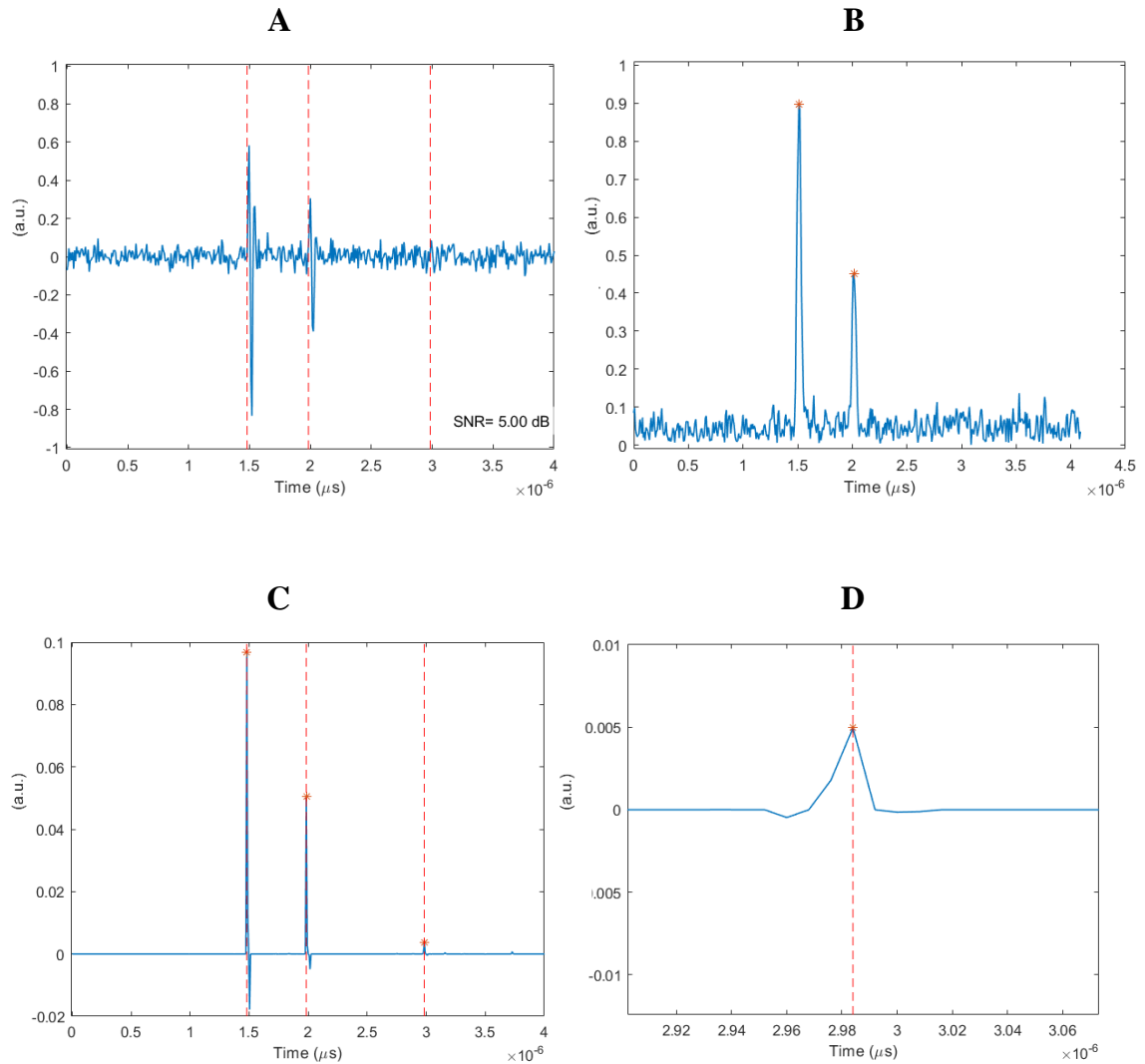
Figure 4.11 The Diagrams present 2 cases: the first raw is the signal and peak detection without the ability to detect the peak in the signal after applying the proposed deconvolution algorithm

4.4. Conclusion and Summary

A set of conditions on the regularization parameter, cost function behavior, PSF estimation latency and time were tested. The results show that the system with the proposed algorithm can behave in a reactive computing sense which describes software

real-time constraint. According to the literature [56], similar applications' latency is in the range of 6-20 ms and that is considered as a real-time operation. The current algorithm computation time is above the upper limit of the range. Nevertheless, it can be improved by migration from the script-based implementation to a compilable code (either host-based or embedded).

The results presented in this chapter confirm that the algorithm has the potential to improve signals and yet operates in real-time. Further testing on animal-sourced samples was performed so the system has the necessary efficacy documentation and gained the potential to be clinically utilized. The initial parameters were selected based on the synthetic data and further used in the system testing presented in the next chapter.

CHAPTER 5.

VALIDATION STUDIES OF THE ALGORITHM BASED ON

ANIMAL MODELS

The system described in the previous chapters was assembled and tested for safety (Appendix 1) for the purpose of further evaluation in the clinical setting.

The purpose of the study was to demonstrate the system and algorithm performance within a controlled clinical environment where the study was conducted on animal models. Chapter 4 presented the methodology of selecting algorithm constants using controlled synthetic signals such that the system clinical performance could be effectively conducted. Although at this stage the device was evaluated on biological samples only, all necessary steps have been taken to confirm device safety and efficacy prior to the initial pilot trial to provide data for further ethical approvals. In general, clinical performance indicators are metrics used to determine the clinical efficacy and studies conducted. The major challenge in determining the diagnostic accuracy and precision was to establish the ground truth (a gold standard measurement method) diagnosis for the animal models. An alternative imaging technology known as Optical Coherent Tomography (OCT) has been used to obtain true values in the semi-invasive approach described in detail in this chapter. Finally, the currently known assessment method known as trans-gingival probing was used to validate the ultrasound-based assessment.

5.1. Introduction - Anatomy of Dental Structures

The attached gingiva represents the keratinized oral mucosa which surrounds teeth and is tightly bound to the underlying alveolar process. Its main functions are to withstand the frictional forces of mastication and to maintain a seal around erupted teeth to prevent an invasion of bacteria [57].
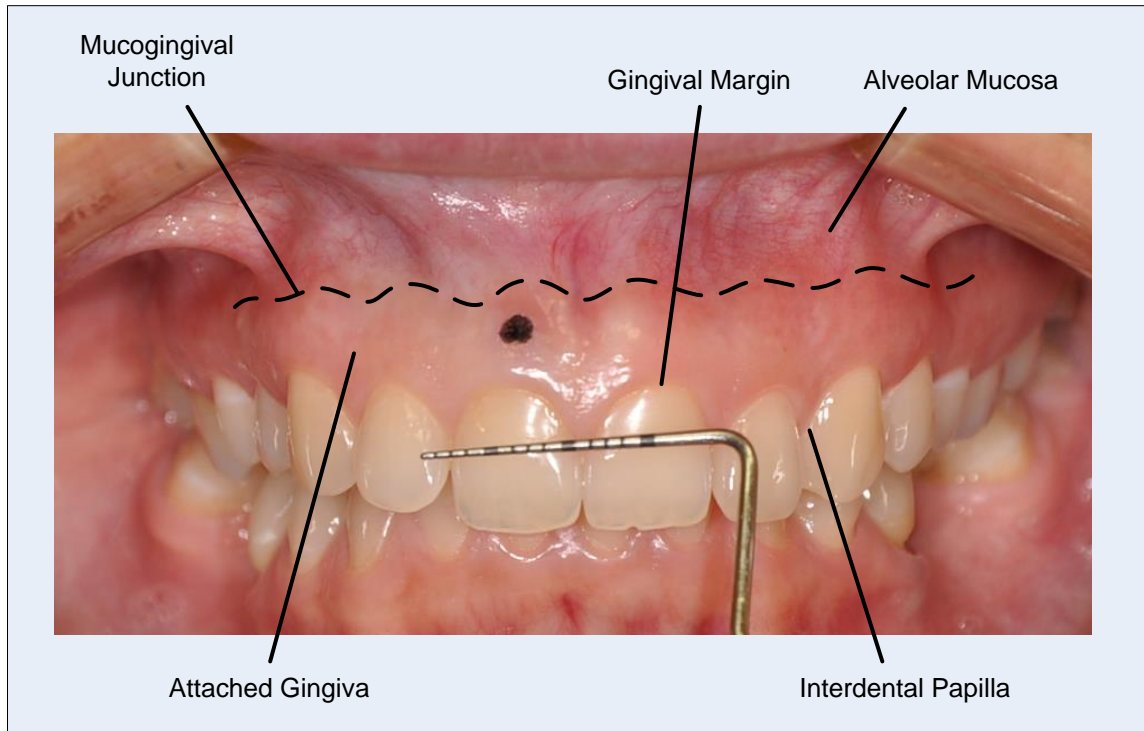
Figure 5.1 The picture presents a view of human periodontium with a reference scale of the division of 1 mm.

The thickness of healthy gingival tissues can vary, not only between individuals but also within the same oral cavity depending on the site. Intra-oral differences in gingival thickness (GT) have been shown between the upper and lower jaws and tooth type [58].
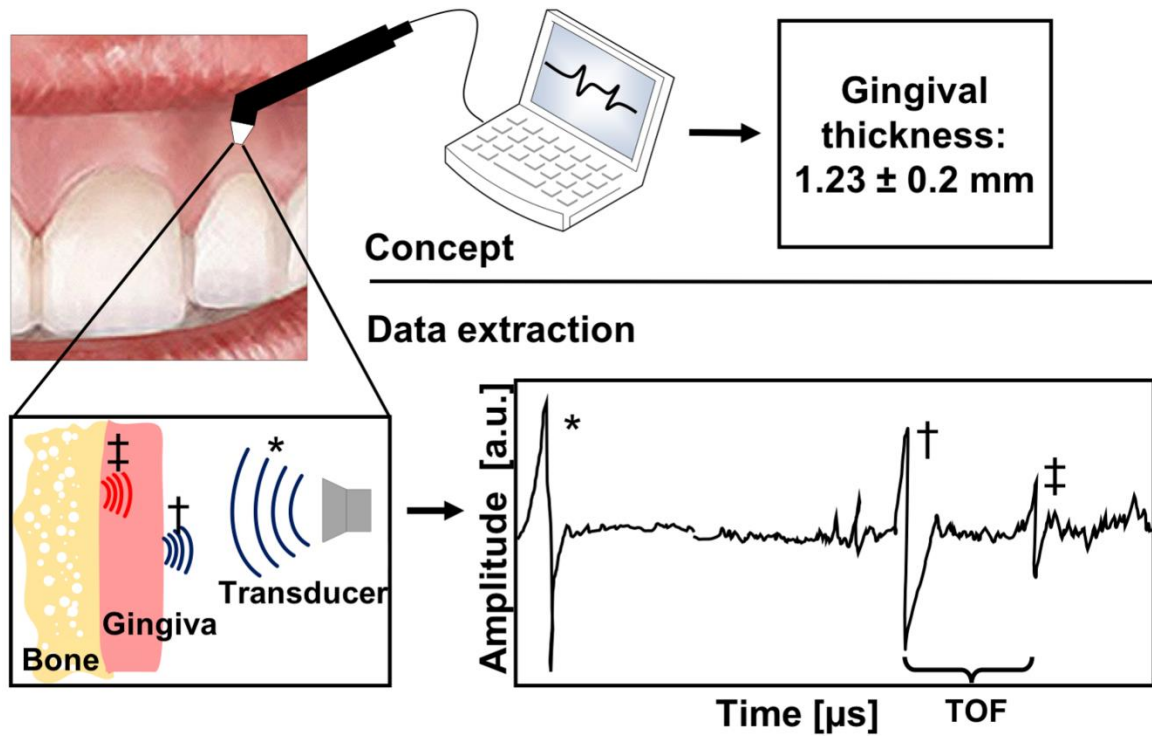
Figure 5.2 Concept diagram of the proposed ultrasonic device operation. * Ultrasound signal, † Reflection from first tissue interface, ‡ Reflection from second tissue interface, TOF – time-of-flight.

Gingival thickness is one of the important factors that determine how this tissue responds to disease or trauma and can have a significant clinical impact on treatment outcomes. For example, thinner tissues are at an increased risk of recession following orthodontics [59], periodontal treatment [60]; [61]), and implant placement [62]compared to thicker tissues. Furthermore, following procedures designed to correct gingival recession defects, thinner tissues have a lower chance of achieving full root coverage compared to thicker tissues [63]. Therefore, accurate assessment of GT is an important part of the treatment planning process. Conventional clinical methods of assessing GT include visual assessment, probe transparency, and trans-gingival probing.
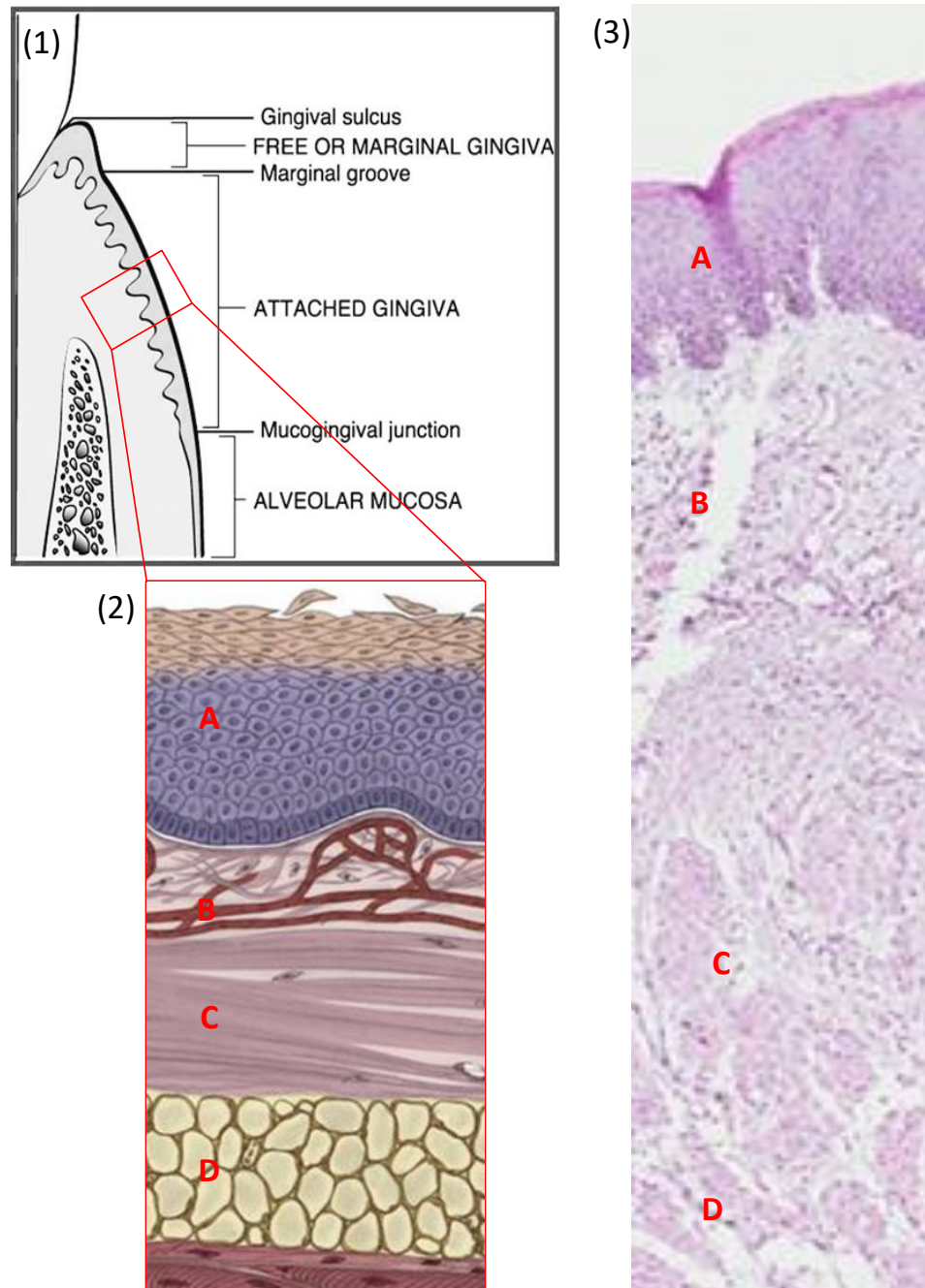
Figure 5.3 The diagram (1) presents a cross-sectional view of the human periodontium with (2) detailed view on the soft tissue structure highlighting.

Visual assessment alone aims to categorize patients into two groups, those with a thin or thick biotype [64]. However, this is not a reliable method for assessment of

GT as misclassification of biotype can occur in approximately 50% of cases irrespective of clinician experience [65].

Probe transparency involves the placement of a periodontal probe into the buccal sulcus and categorization of GT as either thick or thin depending on whether the probe is visible through the gingival tissues [66]. However, there is no specific threshold thickness of GT which could differentiate between sites where the probe was or wasn't visible [67].

Transgingival probing involves the use of a periodontal probe [58] or an endodontic hand-file with a silicone stopper [68] to pierce the gingiva perpendicularly to the tissue surface until resistance is met by the underlying hard tissues. The distance between the instrument tip and silicone stopper can then be gauged with calipers to obtain a direct measurement of tissue thickness. In clinical practice this is the only objective measure of GT, however, it is an invasive technique that can cause considerable discomfort to the patient, usually requiring the provision of local anesthesia before being performed [69]. More recently, ultrasound has been investigated as a safe, non-invasive diagnostic tool to assess gingival thickness [70], with the potential benefits of greater accuracy, and fast data collection [71]. This method involves the placement of an ultrasonic probe on the gingival surface at the site of interest which is able to emit and receive ultrasonic acoustic waves, generally with the help of a coupling agent. By measuring the time difference between the acoustic signals reflected back from different tissue interfaces, i.e. the gingival surface and the underlying hard tissues, GT can be calculated within seconds and to a resolution of 0.1 mm. The majority of ultrasound devices previously tested for GT measurement in the research were originally designed for applications other than intra-oral use. This, in turn, could affect the precision of obtained measurements, for example by using probes with a large diameter (up to 4mm), or with limited access to more posterior sites. Therefore, despite the potential benefits, ultrasound imaging has not been widely adopted as a diagnostic tool in dental clinical practice.

Optical coherence tomography (OCT) is a non-invasive imaging modality capable of producing high resolution cross-sectional and 3-dimensional images of biologic tissues [72]. With a concept similar to ultrasound, OCT instead uses a low coherent light source scanned over the tissue of interest and data from backscattered light is used to recreate images. There is no known detrimental effect on biologic tissues and it is gaining more interest in dentistry due to its ability to capture high-resolution, cross-sectional images in real-time [73]. However, the current technology is limited by penetration depth which can only reach approximately a maximum of 2 mm [74]. Furthermore, due to laser beam tissue attenuation, the image quality for soft tissues drops significantly at depths approaching the 2 mm mark.

In summary, accurate assessment of GT should form part of a complete oral assessment both for diagnostic and therapeutic purposes. However, current clinical practices are mostly based on subjective judgment by the clinician or require invasive techniques that are unpleasant for the patient. Non-invasive imaging techniques have the potential to overcome these problems, however, they have not yet been incorporated into clinical practice due to either limitation in the technology or lack of convenience. Therefore, the aim of this experimental study was to conduct an accuracy assessment of GT measurement with a novel, high-frequency, low-cost ultrasonic device, designed specifically for the dental purpose, in the hopes that this device will provide a viable and clinically acceptable solution to non-invasive, objective GT assessment.

5.2. Material and Methods

5.2.1. Experimental Model

Three fresh porcine mandibles sectioned into quadrants were used as the experimental model. The animals were slaughtered for consumption purposes and all experimental specimens were dispose according to the hospital standards. Each jaw quadrant was numbered, and gingival surfaces were exposed for better accessibility.

Eight measurement sites were allocated per quadrant (four buccal and four lingual), resulting in a total of forty-eight measurement sites. For each site, reference points were created by bonding composite resin material on the corresponding teeth at the level of the free gingival margin. This was carried out in a two-stage technique with a self-etching bonding agent, and flowable composite cured with a 470 nm wavelength light for 20 seconds. Transgingival bone sounding was then carried out at each reference point with a periodontal probe (UNC-15) to detect the level of the bone crest. The measurement sites were then marked on the gingival surface with indelible ink (0.5mm tip diameter) 1mm apical to the identified bone crest.

5.2.2. Transgingival Probing

GT was then assessed by using size 25 endodontic k-files with silicone stoppers (Sybron Endo, Glendora, CA, USA). At each measurement site, the k-file tip with a silicone stopper was placed perpendicularly to the gingival surface. The k-file was then advanced through the soft tissue until the file tip made firm contact with the underlying bone, leaving the silicone stopper at the gingival surface (Figure 5.5c). The file was then transferred and fixed to a metal reference block (Albuquerque Industrial, Forest Hills, NY, USA) of known width (1.52 mm) and a photograph taken at a set distance perpendicular to the file and reference block. The distance from the file tip to silicone stopper was measured digitally with image processing software (ImageJ, National Institutes of Health, Maryland, USA), using the metal reference block to calibrate the dimensions of the image (Figure 5.5d). The digital measurement of each file was repeated 10 times, saving the mean and standard deviation for each measurement site.

5.2.3. Optical Coherence Tomography

The swept-source OCT unit (Vivosight, Michelson Diagnostics, Kent, UK) produces a low coherent light (~1305 nm) which enters the Michelson interferometer,

Figure 5.4c [75]. One beam is directed to a movable reference mirror arm and the other to a sample arm. Both the back-reflected reference beam and the back-scattered beam from the sample arm are interfered with and captured by a photodetector. The interference signal is detected if the length of the back-reflected light is in the range of the coherence length of the main source [76]. Due to the known reference mirror position, the depth into the sample structure can be determined (depth resolution). The system has 7.5 μm of optical resolution laterally and 5 μm optical resolution axially and it can scan an area of up to 6 mm (width) by 6 mm (length) with up to 2.0 mm of penetration depth.
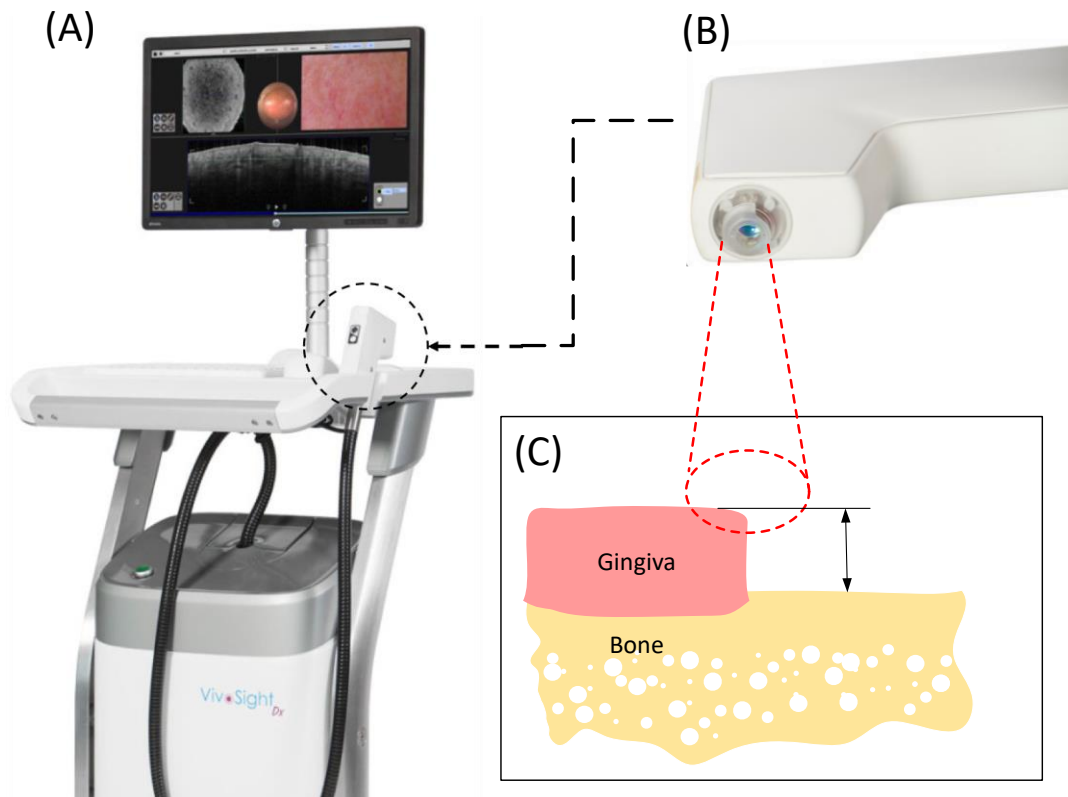
Figure 5.4 The diagram represents the OCT unit (A), the OCT probe (B) as well as the experimental measurement setup (C). The setup represents an illustration of the raised flap so that the accurate gingival thickness measurement representing true values was obtained based on the light reflation from both the gingival surface and the surface of bone [77]**.**

Upon completion of the ultrasonic and trans-gingival probing measurements, full-thickness mucoperiosteal flaps were raised with vertical incisions passing through the measurement sites (Figure 5.6e). OCT images were taken at each measurement site ensuring the probe was placed over the incision lines. In this way, GT could be assessed by measuring the distance between the gingival surface and exposed bone on the cross-sectional OCT images (Figure 5.6f). Measurements were repeated 10 times per image with ImageJ (National Institutes of Health, USA), saving the mean and standard deviation for each measurement site. It was assumed that this assessment represented the true GT value.
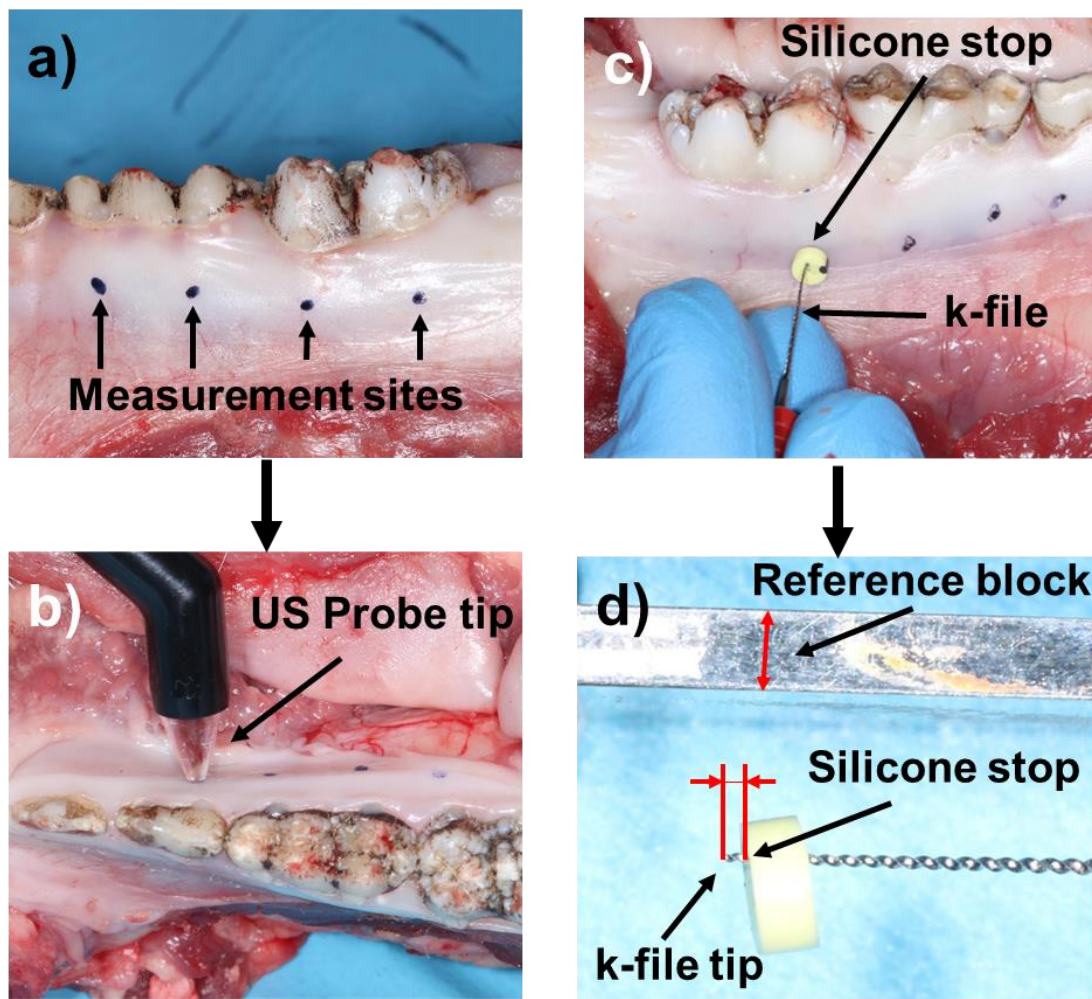
Figure 5.5 Methods used in the experiment: a) Marking of measurement sites on gingival tissue, b) Ultrasound (US) measurement at marked sites, c, d) TGP at marked sites with k-files and measurement using reference block.
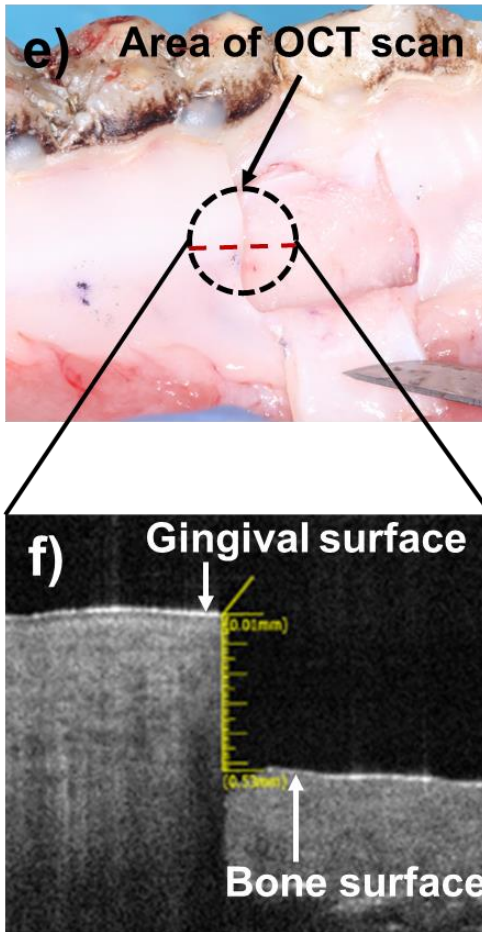
Figure 5.6 Methods used in the experiment: e) Elevation of full-thickness gingival flap through marked sites, f) OCT scan with measurement.

5.2.4. Statistical Analysis

A repeated measure analysis of variance (ANOVA) was conducted using SPSS software (IBM Corp., USA) to test for differences in GT measurements carried out by the three methods used, i.e. ultrasound, trans-gingival probing and OCT. Repeatability and reproducibility of the ultrasound device was assessed by calculation of Lin's concordance correlation coefficient (LCC) and displayed graphically on Bland-Altman plots with Stata®14 software (StataCorp LLC, USA). The Intraclass Correlation Coefficient (ICC) was calculated with Stata (StataCorp LLC, USA) to assess the agreement of ultrasound measurements between the two examiners.

5.3. Study Results

5.3.1. Mean Values Obtained by Each Method

The mean and standard deviation in terms of GT across all measurement points for ultrasound, OCT, and trans-gingival probing (TGP) was calculated (Figure 5.7). Obtained results were assessed graphically for normality. The Mauchly's test indicated that the assumption of sphericity had been violated, $\chi^2(2) = 28.242$, $p = 0.00$ so for that reason repeated measures ANOVA with a Greenhouse-Geisser correction was used. There was a statistically significant difference in mean GT observed by different measurement methods ($F(1.371, 64.437) = 17.414$, $P < 0.01$). The post hoc test using the Bonferroni correction revealed that mean ultrasound results compared to those obtained with OCT were not statistically significant ($p = 0.89$). However, statistically significant differences were found when comparing both OCT and ultrasound measurements to TGP measurements $p<0.02$ and $p<0.01$, respectively (Figure 5.7).
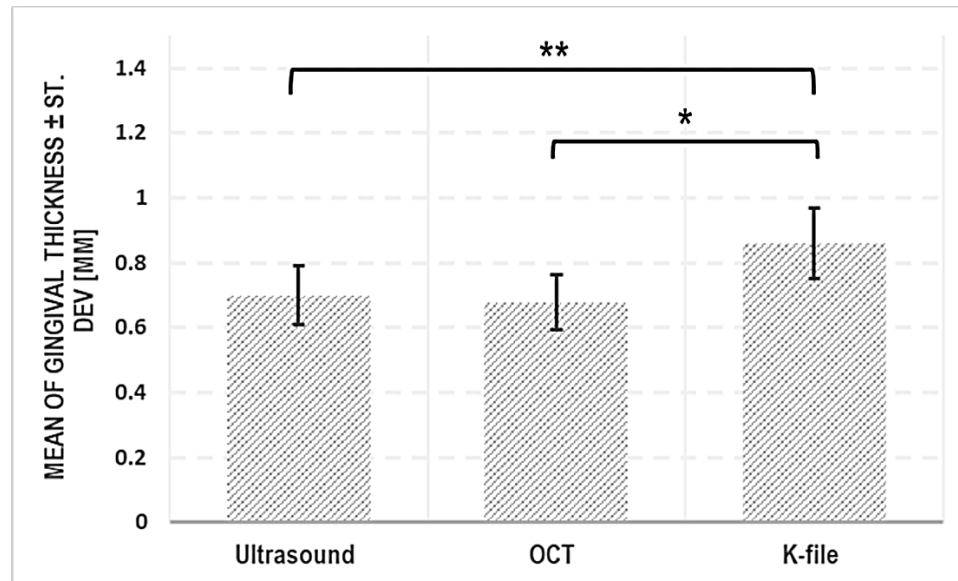
Figure 5.7 Bar chart displaying mean (±SD) GT values measured by US, OCT and k-file (TGP), *p<0.02, **p<0.01.

5.3.2. Repeatability and Reproducibility

The repeatability of ultrasound measurements assessed by LCC was 0.625 (95%CI0.539-0.710), whilst the reproducibility between two examiners was 0.591 (95%CI0.499-0.683). The ICC between two examiners was 0.6 representing substantial agreement [78]. The agreements between repeated ultrasound measurements and between examiners are displayed graphically in Bland-Altman plots (Figure 5.8).
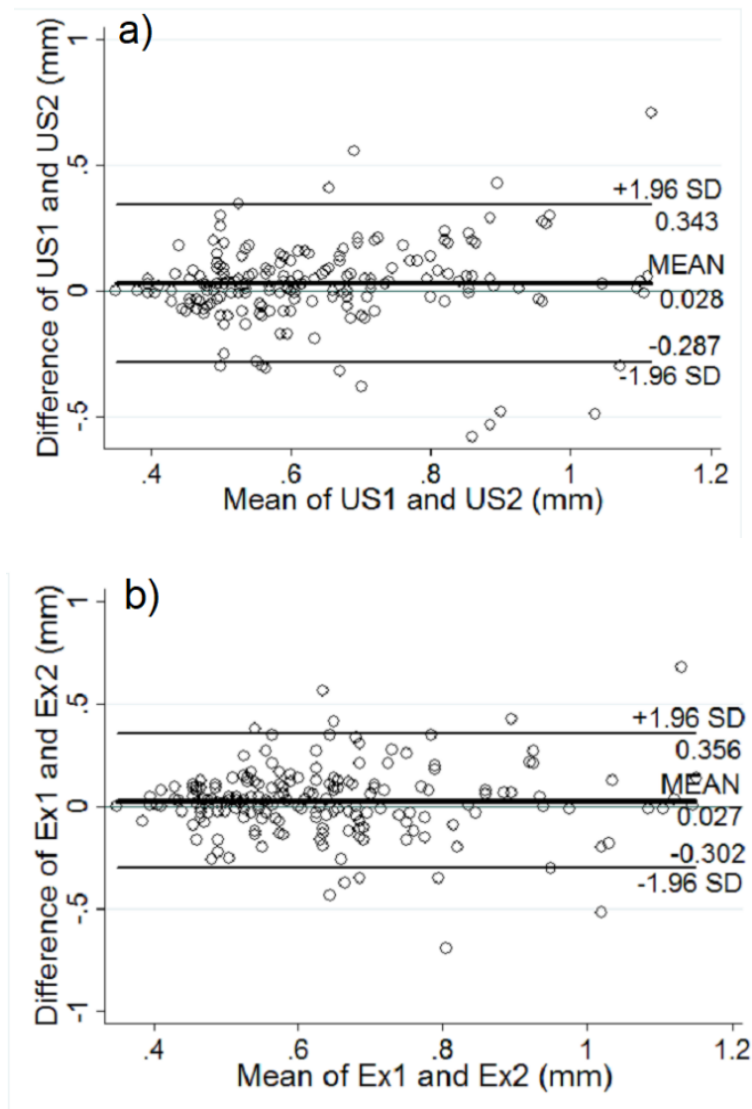
Figure 5.8 Bland Altman plots showing the difference between GT values assessed by ultrasound plotted against the mean of the pair assessed by; a) two consecutive measurements (US1 and US2), b) two examiners (Ex1 and Ex2).

Ultrasound versus OCT

The agreement between measurement methods was found to be the highest for ultrasound versus OCT with an LCC value of 0.594 (95% CI0.426-0.763). Trueness using Bland-Altman plots was investigated where ultrasonic measurements were compared with the results obtained based on OCT analysis and the agreement between paired readings was moderate (Figure 5.9a). Overall, the plot presents random distribution and minimal bias between true values and ultrasound results.

TGP versus OCT

LCC coefficient was 0.230 (95%CI0.046-0.415) for TGP versus OCT indicating fair agreement between these two methods. A Bland-Altman plot displaying the agreement between methods is shown in Figure 5.9b.

Ultrasound versus TGP

LCC coefficient for ultrasound versus TGP was 0.008 (95%CI-0.128-0.145) indicating poor agreement between these two methods. It should also be noted that the mean difference, in this case, was equal to -0.226 and it departed from zero significantly based on the estimated confidence interval (Figure 5.9c).
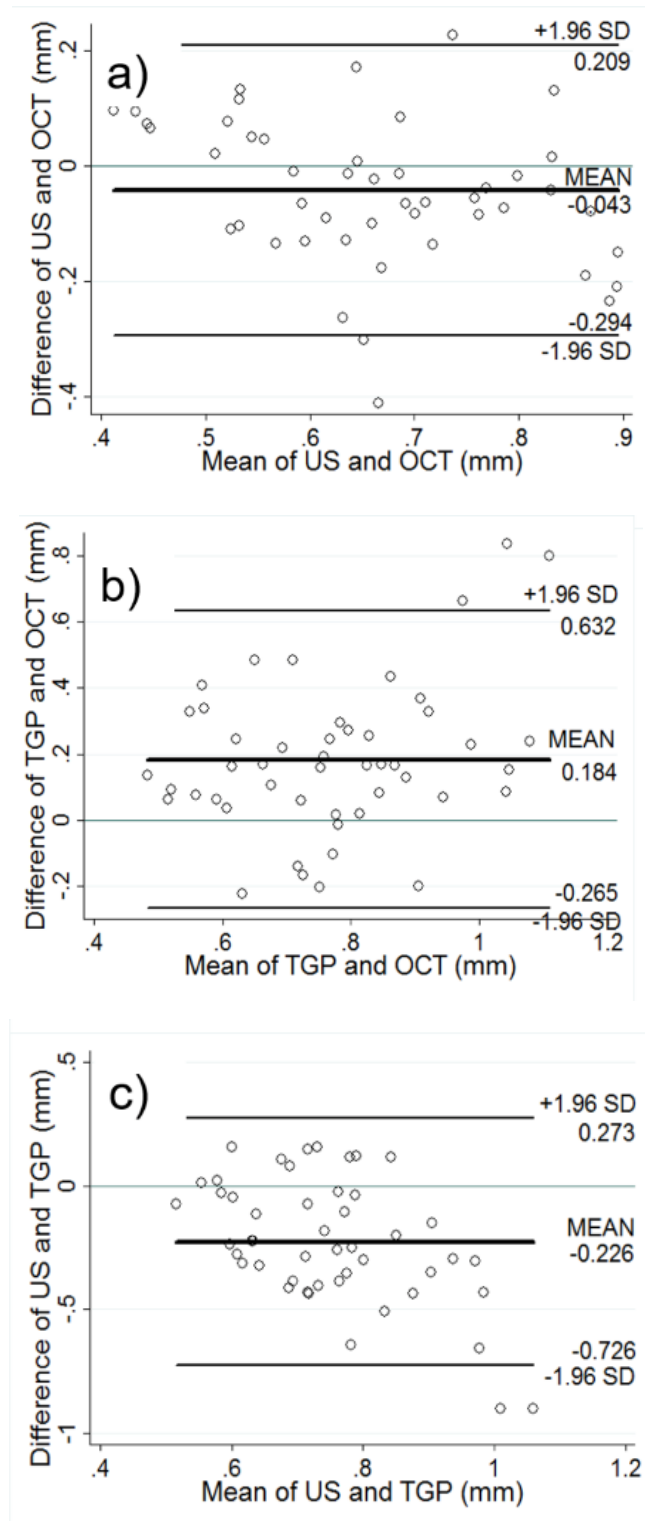
Figure 5.9 Bland Altman plots showing the difference between GT values plotted against the mean of the pair, assessed by; a) US and OCT, b) TGP and OCT. c) US and TGP.

5.3.3. Pilot Study Summary

This study demonstrated the ability of a novel dental ultrasound device to assess GT non-invasively. The mean value for GT measured by ultrasound closely resembled the mean value obtained by direct measurement with OCT, which may be considered the true value. The difference in mean GT measurements using ultrasound and OCT was 0.02 mm (p=0.89). In contrast, the difference in mean GT values between OCT and TGP, which is a commonly used invasive technique, was 0.18 mm (p<0.02). Furthermore, when assessing the correlation between the three measurement methods, the agreement between ultrasound and OCT was satisfactory (LCC 0.594) and greater than the agreement found between TGP and OCT (LCC 0.230), with a tendency found for TGP to overestimate measurements compared to GT true values. Taken together these findings indicate that within this study, ultrasound was a more accurate method of GT assessment than TGP.

The repeatability and reproducibility of ultrasound measurements were evaluated by assessing the agreement between paired readings and the agreement between two examiners. The correlation coefficients of 0.625 and 0.591 respectively indicate substantial levels of repeatability and moderate reproducibility [78]. The possible reasons for not obtaining higher levels of agreement for repeatability and reproducibility are suspected to be related to several factors including errors related to the repositioning of the probe, angulation of the probe, compression of the soft tissues during probe placement, and anatomical factors such as bone topography and proximity to the bone crest where the reflected ultrasound signals could have been received from the tooth surface instead of the underlying bone. For that reason, it is important for the system to be perfectly suitable for its application. The ultrasound device used in the present study was specifically designed to match parameters with tissue characteristics, topography, dental geometry, and accessibility. The main benefits of the probe design are the narrow probe tip diameter (1.5 mm), contra-angled handle, and ability to use water as a transduction medium which would enhance its clinical utility for intra-oral applications (Figure 5.10).

Other imaging techniques such as OCT will have an increasing role to play in dentistry and periodontology as they are non-invasive and can be used without detrimental effects on the patient [72]. However, the current technology is limited by penetration depth, especially in soft tissues [74]. In the present study, the limitation related to the laser beam tissue attenuation was overcome by exposing the bone surface. This allowed direct and precise measurements to be taken to a resolution of 0.01 mm to obtain the true GT value as a benchmark for comparison against ultrasound and TGP.

When ultrasound results were compared with TGP there was no agreement between methods with a tendency for TGP to exceed ultrasound measurements. This could have been due to bone penetration by the k-file and errors included in the value reading procedure. Consequently, LCC indices showed no correlation when TGP results were compared to ultrasound (LCC 0.008). These findings agree with previous studies comparing GT measured by ultrasound and TGP, which demonstrate that the latter overestimates GT compared to ultrasound. Bednarz et al. found the difference in mean GT measurements between ultrasound and TGP with endodontic k-files to be 0.044 mm. This was found to be statistically significant and furthermore in that study ultrasound was found to be more accurate when measuring thinner tissues [69]. It was also found that the mean difference between the two methods at mid-buccal and interdental papilla sites was 0.22 mm and 0.49 mm, respectively [58]. These were found to be statistically significant and the authors concluded that ultrasound assessment was more accurate, quick and atraumatic. In contrast, recently found ultrasound exceeded measurements compared to TGP with a periodontal probe at lower incisors in the range of 0.11-0.16 mm [79]. However, as mentioned in their conclusions it was not possible to comment on the accuracy of the different methods as they were uncertain of the GT true value. Another limitation they mentioned was related to the ultrasound device used in their study which, in addition to having a wide probe diameter of 3mm, had a resolution of 0.1 mm which was lower than the digital caliper they used for TGP measurements.
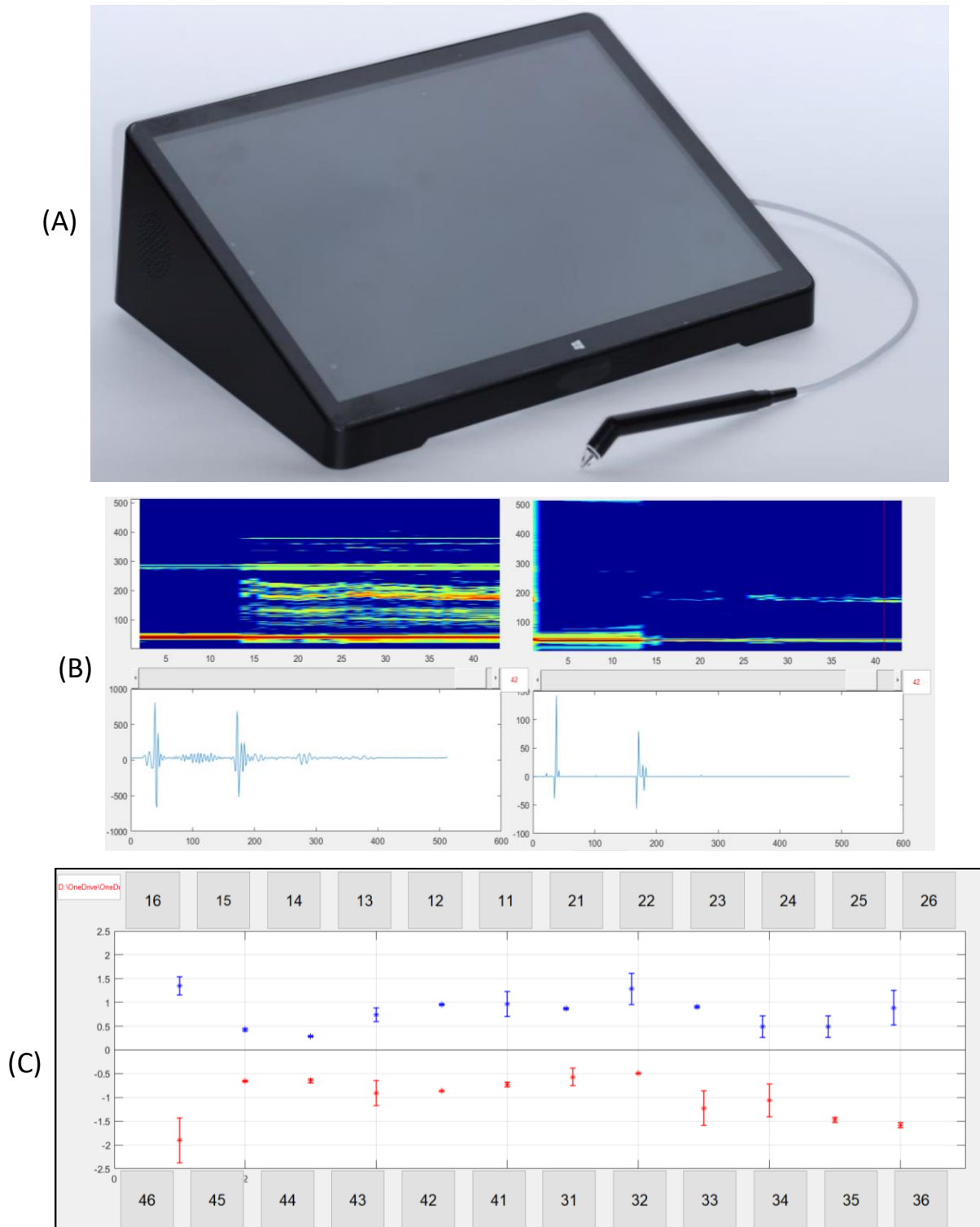
Figure 5.10 (A) The clinical version of the device developed for clinical testing. (B) Represents the research view in the software package, the left side presents the results before and right after performing the signal enhancement with the deconvolution algorithm described in Chapter 3. (C) Presents database window where measurement results are presented with error estimations.

More commonly used techniques to discern thick or thin gingival biotypes include subjective assessment such as visual assessment and probe transparency. However, visual inspection alone is not a reliable method for assessment of GT as misclassification of biotype can occur in approximately 50% of cases irrespective of clinician experience [66]. With regards to probe transparency, visibility of the probe is usually associated with thinner measurements of GT, however, there is no specific threshold thickness of GT which could differentiate between sites where the probe was or wasn't visible (Frost et al., 2015). Alternative methods for assessing GT have included plain radiographic assessment of the soft tissues [80] and cone-beam computed tomography [81]. However, the use of these techniques in routine clinical practice for assessment of GT cannot be justified due to the potentially harmful exposure to ionizing radiation. Therefore, the potential benefits of ultrasound are clear given the non-invasive, safe, fast and accurate results that can be produced. Furthermore, the potential indications for ultrasound are not limited to the gingival tissues but could also be applied to peri-implant tissues for soft and hard tissue assessment during different phases of treatment [82].

The ability to estimate the thickness of the gingival tissue being measured ultimately relies on converting the signal arrival times into thickness. This conversion requires knowing the speed of sound of the tissue. The B-scan image in Figure 5.11 shows (A) TOF through water and (B) TOF through gingival tissue located on the microscope slides. Average TOF values through water and tissue were 1.32 µs and 1.25 µs, respectively. A schematic representation of the experimental setup shows how the sample was arranged in order to perform the measurement. Buccal gingival site gingiva was used. The average speed of sound in a single porcine gingival tissue sample was calculated to be 1564 ± 21 m/s. Although the goal of experimental assessments was to calculate the final gingival thickness, the focus of the conducted algorithmic enhancement lies in the timely TOF extraction. The speed of sound in the sample was obtained and used to calculate the gingival thickness.
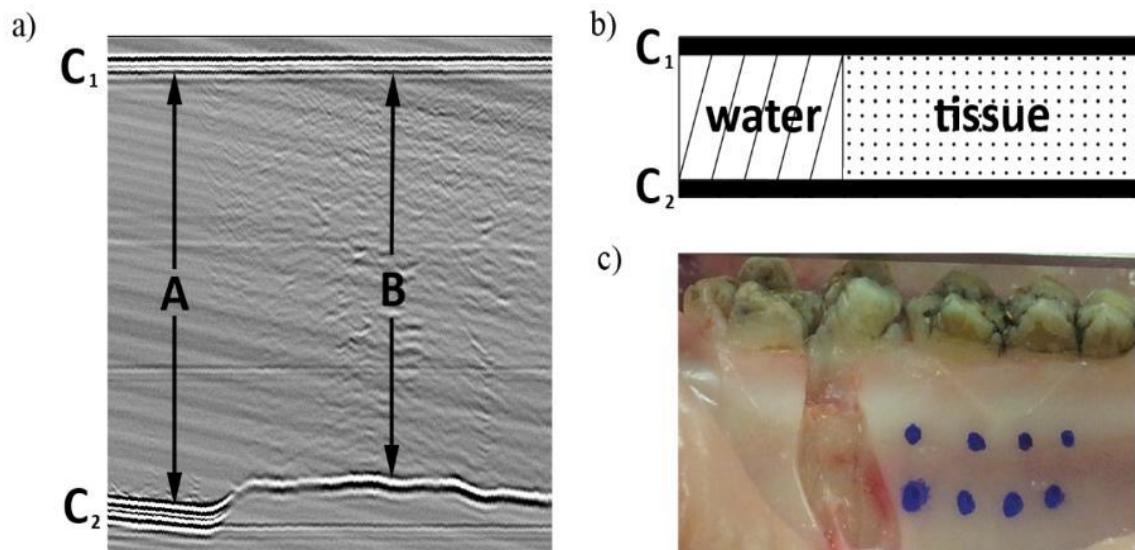
Figure 5.11 (a) The B-scan showing (A) TOF through water and (B) TOF through the gingival tissue, held in place between microscope slides (C1 and C2). Average TOF values through water and tissue were 1.32 μs and 1.25 μs, respectively (b) A schematic representation of the experimental setup (c) The site on the buccal gingival surface of the fourth quadrant from which tissue was excised.

This study helps to establish a new standard for gingival assessment were quick, non-invasive and efficient measurements are possible. All the clinical factors that can potentially contribute to the variability of results from a measurement method perspective were comprehensively studied and showed the ultrasound technology excellence. The system has a high potential for clinical usability due to the low-cost, automated data management and overall assessment rapidness while maintaining comparable and better accuracy.

The study described in the chapter has confirmed the clinical applicability of the proposed and developed system as well as it provided data to reassure the quality of measurements. Additionally, the system was tested in terms of practical usability in clinical settings, ergonomics and software simplicity.

CHAPTER 6.

EXTENDED STUDIES: DECONVOLOUTION ENHANCED

ULTRASOUND-BASED SYSTEMS

In this chapter additional directions of the high-frequency ultrasound technology that can benefit from the proposed algorithm have been described. Several developments and studies have been undertaken to verify the applicability and potential value behind targeted proof of concepts. Medical disciplines such as dentistry and dermatology have been further explored as directions where ultrasound with the proposed algorithm can provide improved diagnostic information and enable quantitative measurements.

In general, the need for ultrasound technology improvement and application-based exploratory studies are important and needed due to benefits such as non-invasiveness of the technique. The most popular diagnostic method thus far in dentistry is x-ray imaging which has been repeatedly described in the literature as the method that causes long-term carcinogenic effects. This chapter includes a collection of studies performed on proof-of-concept prototypes designed and developed to characterize and enable further project progression.

6.1. Alternative Project Developments and Directions

The hard and soft dental tissue assessment is necessary for improved predictability of outcomes in surgical procedures. For the following reason, further investigation of gum thickness in clinical pilot studies has been proposed. Additionally, a new direction of experimental studies related to alveolar crest assessments is suggested along with a new device prototype. Lastly, the concept of a new system for implant navigation using improved axial resolution based on the discussed algorithm has been proposed and patented.

6.1.1. Ultrasound Assessment of Gingival Tissue – Clinical Evaluation.

The following clinical pilot evaluation has been approved by the ethical boards at both involved institutions. The health and safety hospital regulations are followed throughout the studies. The ultrasound system described in the previous chapters was used according to a manual (Appendix 1 - Instruction for use: safety, disinfection and study use). The main advantages are that this system is painless (non-invasive), quick (each scan takes approximately 1-2 seconds to complete), user-friendly (simple operation for the user and an easy interface to quickly view or diagnose problems), and radiation-free (requires no harmful external radiation). The device consists of a probe with a built-in unique ultrasonic transducer and an enclosed unit for signal generation and acquisition. During the measurement, the practitioner gets the tip of the probe (1.5mm in diameter) in contact with the specific measurement location on gums (Figure 6.1). A drop of water will be used for ultrasonic wave coupling (in traditional ultrasound an ultrasonic gel is used). The system requires angular adjustments in order to receive measuring values in a timely manner. The prototype analyses the signal and informs the user by generating audio signals about an acceptable angular position, it conducts the calculations and stops the acquisition. Then, the system is ready for data to be saved and can proceed to the next measurement point.

Proposed pilot study protocol:

- ultrasound measurements of gingival thickness:

- patients' preparation according to the dental and hospital standards.

- device preparation according to instruction for use.

Measurement location:

- upper and lower teeth, from right to left first molar

- one measurement per tooth

- mid-buccal, tangent to the mucogingival junction, within the keratinized tissue.
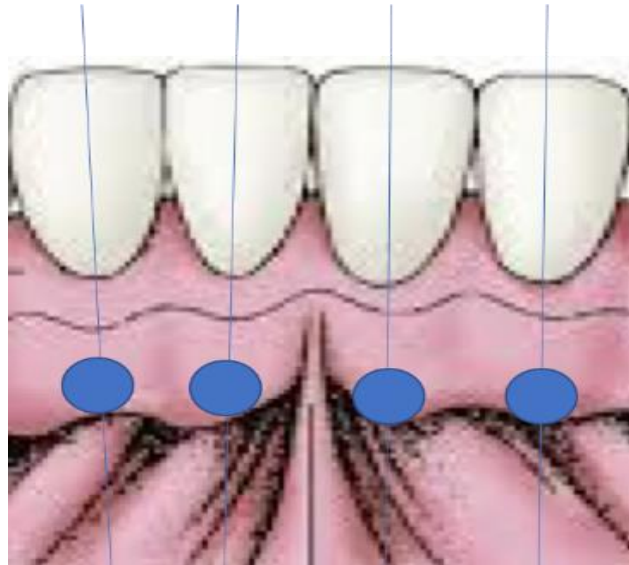
Figure 6.1 Ultrasound measurement locations (blue dots), located mid-buccal (blue lines) and tangent to MGJ within KT.

Following the clinical examination, clinician feedback on the use of the ultrasound device for gingival thickness measurements will be collected. These comments will be used for improvements to the device's design. The ultrasound gingival thickness measurements obtained from study participants will be compared against conventional visual examination and dental probing. This comparison will validate the use of the ultrasound device to objectively define clinical gingival thickness.

6.1.2.   Sparse Deconvolution Algorithm for Ultrasound Dental Calipers.

An important factor in determining dental implant success is the anchorage provided by the width of the alveolar bone ridge at the location of the implant site obtained during the pre-surgical assessment [83]. Ridge mapping is a measurement procedure to ensure that the diameter of an endosseous screw implant does not exceed the dimensions of available bone. The major problem is estimating the thickness of bone since the mucosal contour can mask the actual dimension of the alveolar ridge. Bone evaluation limited to the use of panoramic and or periapical radiographs is insufficient, as it provides only two-dimensional information (mesial-distal view). Other invasive techniques for measuring alveolar bone ridge width have been developed and used [84], [85], [86], [87]. Coned-Beam Computed Tomography (CBCT) and ridge mapping (k-file and Wilson caliper) methods are used for the alveolar bone assessment allowing practitioners to extract information on the bone width. However, although CBCT scans are inherently regarded as an accurate way of measurement, there have not been many published studies confirming this [88]. In ridge mapping, the area of tissue being measured is generally anesthetized. In the k-file method, the silicone stopper is initially fitted at the end of the needle and is pushed back as the needle gradually penetrates into periodontal soft tissue. When the needle is removed, the displacement of the stopper provides an estimate of the gum thickness and using an impression model, the bone width can be calculated. The same concept applies when utilizing a Wilson caliper, except that two needles are present on each side allowing for direct measurements. Two points vertically down on the soft tissue ridge crest on both buccal and lingual areas are measured and joined by pencil on a diagnostic cast. The disadvantage of these common methods is that they both are invasive techniques.

The goal of this research is to develop new technology for the alveolar bone ridge width measurement that is high in accuracy and reliability and is most importantly, non-invasive. Ultrasound methods have gained research interest over the past decades, fit these conditions and have shown promising results in dental

applications. In general, the ultrasound technology in the field of medical diagnostics has achieved renowned success as a result of its portability and generally low cost in comparison to other available modalities. At the same time, it has attained a comparably high resolution, as well as a lack of harmful effects. There is a niche for ultrasonic devices in highly specified, narrow-band applications.
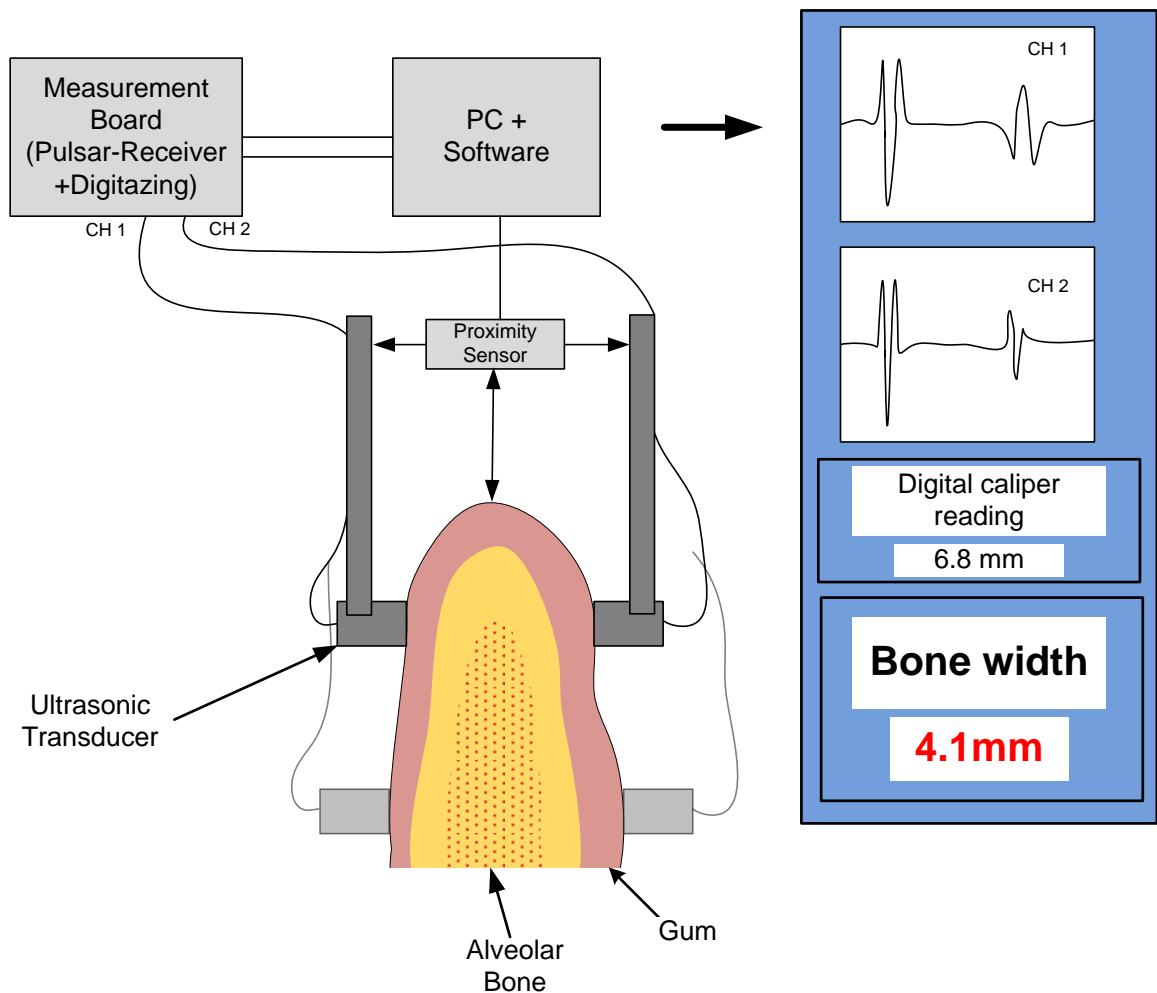
Figure 6.2 The diagram presents a functional concept of the dental caliper for bone thickness assessment.

Requirements posed by mechanical parameters, geometry, and accessibility of objects in most of these cases limit the usage of traditional ultrasonic systems and

generate area for a study required for new developments. To date, there is no real-time ultrasonic dental system dedicated to measuring the alveolar ridge width that aids dentists in diagnosing and monitoring treatment progression by providing high accuracy measurements without subjecting the patient to repeated harmful ionizing radiation or surgical insult and anesthesia. The proposed technology is based on short-pulse waves emitted by the ultrasonic transducers simultaneously from buccal and lingual sides of the bone ridge; the thickness of the soft tissues can be calculated with using developed sparse deconvolution algorithm (Chapter 3 and 4) and subtracted from overall ridge thickness measured with other a calibrated Hall sensor to obtain internal bone width measurement (Figure 6.2).

To validate and research methodologies the following sequence of prototypes has been developed and tested (Figure 6.3 - 6.5). Firstly, the proof-of-concept laboratory setup of the system was assembled and tested (Figure 6.3). The limitations of the early development were overcome in further prototypes. The third and latest prototype was equipped in custom electronics for displacement measurements (Figure 6.5).
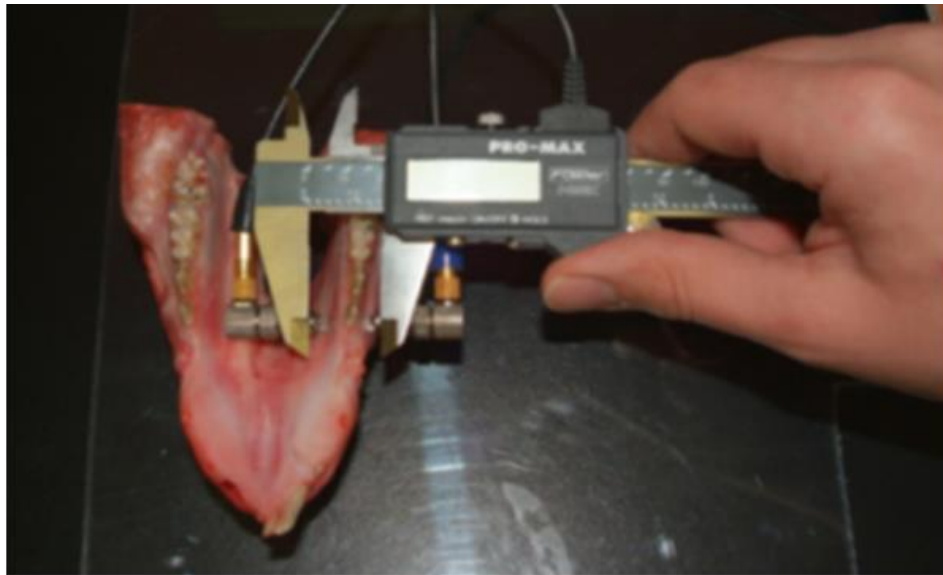
Figure 6.3 The first prototype for proof of concept evaluation. A measurement caliper with attached ultrasound transducers.
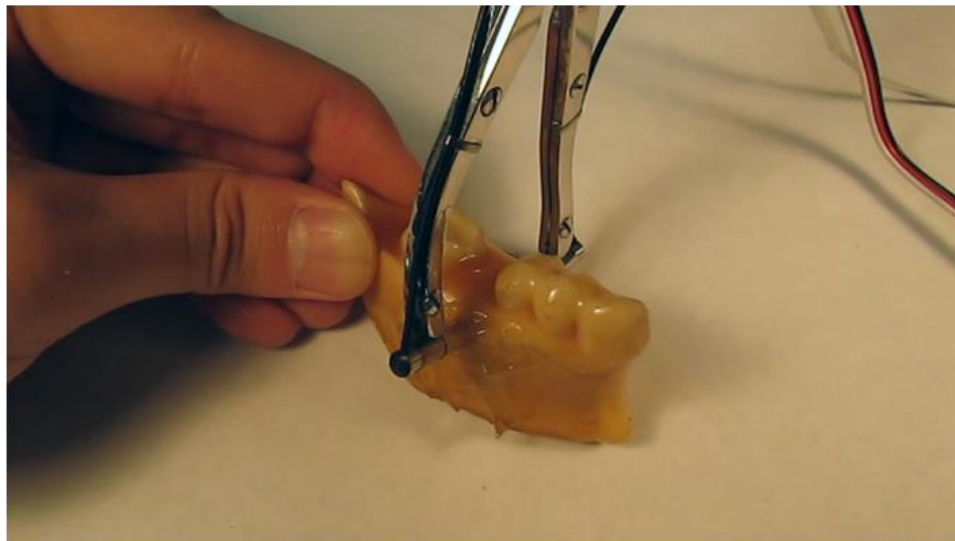
Figure 6.4 The second prototype built based on a Wilson caliper (the original needles were removed and replaced with custom ultrasound transducers). The prototype was equipped with custom electronics with a built-in multiplexer so that the 2 channels could be digitized, the unit was based on an embedded PC. (below) The picture presents an experimental setup with the calipers and a phantom

Figure 6.5 The third prototype equipped with a custom, developed an electronic board for proximity data acquisition highlighted in Figure 6.2.

6.1.3. Portable Ultrasound Device for Fingernail Characterization.

Human fingernails may potentially be a useful biomarker in assessing certain disorders of the body by both their appearance and texture. With the use of a hand-held, portable ultrasonic device a user may have the ability to quantitatively assess the progression of fingernail properties on-the-spot and over the long term. This device would be applicable to both clinical and cosmetic applications alike. Its application in

the medical field to chemotherapy patients in a pilot study is also introduced. No device is currently available to quantitatively investigate the properties of fingernails based on ultrasound characteristics.
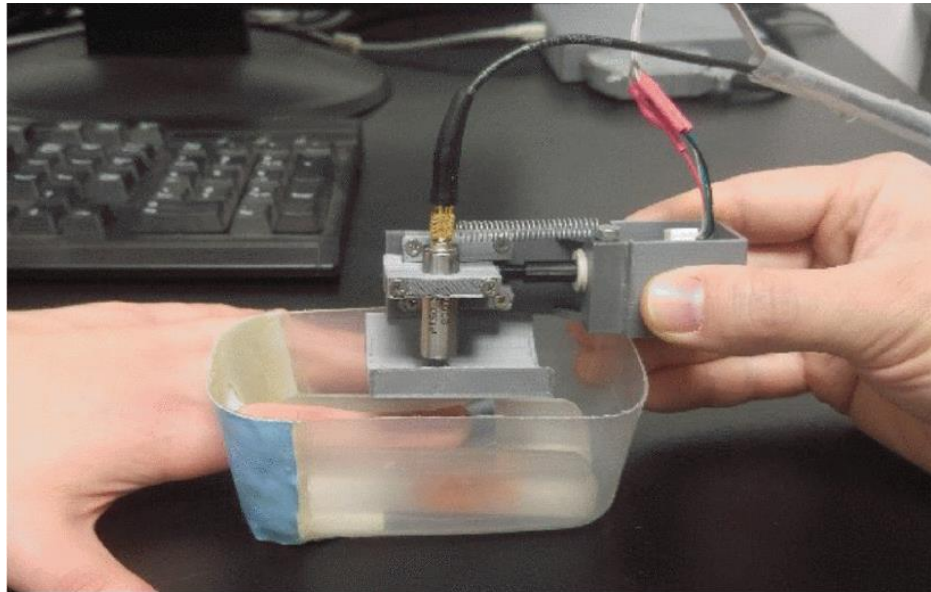
Figure 6.6 Experimental setup for fingernail properties assessment. The ultrasound transducer mounted into a micro scanner with a displacement actuator.

Limited information is available in regard to fingernails assessment using ultrasound-based methods and no major machinery or technologies have been implemented or standardized for the examination of nails. Qualitative information such as photographs or visual inspection limits the amount of information that can be collected and studied. Ultrasound provides noninvasive, quantitative data that reveals the TOF through the nail plate by using pulse-echo B-mode scanning (Figure 6.6). By using a higher frequency, the depth penetration was sacrificed for greater spatial resolution for the gain of a more detailed analysis. The device prototype was created and tested at the Windsor Regional Cancer Centre in Windsor, Ontario, Canada. This study was the first step in validating the useful application of this device [89], [90].

6.2.   Future Project Considerations

The following research areas of interest are believed to benefit from developments described in the previous chapters. They have been evaluated in terms of importance and potential value for both patients and doctors. An initial study scope was assessed and described below.

6.2.1.   Ultrasound for Alveolar Bone Quality and Quantity Assessment.

Dental implants are becoming the standard and the best solution for teeth replacement. Numerous studies show that dental implants stop the progressive loss of bone over the long term and provide a stable and effective tooth replacement. It is well-established that a primary factor in providing for the success of a dental implant is the crestal bone in which it's placed. Therefore, establishing whether the quality of the crest bone is adequate, has become one of the most important aspects in determining implant placement long-term success. The aim of this research direction is to develop an easy to use, compact ultrasound dental system intended for the noninvasive and accurate evaluation of the edentulous alveolar bone quality and quantity in the region planned for implant placement. The device will be able to differentiate between the 4 types of bone recognized in dentistry. The device prototype is comprised of a dental caliper-shaped probe with embedded miniaturized ultrasonic transducers and a monitor/tablet unit to which the probe will be connected (Figure 6.5c). During measurement, the transducers emit/receive completely harmless ultrasonic waves. The waves propagating through the soft and hard tissues from both buccal and lingual sides will generate a signal containing the information correlated to bone quality. The signal will be further processed by the device and the obtained results displayed in real-time. The dentist will be able to assess both the quality of the crestal bone and, if necessary, map the cross-sectional thickness profile of the crestal bone. The user-friendly interface will guide the dentist through the measurement steps and display the results in a convenient format. The offered device will assist the dentist in making a decision about the necessity of

gum and/or bone augmentation, estimate proper implant dimensions prior to the implant placement procedure, and limit unnecessary exposure of patients to ionizing radiation (especially 3D imaging). The device will help to evaluate whether the quality of the regenerated crest bone after grafting is sufficient for drilling and implant placement. It will also help to assess changes in the crestal bone density as a function of time after the implant has been placed.

6.2.2. Demineralized Dental Tissue Diagnostics

This direction and studies aimed to explore demineralization detection abilities and conduct a volumetric assessment of caries in extracted teeth using ultrasound, Optical Coherence Tomography (OCT), and x-rays imaging (micro CT). Sound and carious extracted human molars were collected under ethical approval at the Eastman Dental Institute, London, UK (N>12). Four groups were created using the International Caries Detection and Assessment System (ICDAS) score 2 to 4 (incl. control). All samples were scanned using micro CT and OCT for demineralization and cavitation volume estimations. Longitudinal (~200 um thick) and transverse sections across the ranked lesions were prepared before being assessed histologically. The ultrasound-based assessment was carried on serial transverse sections. This enabled to gradually image through the cavities to determine the boundaries between healthy and demineralized tissue. The obtained data were used to recreate and calculate the carious volume. Following comparative A-Scan analyses of the ranked ICDAS lesions, we identified unique ultrasound and OCT scattering markers which could be correlated to tooth histology. Following this, the methods for caries volumetric assessment based on the multi-modality imaging techniques have been examined. The calculated concordance coefficients between estimated volumes show good correspondence. Finally, the volumetric correlation between ultrasound & OCT scans and ICDAS was reviewed as a potential clinical diagnostic approach.
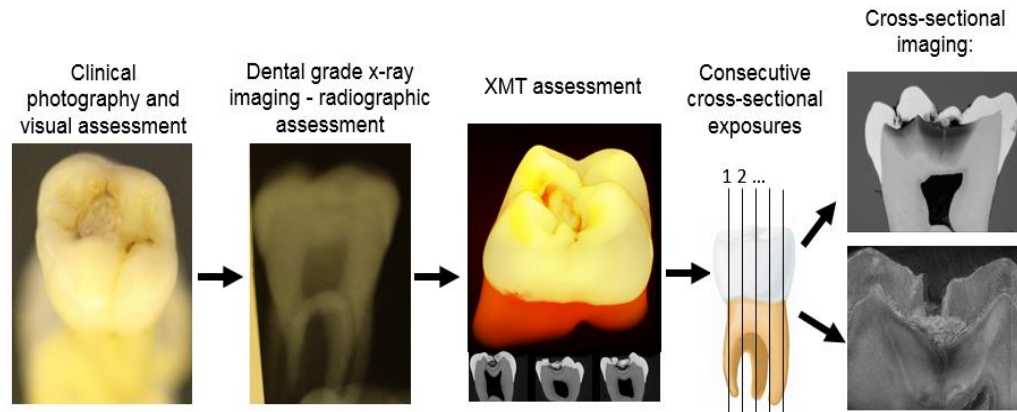
Figure 6.7 The diagram presents the consequent study methodology for hard tissue demineralization assessment. Ultrasound imaging was performed on the cross-sectional exposures (upper right example)

The optical and ultrasonic methods used in the study proved to be a possible alternative to ionizing radiation techniques used in current clinical settings. Further improvements in the experimental design will eliminate the necessity of surface exposers so the OCT and ultrasound could be used as complementary technologies.

6.2.3.   Ultrasonic Image-Guided Positioning System for Dental Implants

To navigate the implant position according to prior X-ray planning (Figure 6.8). Ultrasonic data analysis and fusion with cone-beam computed tomography data with a presence of fiducial markers (Figure 6.9) The main goal of the proposed technology is to improve the current dental implant procedure. Benefits include eliminating guesswork in the freehand implant placement, exclude a costly surgical guide from the guided surgery procedure (details in Appendix 2).
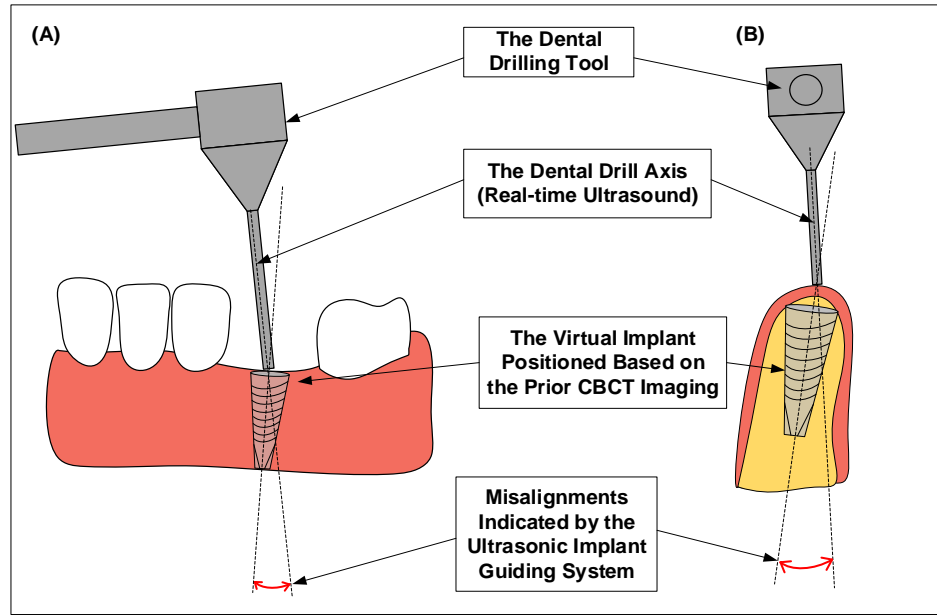
Figure 6.8 Diagram representing mesial-distal (A) and cross-sectional (B) view of the implant site, a virtual implant (positioned based on CBCT data, pre-surgery planning), a dental drill (real-time ultrasound data), and the misalignment between the implant axes and drilling direction.
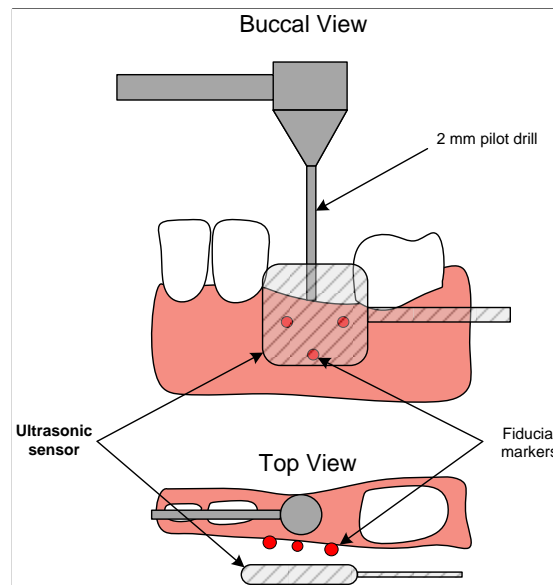
Figure 6.9 Illustration shows an implant placing area, a dental tool with a 2 mm pilot drill placed on the crest, three fiducial markers attached to the surface and the ultrasonic probe head.

CHAPTER 7.

CONCLUSION

Ultrasonography allows clinicians to obtain diagnostic images in a cost-effective, convenient manner without exposure to potentially harmful ionizing radiation. The ultrasonic device sends pulses of high-frequency sound waves inaudible to the human ear into tissues being investigated. The sound waves are reflected by tissues differentially with different degrees of acoustic impedance to sound based on their density/anatomical structure. The reflected sound waves are detected and recorded after the interaction by the same probe, resulting in carrying a piece of information about the tissues that can be transformed into an image or diagnostic results. Traditionally, ultrasound has been used more for assessment of soft tissue, but technological advances and further research have allowed for the expanded application to hard tissues as well. The use of ultrasound has been investigated in dentistry and summarized in the recent literature [12].

This dissertation combines knowledge gained in electronics and physics (ultrasound wave propagation and signal processing) and introduces the sparse deconvolution algorithm into dental diagnostic applications. It is believed that the current advancement depends on the development of digital processing methods, early prototyping, and integration of the system design. The following considerations dramatically accelerate the overall system improvements and clinical implementation. The goal of this dissertation was to address problems such as accuracy, uncertainty and computation time by proposing algorithmic solutions and testing its ability. The utilization of digital signal processing for optimizing operation, enhancing SNR that simplifies feature extraction was essential and necessary to accelerate execution at runtime. It also allows shortening the clinical time spent on diagnostics and simultaneously promotes ultrasound as a commercially viable method. The algorithm was adopted and implemented in the script-based programming environment so it could be modified and adjusted at execution. It also allows test vectors analysis to be effectively implemented. A set of simulations based on synthetic signals were performed for preliminary investigation. The algorithm characteristics have proven ability to enhance signals and results show the satisfactory time of flight extraction.

The encouraging simulation results and collected parameters supported further in vitro experiments. A clinically focused study was designed to verify the developed device with the built-in algorithm used against the current gold standard, visual inspection, and invasive diagnostic method based on OCT created for true value measurements. The repeatability and reproducibility of ultrasound measurements were evaluated by assessing the agreement between paired readings and the agreement between two examiners and showed highly satisfactory outcomes. The framework of the system operation was verified and validated for future embedded implementation.

The aim of the system enhancement and optimization has been achieved; a non-invasive, ultrasound-based gingival thickness measurement device was developed and improved in the pilot evaluation. The future of the project can be twofold and involve further studies in applications such as dental calipers and implant navigations. Both

directions will require algorithm adjustments and optimizations for specific tissue structures.

APPENDIX 1

Instruction for Use of the Ultrasound Diagnostic System

> The Institute for Diagnostic Imaging Research, University of Windsor
> Windsor, Ontario, Canada
>
> Ultrasound Dental Device
> UDS201705001

Introduction

The purpose of this document is to provide instructions for use for the investigational Ultrasound Dental Device UDS201705001 only (hereafter referred to as "Device"). These instructions contain all necessary information for the safe and effective usage of the Device. These instructions are provided only within the framework of the research study related to the Health Canada Application (hereafter referred to as "Study").

Device Description:

Gingival thickness (biotype) has a significant impact on the outcome of dental restorative and regenerative therapy for a broad segment of patients. The assessment of periodontal biotype is critical when selecting appropriate protocols in the field of dental

surgery. The presented device consists of a miniaturized probe with an ultrasonic transducer, electronics responsible for signal generation and acquisition, as well as software required for data analysis. The Device is a comfortable system to be used by trained clinicians (dentists). Based on the used technology, the Device produces low energy level ultrasound pulsed wave (similarly as to the pachymeters used in ophthalmology). The Device is non-invasive, battery operated and produces only sub-threshold signals (please see: Acoustic Output Parameters). The system is based on a popular pulse-echo method used in medical ultrasound. The ultrasonic transducer is commercially available, and it has been used in other fields of medicine. The system has been tested and it is safe to be used in the clinical setting.

Components and Accessories

The Device consists of two main components: the main unit and the ultrasound probe (Figure 5.). The Device package also includes an external power supply to be used only for recharging the internal battery while the Device is not in clinical use. Additionally, the system is equipped with disposable dental sleeves (commercially available) to protect from the cross–infections.

Acoustic Output Parameters

The system prototype has been evaluated according to guidelines provided by Health Canada. The setup instruction provided by the National Physical Laboratory, London, UK were used. A hydrophone (Onda HGL-0400) attached to an amplifier (Onda AH2010025) was used to measure and characterize a sequence of pulses generated by the ultrasonic transducer. The voltage of the hydrophone as a function of time is proportional to the acoustic pressure p(t) at the active element of the hydrophone with an assumption that the maximal signal value in the special domain was found (values referred further as special-peak). The signal was recorded on a 50 Ohm impedance matched oscilloscope and further calculations were conducted in script-based software.
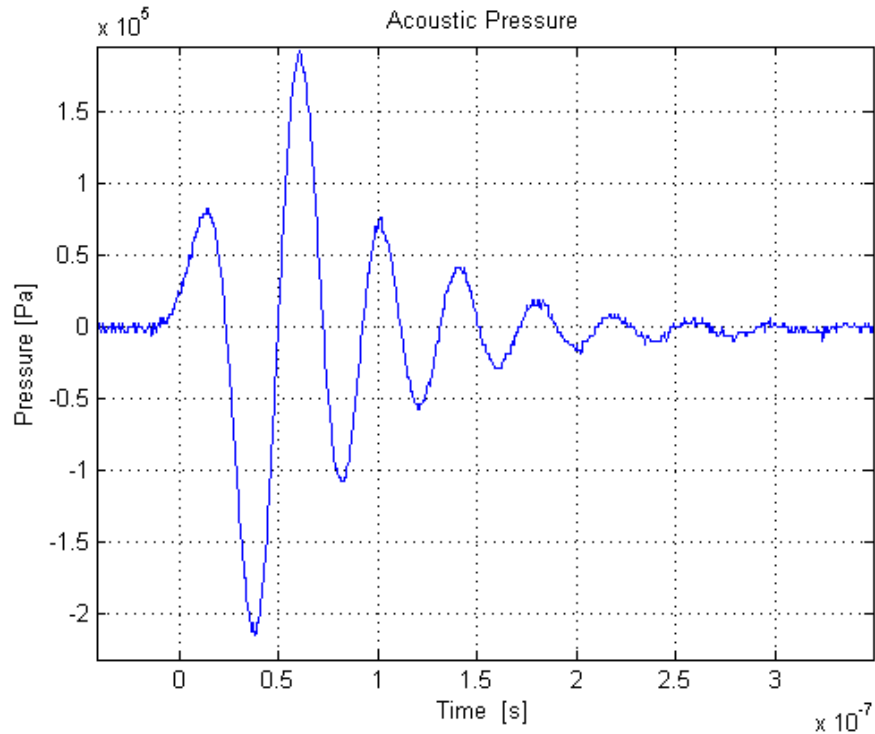
Figure 7.1 The acoustic pressure distribution of a singular pulse. The peak negative pressure amplitude is equal to 215KPa.

The pulse-pressure-squared integral Pi has been calculated. Based on that the signal time duration has been estimated and it is equal to 1.25 times the interval between the time when the time integral of the instantaneous acoustic pressure squared reaches 10% and 90% of the final value of the total integration. The pulse repetition has been set in the system hidden settings (these are not available for the end-user) to 120us and the value was reconfirmed during the measurements on the oscilloscope. Under the assumption of a plane progressive wave, the intensity can be derived from the acoustic pressure by following the formula: $I = p^2/\rho c$.

Figure 7.2 Acoustic output measurement setup.

Figure 7.3 Preamplifier connected directly to the oscilloscope.

Figure 7.4 The hydrophone and the evaluated probe lined up in the testing tank.

Table 7.1 The acoustic output exposure levels.

Parameters:	$I_{SPTA.3}[\frac{mW}{cm^2}]$	$I_{SPPA.3}[\frac{W}{cm^2}]$	MI
FDA (Abdominal, Intraoperative, Pediatric, Small Organs)	94	190	1.9
Measured	**0.7**	**1.21**	**0.48**

$I_{SPTA.3}$ – Derated Spatial-Peak Temporal-Average Intensity

$I_{SPPA.3}$ – Derated Spatial-Peak Pule-Average Intensity

MI – Mechanical Index

Instructions for Installation of the Investigational Device

The Device will be placed on the medical cart next to the dental chair while in use. The device does not require a specific installation procedure other than the probe attachment (the study coordinator will be specifically instructed on how to attach the probe). The system is pre-configured and automatically starts the data acquisition procedure after powering up and system booting process.

Storage and Handling Requirements

Upon the experimental measurements' completion, the Device will be stored according to the protocol of clean dental supplies and recharged in the technicians' room.

Preparation for use (intended cleaning, disinfection, re-use, sterilization)

After booting the system and the designated dental software initiation the user is required to place the probe perpendicularly on a calibration phantom provided with the device in order to verify proper performance and calibration. After the calibration test, the device is ready to be used.

Cross-infection prevention: The Device requires an application of a cross-infection prevention foil on the touch screen and the probe handle (disposal protection barrier at any contact surfaces).

The device will be prepared for use according to the dental disinfection protocol for a semicritical patient-care device. It is considered semi-critical due to contact with mucosal membranes. Since the ultrasound probe is not heat-tolerant and cannot be sterilized it will be cleaned with high-level disinfectant (Mikrozid wipes are a compatible method of high-level disinfection for UDS probe). Additionally, to increase protection level the probe will be placed in a disposal protection barrier during assessments.

Table 7.2 Technical specifications of the device.

Specifications:
Color: Black
OS: Windows 10
CPU: Intel Cherry Trail Z8350 Quad Core
GPU: Intel HD Gen8 Graphics
RAM: 4GB DDR3L
ROM: 64GB eMMC
Screen: 10.8 inch
Display: IPS, Capacitive Touch Screen
Resolution: 1920*1280 pixels
Card Extended: Support TF card up to 64GB

Basic Functions:
Video Format: MEPG 1/2/4, H.263/H.264, RMVB, WMV/VC-1, MVC, AVS, MJEPG (Support 1080P)
Audio Format: MP3/WMA/WAV/OGG/FLAC/ALAC/APE/AAC/AC-3/
Picture Format: JPG/JPEG/BMP/GIF/PNG
3G: No
WiFi: 802.11 b/g/n
Bluetooth: Bluetooth 4.0
HDMI: Yes
GPS: No
Battery: 10000mAh
Multi-language: Support

Ports:

2 x USB ports
1 x HDMI port
1 x RJ45 LAN Port
1 x TF card slot

1 x Earphone jack
1 x 5V/3A DC Power port (**Only to be used while not in clinical use!**)

Dimension: 255*173.5*70 mm
Weight: 1020g
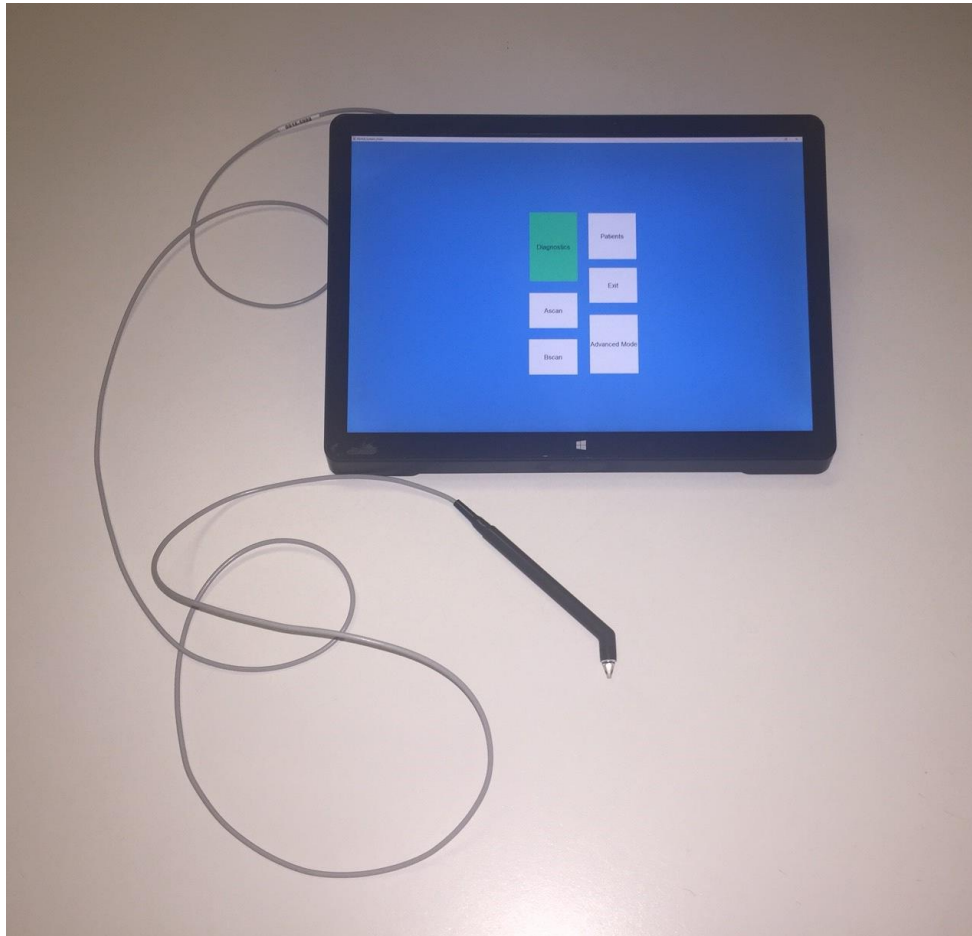
Figure 7.5 The device with the measurement probe.

Warnings:

- The Device must be used only under the guidance of a trained professional involved in the Study.

- Any deviation from the Study protocol and from the instruction of use is strictly prohibited.

- The device contains no user-serviceable parts. In case of perceived or suspected malfunction please contact the Study coordinator.

- DO NOT use the Device if you have any implanted electrical devices, such as a pacemaker.
- DO NOT place the Device on areas other than gingiva and fingernails.
- DO NOT attempt to use external sources of electricity to power the Device. The Device should only be powered by the internal battery.
- DO NOT hit or expose the Device to vibration, as it contains fragile elements.
- DO NOT expose the Device to water or direct sunlight.

Usage

1. Before each use, make sure that the device is functional, and that the battery is charged.
2. Before each use, make sure that the Device is cleaned, protected and disinfected according to dental standards.

Contacts

For any questions about the Device or the Study, please contact the Study principal investigator.

APPENDIX 2

Patent – Ultrasonic Device for Dental Implant Navigation

(12) **United States Patent**
Slak et al.

(10) **Patent No.:** **US 9,986,968 B2**
(45) **Date of Patent:** **Jun. 5, 2018**

(54) **ULTRASONIC DEVICE FOR DENTAL IMPLANT NAVIGATION**

(71) Applicant: **UNIVERSITY OF WINDSOR**, Windsor (CA)

(72) Inventors: **Bartosz Slak**, Windsor (CA); **Emil Strumban**, West Bloomfield, MI (US); **Roman Maev**, Windsor (CA)

(73) Assignee: **University of Windsor**, Windsor, Ontario (CA)

(*) Notice: Subject to any disclaimer, the term of this patent is extended or adjusted under 35 U.S.C. 154(b) by 53 days.

(21) Appl. No.: **14/956,247**

(22) Filed: **Dec. 1, 2015**

(65) **Prior Publication Data**

US 2016/0157815 A1   Jun. 9, 2016

Related U.S. Application Data

(60) Provisional application No. 62/088,511, filed on Dec. 5, 2014.

(51) **Int. Cl.**
A61C 3/00	(2006.01)
A61B 8/08	(2006.01)
A61C 8/00	(2006.01)
A61B 5/055	(2006.01)
A61C 1/08	(2006.01)
A61B 6/14	(2006.01)
A61B 6/03	(2006.01)
A61B 6/00	(2006.01)
A61B 8/00	(2006.01)

(52) **U.S. Cl.**
CPC *A61B 8/0841* (2013.01); *A61B 5/055* (2013.01); *A61B 8/5261* (2013.01); *A61C 1/084* (2013.01); *A61C 8/0089* (2013.01); *A61B 6/032* (2013.01); *A61B 6/14* (2013.01); *A61B 6/4085* (2013.01); *A61B 8/4483* (2013.01); *A61B 8/463* (2013.01)

(58) **Field of Classification Search**
CPC A61C 1/084; A61C 8/0089; A61B 8/0841; A61B 8/5261; A61B 5/055; A61B 6/032; A61B 6/14; A61B 6/4085; A61B 8/4483; A61B 8/463
See application file for complete search history.

(56) **References Cited**

U.S. PATENT DOCUMENTS

2007/0073136 A1*	3/2007	Metzger	A61B 17/1637 600/407
2011/0015521 A1*	1/2011	Faul	A61B 34/20 600/426

(Continued)

OTHER PUBLICATIONS

G. Pellegrino et al., "A new navigation system for dental Implantology," Clinical Oral Implants Research, vol. 25, Issue S10, p. 297 (2014).

(Continued)

Primary Examiner — Heidi M Eide
(74) *Attorney, Agent, or Firm* — Womble Bond Dickinson (US) LLP

(57)   **ABSTRACT**

The present invention providing a real-time positioning ultrasonic system that locates the dental implant drill bit relative to placed reference points or fiducial markers, and guides the drill entry point and angular trajectory, so that drilling is effected in the most optimum location in the jaw bone, as planned based on pre-surgery cone-beam computed tomography scans.

20 Claims, 4 Drawing Sheets
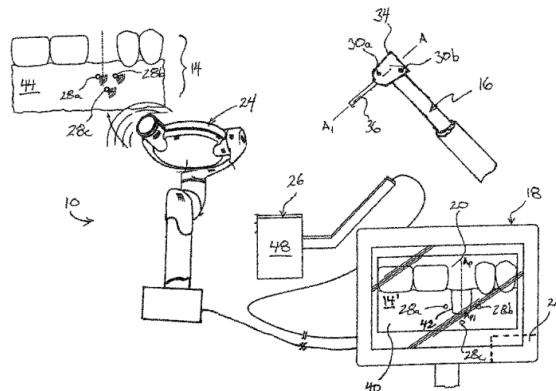
US 9,986,968 B2

Page 2

(56)   **References Cited**

U.S. PATENT DOCUMENTS

2012/0015329 A1*   1/2012   Gross A61C 1/084
                                                                433/215
2015/0196369 A1*   7/2015   Glossop A61B 19/54
                                                                600/409

OTHER PUBLICATIONS

Satoshi Yamaguchi et al., "Intuitive Surgical Navigation System for Dental Implantology by Using Retinal Imaging Display," Chapter 13, pp. 301-317 (Aug. 2011).
George A. Mandelaris, et al., "Computer-guided implant dentistry for precise implant placement: combing specialized stereolithographically generated drilling guides and surgical implant instrumentation," The International Journal of Periodontics & Restorative Dentistry, vol. 30, No. 3, p. 275-281 (Jun. 2010).
"SIMPLANT® Guided Surgery—Delivering restorative driven implant treatment," Dentsply Implants, 12 pgs. (2014).
"SIMPLANT® Introducing SIMPLANT® 16—The key to unlocking digital potential," Dentsply Implants, 2 pgs. (2014).
"Prosthodontics Guided Surgery", University of Michigan —School of Dentistry, accessed at: http://www.dent.umich.edu/about-school/department/bms/prosthodontics/guided-surgery   on Sep. 27, 2013, 1 page.

* cited by examiner

Fig. 1

Fig. 2

Fig. 3

Fig. 4

Fig. 6

Fig. 5
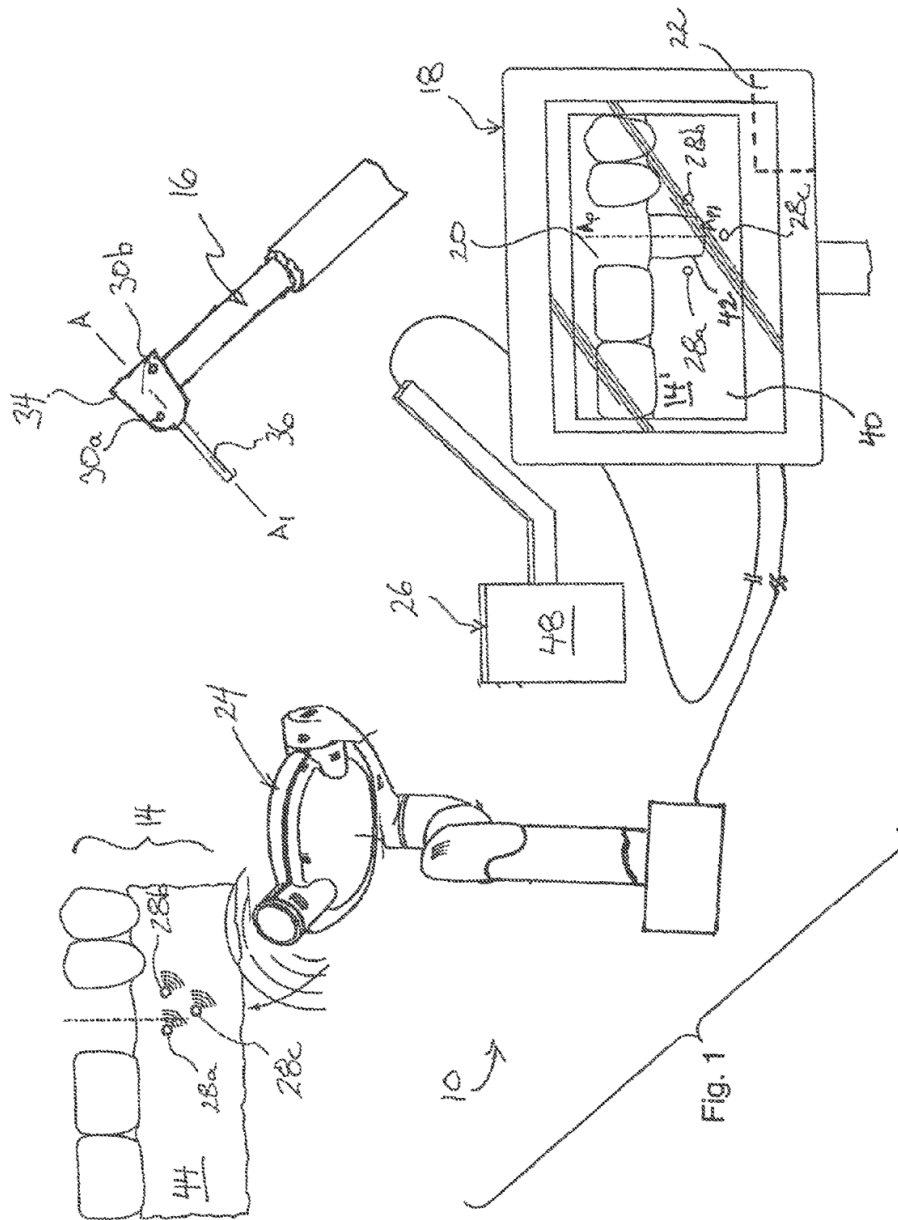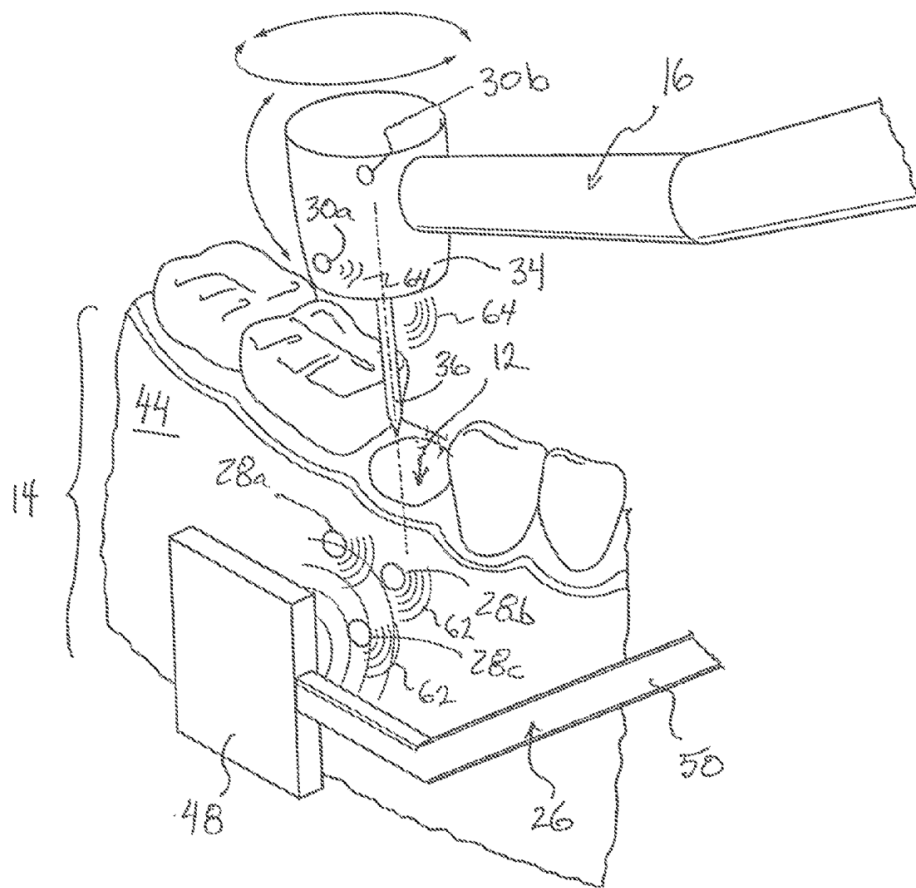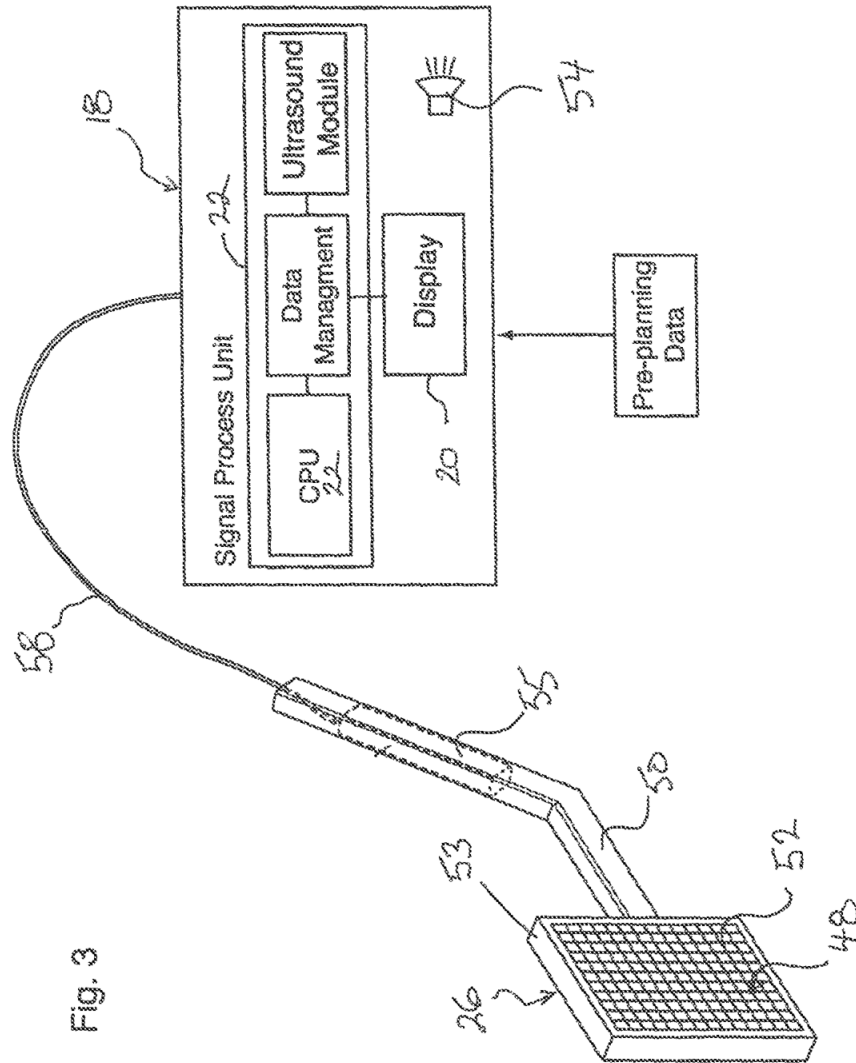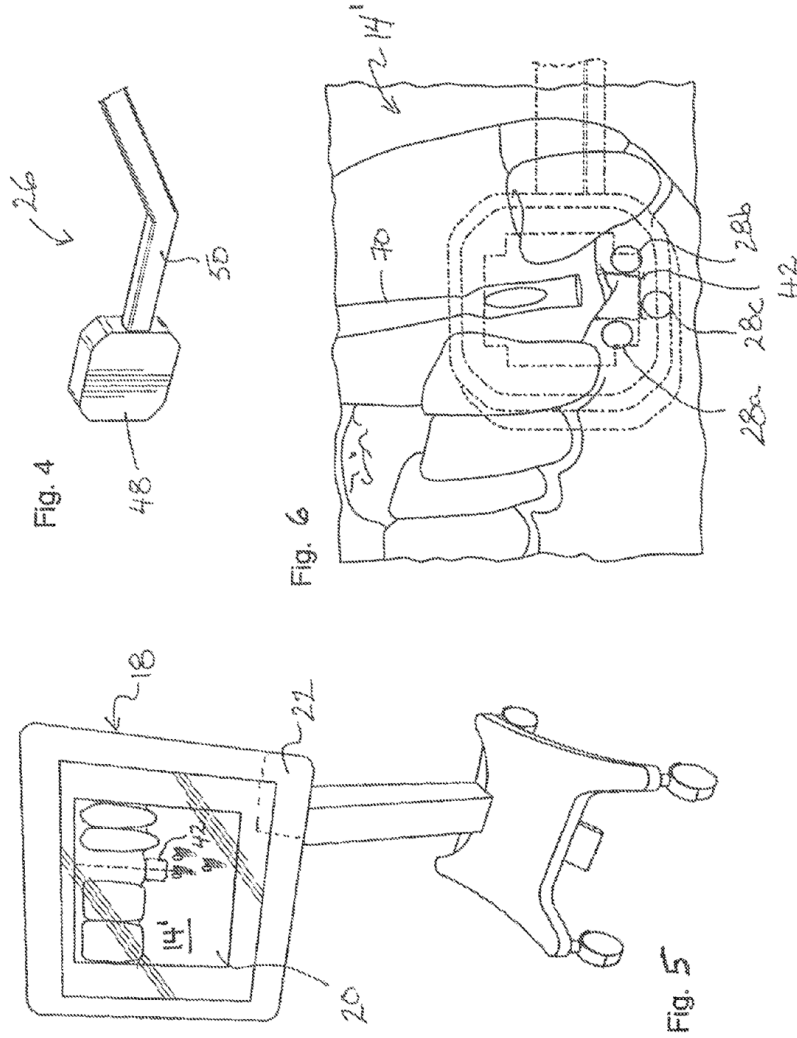
US 9,986,968 B2

1

ULTRASONIC DEVICE FOR DENTAL IMPLANT NAVIGATION

RELATED APPLICATIONS

This application claims priority and the benefit of 35 USC § 119(e) to U.S. Provisional Patent Application Ser. No. 62/088,511, filed 5 Dec. 2014, the disclosure of which is incorporated herein by reference in its entirety.

SCOPE OF THE INVENTION

The present invention relates generally to the field of medical ultrasound. More particularly, the present invention relates to the field of ultrasound navigation systems intended for medical implants, and most preferably dental implantology. Preferably, the invention provides an ultrasonic-based system that provides a medical practioner with a visual display which facilitates real-time guidance or location identification of an implant drill relative to an intended implant site in a patient's bone or tissue.

BACKGROUND OF THE INVENTION

Permanent dental implants have become a common method of replacing missing teeth. Prosthetic replacement teeth are supported by screws set into the jaw bone directly beneath the location where the tooth or teeth are missing and the replacement teeth are formed or mounted on the ends of the implant screw that protrudes above the gum line. The procedure of placing these screws into the jaw bone is done virtually blind by the dentist. As a result, there are many cases where implant screws are not properly placed, resulting in the failure of the dental implants and the removal and replacement of the implants with new implants or removable dental bridges anchored to adjacent teeth.

One important factor to the long term success of permanent dental implants resides in that the supporting screw is centered in the bone mass of the jaw at an angle directly under the load force that will be placed on the implant. The mechanical screw thread must be fully engaged with the jaw bone at a torque force that is less than the thread breakout force in the bone. The mechanical structure of implant screws is preferably such that it does not permit the implanted tooth to move or create pressure on the natural teeth next to the implants.

To ensure the pilot hole for the implant screw is properly placed, x-rays are taken, studied and reviewed to determine the best screw location and alignment. In most cases, the dental surgeon references the teeth he can see with x-rays or radiographs and positions the entry and alignment of the drill on visual observations. Conventional methods for dental implant placement typically involve freehand positioning based on subjective data such as visual examination with invasive bone structure exposure. Unfortunately, this method relies on specialist's skills and experience, extends the healing time and increases the risk of possible infection.

Custom fixtures that anchor on adjacent teeth with guide holes to properly align the drill have been attempted with limited success. Issues exist with the cost of fixture creation and the time required to place the fixture, and which unduly lengthen the time to the procedure, both in productivity for the doctor and comfort for the patient. As a result many dentists have reverted back to the freehand method, using the adjacent teeth as references to position and aligning the drill based on what was observed in the x-ray and accepting the failed procedures as the risk involved.

2

More sophisticated methods involve using cone-beam computed tomography (CBCT) data for implant placement planning, and CAD/CAM-based dental drill guide fabrication. The main utility of the guide is to transfer pretreatment planning information to the surgery site. The guide is usually made out of plastic and it is supported on residual or adjacent teeth, or in other cases attached with specially designed mini implants. Typically, such guides require the formation of metal sleeves which are immersed in plastic, and which act as jigs for positioning and depth control of the dental drill bit. Such system are personalized, entirely designed and fabricated based on pretreatment CBCT scans of the patient. Due to its complexity, involved risk and required accuracy, the guide fabrication is centralized and completed by professionals which increases the cost and considerably extending the restoration timeline.

SUMMARY OF THE INVENTION

Accordingly, to at least partially overcome some of the disadvantages associated with prior art devices, the present invention provides a system for facilitating the placement of implants, and in a preferred aspect, dental implants. The system incorporates a sensor which electronically communicates with a display, and which allows for substantially real-time imaging and display of an implant drill relative to a patient's particular biological area of interest, such as the intended area for implant placement.

The system operates in conjunction with a suitable imaging apparatus such as an x-ray apparatus, CBCT apparatus, magnetic resonance imaging apparatus (MRI) or the like, and which is operable to produce and store an output scanned image of the patient's intended implant area. The scanned image may be in a number of possible formats, including as a radiographic image, as well computer generated two-dimensional and/or three-dimensional images. The imaging apparatus may be located on site, or remotely, as for example at a hospital or clinic, with prepared output scanned image file being exported either electronically, or stored on portable storage media, such as a CD Rom, flash drive or other portable memory.

The system is provided with a processor having memory for receiving the output scanned image, and which electronically communications with a guidance system display. The system further includes a sensor assembly, and more preferably, an ultrasonic-based sensor assembly which operates in real-time to the processor for projection graphically an output on the data signals representing the position and/or orientation of a drill bit relative of the intended implant area. More preferably, the system operates in conjunction with one or more fiducial markers which are placed in the biological area of interest, and on the implant drill or other medical apparatus. Thus fiducial markers are positioned to allow for the correlation of the output scanned image produced by the imaging apparatus and the position of the drill bit and/or drill head detected by the ultrasonic sensor. The system may for example include software operable to automatically correlate the positioning of fiducial markers identified in the scanned output image with fiducial markers detected by the ultrasonic sensor. The system may therefore output on the display a visual representation of the drill and/or drill bit position in substantial real-time relative to the stored image. In this manner, the practioner may be able to view in substantially real-time the implant drill as it moves relative to the intended implant area.

In a most preferred construction, the fiducial markers are provided as part of a fiducial spatial coordinate system, in

US 9,986,968 B2

3

which three or more fiducial markers are fixed in position relative to the intended implant area, and in the case of a dental implant system in the patient's mouth. Alternately, one or more geometric or needle-shaped fiducial markers in the form of gold spheres may, for example, be used. Further, positional markers, and more preferably additional fiducial markers, are positioned on the drill or drill head in a predetermined orientation relative to a drill bit axis.

The applicant has appreciated that the present invention may thus provide an implant placement system, and preferably a dental implant drill guidance system which incorporates a drill and sensor arrangement which is cost effective, small and which is chosen to have a minimum effect on patient comfort. The present system further may work well with conventional implant placement methods and equipment, without adding to the overall length of the implantation procedure.

In another embodiment, the present invention provides a method and an apparatus for medical implant positioning, and preferably a dental implant positioning as part of placement procedure. Preferably, the present invention provides a real-time positioning ultrasonic system that locates the dental implant drill bit relative to one or more placed reference points or fiducial markers, and provides guidance as to the drill bit point and angular trajectory, so that drilling may proceed in the most optimum location in the jaw bone. More preferably, the intended implant position is pre-planned, based on a preselected orientation, imagery and/or pre-surgery MRI or cone-beam computed tomography scans. The pre-planned implant position may thus be modelled and stored in the processor memory for simultaneous projection to the display with the output scanned image.

The system display thus may graphically or visually locate and guide in real-time an implant drill relative to the optimum implant placement model. The system further may provide guidance as to the drill entry point, angular trajectory, and/or positional depth, such that drilling occurs in the most optimum location in bone, as determined from pre-procedure modelling and/or x-ray based calculations.

In another preferred embodiment, an ultrasonic system is proposed which tracks the drill bit location in real-time using designed fiducial markers, more preferably the markers are made of materials which create a strong contrast for both ultrasound and radiograph or x-ray images. Suitable fiduciary markers would therefore include those made from materials such as gold or amalgam. Other materials such as carbon, polymer and gutta-percha may, however, be used. In one use, one or more fixed reference markers or points are placed by a practitioner as part of a reference fiducial spatial coordinate system before CBCT scans are taken. The fixed fiducial markers preferably placed in close proximity to the intended implant placement or drilling area. After obtaining 3D x-ray data from the CBCT scan, the surgeon can pre-plan the implant surgery to select and model a preferred implant placement orientation using a virtual implant, as for example, by employing drag and drop tools in suitable implantology software. In this manner, it is possible to select the best implant screw or body placement trajectory for the particular host-patient's anatomy. The information about the optimal implant placement is then saved and sent to the guidance system display.

During the implant placement procedure, the ultrasonic probe is situated adjacent or in the mouth area in close proximity to the intended implantation site. The ultrasonic probe is preferably selected with a probe head which is sized to be comfortably received by the patient and contains a multi-element ultrasonic transducer array which is operable

4

to form a space distributed ultrasonic beam. The probe head is preferably placed in a position selected to detect reflected ultrasonic signals from both the fixed reference fiducial markers, as well as fiducial markers on the drill or drill head at the same time. During one preferred mode of operation, the system processes received data representing the relative 3D positioning of the reference fiducial markers and fiducial marker position on the drill and calculates the current angulation and position of the drill bit relative to one or more of the reference fiducial markers previously imaged in the received pre-operative CBCT planning data. The system preferably enables the medical practioner or implantologist to observe on a monitor in real-time, drill bit position related to image intended implant area by generating and displaying graphically or by sensing a rendering of the drill bit position on the display. Optionally, the system may operate to provide visual and/or available warning informing about necessary corrections to correct drill bit penetration depth or to re-align the drill bit with the pre-planned trajectory. Preferably the system operates whereby in event that the sonic probe moves during the procedure, a displayed image may change, but the orientation of the drill relative to the reference points remains the same, and is continuously calculated by the matching algorithm.

Accordingly, in one aspect the present invention resides, a device for drill bit navigation in dental implant placement process, comprising: a tracking system which supplies information for guiding the drill bit during implant bed preparation by means of an output unit, said device producing a three-dimensional volume data set for the implant placing area, drill bit and fiducial markers by means of ultrasound imaging through an ultrasonic probe, said three-dimensional volume data set is used by said tracking system and exhibited by the output unit, wherein the output unit is a screen display, on which the implant placing area, drill bit, fiducial markers and a preplanned implant bed position are displayed in real-time during the implant bed preparation, and said screen display presents incorrect angulation of the drill bit when the preplanned positional path and the actual positional path of the drill bit deviate. More preferably, the device, produces an audible alarm should at any time the sonic probe not has three fiducial markers within the sonic probe vision area. The device may further have an image refresh rate greater than 30 times per second.

In another aspect, a dental implant placement system comprising: at least one fiducial marker adapted for placement in an intended implant area of a patient's mouth, said fiducial marker being detectable by both an ultrasonic sensor assembly and an imaging apparatus selected from the group consisting of an x-ray apparatus and a cone-beam computed tomography (CBCT) apparatus; an output assembly having a display electronically coupled to said ultrasonic sensor assembly and said imaging apparatus, the imaging apparatus being operable to produce and output on said display a three-dimensional image of said intended implant area; a drill assembly comprising: a drill bit actuable to form a bore in the patient's jaw at the intended implant area; and positional markers being detectable by said ultrasonic sensor assembly to provide an indication of an orientation of said drill bit in said patient's mouth, wherein the output assembly is operable to correlate the positional markers detected by said ultrasonic sensor assembly to said fiducial markers, and to output on said display a visual representation of said drill bit position relative to said three dimensional image.

In a further aspect, the present invention resides in An implant placement system comprising: at least one fiducial marker adapted for placement in an intended implant area of

US 9,986,968 B2

5

a patient's bone, said at least one fiducial marker being detectable by both an ultrasonic sensor assembly and an imaging apparatus selected from the group consisting of an x-ray apparatus, a magnetic resonance imaging apparatus and a cone-beam computed tomography (CBCT) apparatus; and an output assembly electronically coupled to said ultrasonic sensor assembly and said imaging apparatus, the output assembly including a display, and wherein the imaging apparatus is operable to produce and output to said display a visual image of said intended implant area, a drill assembly comprising: a drill bit actuable to form a bore in the patient's bone at the intended implant area; positional markers being detectable by said ultrasonic sensor assembly to provide an indication of an orientation of said drill bit relative to the intended implant area; and wherein in use, the output assembly is operable to correlate the positional markers detected by said ultrasonic sensor assembly to detected ones of said fiducial markers, and to display on said display a visual representation of said drill bit position relative to said visual image based on said correlation.

BRIEF DESCRIPTION OF THE DRAWINGS

FIG. 1 shows a schematic view of dental implant placement system for use in positioning a dental implant in a human periodontium in accordance with a preferred embodiment of the invention;

FIG. 2 is a partial perspective view showing the operation of an ultrasonic probe of the system of FIG. 1, in sensing the position of a drill bit position during drilling operations;

FIGS. 3 and 4 illustrate schematically the ultrasonic probe used in the sensing of drill bit position shown in FIG. 2;

FIG. 5 illustrates schematically the guidance system processor and video display used in the system of FIG. 1; and

FIG. 6 illustrates schematically a real-time output display of a visual graphic shown on the display video of FIG. 5, showing the relative movement of a sensed drill bit, relative to the patient's jaw bone during implant drilling.

DETAILED DESCRIPTION OF THE PREFERRED EMBODIMENTS

Reference may be had to FIG. 1 which illustrates a dental implant placement system 10 in accordance with a preferred aspect of the invention. The implant placement system 10 is adapted to image and guide in real-time, the formation of desired implant bore 12 (FIG. 2) at an intended implant placement area 14 of patient's mouth. The implant placement system 10 includes a dental drill 16, an output display assembly or a signal processing unit 1 which includes a high resolution pixel display 20 and an internal processor 22 having storage memory and stored data management software, and which is electronically coupled to both a cone-beam computed tomography (CBCT) apparatus 24 and an ultrasonic sensor assembly 26. As will be described, the CBCT apparatus 24 and ultrasonic sensor assembly 26 each operate to detect fixed reference fiducial markers 28a,28b, 28c which are positioned on the patient's teeth or over the jaw bone 44 at or adjacent to the intended implant placement area 14. The ultrasonic sensor assembly 26 is further operable to detect and sense fiducial markers 30a,30b positioned on the dental drill 16 as part of a fiducial spatial coordinate system. Preferably, the fiducial markers 28,30 are spherical in shape with the diameter greater than the resolution of that used in the CBCT apparatus 24 and sensor assembly 26.

In FIG. 1, the fiducial markers 30a,30b are shown in a preferred configuration as being positioned in on the head 34

6

of the dental drill 16. Most preferably, the fiducial markers 30a,30b are pre-positioned in a known orientation relative to the drill chuck assembly such that in use of the implant placement system 10, when sensed, the fiducial markers 30a,30b provide information respecting the relative orientation of the drill bit axis A-A$_1$ relative to the implant placement area 14. Additional fiducial markers may also be provided along the length of the drill bit 36 or drill head 34. The system 10 may thus accurately monitor the forward progress of the drill bit 36 into the jaw bone 44 to ensure that the depth of the formed drill hole 12 is correct and in accordance with plan and technical requirements of the dental implant manufacturer.

FIG. 1 shows best the CBCT apparatus 24 as operable to generate and output to the signal processing unit 18 for viewing on the display 20 a scanned three-dimensional image 14' of the intended implant area 14 of the patient's mouth. Most preferably, the output three dimensional image 14' is stored in the memory of the internal processor 22 as computer generated graphic image. Preferably, the display 20 is provided with a touch screen 40 or other suitable user interface. The interface allows the medical practioner/dentist to input into the processor 22 and generate as part of the displayed image 14', a model 42 of an optimum implant bore hole. The model 42 is input so as to display as part of the image 14' indicia showing the optimum bore angular orientation and/or sized depth relative to the patient's jaw bone 44 to achieve the correct positioning of the desired implant (not shown) in a screw or press fit manner. The signal processing unit 18 is operable to output to the display 20 a visual image of the implant bore model 42 concurrently as part of the output three-dimensional image 14', illustrating schematically the optimum bore placement relative to the patient's jaw bone 44. More preferably, the processing unit 18 further generates and displays with the image 14' a graphic or indicia representative of the drill bit 36 placement at the intended placement area 14 as it moves relative to the jaw bone 44.

As shown best in FIGS. 2 to 4, the ultrasonic sensor assembly 26 includes an ultrasonic sensor head 48 which is mounted on a positioning arm 50. The sensor head 48 is sized to allow for its positioning within the patient's mouth and adjacent to the intended placement area 14, so as to be operable to sense simultaneously both the fixed reference fiducial markers 28a,28b,28c, as well as the fiducial markers 30a,30b mounted on the drill 16. The sensor head 48 is selected to sense and transmit to the signal processing unit 18 data signals representative of sensed relative positioning of the fiducial markers 28a,28b,28c,30a,30b, thus providing data from which the relative drill bit 36/jaw bone 44 position may be determined. Fiducial markers 28a, 28b, and 28c provide reference points to merge the various image data to one common reference frame.

Furthermore FIG. 3, shows the ultrasonic sensor head 48 as preferably includes a multi-element transducer matrix 52 within a biocompatible enclosure 53. The ultrasonic sensor assembly 26 may also have a built-in electronic control block 55 responsible for direct transducer control, and which is located in the positioning arm 50. The electronic block 55 is connected to the signal processing unit 18 by a suitable digital cable 58. The stored data management software in the processor 22 electronically communicates with the array transducer control block 55 to create and manipulate emitted ultrasonic beams.

The ultrasonic waves reflected by the fiducial markers 30a,30b which are placed at known locations on the drill head 34 are received by transducer matrix 52 and connected

119

US 9,986,968 B2

7

to data signals. The signals are sent to the processor **22** that uses the known relationship between **30***a*, **30***b* and drill bit **36** to calculate the axis A-A₁ of vertical drill bit **36** then uses common fiducial markers **28***a*, **28***d*, **28***c*, alignment to position (depth and angle of drilling) relative to the jaw bone **44**. In particular, the signals **62,64** reflected respectively from both sets of the fiducial markers **28***a*,**28***b*,**28***c*,**30***a*,**30***h* are acquired by the probe head **48**, converted to electrical signals, and sent to processor **22** for further processing. Concurrently the sensed position of the reference fiducial markers **28***a*,**28***b*,**28***c* detected by the sensor assembly **26** is used to correlate the sensed drill **16** position with the input image **14'**. Based on the detected signals **62,64**, a secondary graphic image **70** representative of the drill bits **36** is preferably generated, and which is representative of the drill position and orientation. The secondary graphic image **70** is displayed on the display **20**, overlain on the 3D image **14'**. The secondary graphic image **70** is preferably created and analyzed by extracting features and aligning reference points between the two modalities data, namely, the reference data of the fixed fiducial markers **28***a*,**28***b*,**28***c* and the second fiducial markers **30***a*,**30***b*. The processor **22** thus operates to accurately merge the input 3D virtual model image **14'** based on the CBCT scan with live ultrasonic generated images.

In use of the system **10**, a dental surgeon may place three or more spherical reference fiducial markers **28***a*,**28***b*,**28***c* semi-permanently, as for example with adhesive onto the patient's gum tissue and/or teeth, at the intended implant area **14** where the surgery is to take place. The intended placement area **14** is then imaged, by the CBCT apparatus **24** to generate and output the scanned image **14'** to the signal processing unit **18**. The generated x-ray images are preferably then stored in the signal processing unit **18** processor memory and illustrated on the display **20** where the surgeon analyses the site conditions, and determines the optimum position and angle for the implant screw(s). Most preferably, the optimum implant screw center line(s) and depth is calculated and plotted directly as part of the displayed image **14'** using the touch screen **40**.

Following initial scanning by the CBCT apparatus **24** and the determination and input of the model **42** into the processor **22**, the ultrasonic assembly **26** and dental drill **32** are then used in conjunction with the displayed 3D image **14'** to form the desired bore **12** having the optimum configuration.

The implant placement system **10** is operated for optimum drill guidance in real-time. As shown best in FIG. **2**, the ultrasonic sensor assembly **26** is used concurrently with the operation of the dental drill **16** to accurately locate the point of entry and then precisely align the implant drill bit **36** with the predetermined optimum trajectory of the modelled bore hole **42** to form the bore **12** in the patient's jaw bone **44**. In use, the positioned fiducial markers **28***a*,**28***b*,**28***c*,**30***a*,**30***b* that are visible in the real-time ultrasonic image to guide the drill bit **36**.

The patient is thus prepared for surgery and the ultrasonic sensor head **48** is placed in the intended implant placement area **14** of the patient's mouth, in an orientation directed at the intended implant location. Optionally, the ultrasonic probe head **48** may be coupled with the implant placement area **14** by means of water or gel-based agent. Preferably, the system display **20** operates to output concurrently two images on the screen **40**: one based on the initial scanned x-ray image **14'**, with the plotted centerline of modelled bone **42** locations; and the second being the generated secondary image **70** representative of the actual drill bit **36** position, as determined a live feed from the ultrasonic sensor head **40** and the relative drill **16**.

8

Referring to FIGS. **2** and **6** there is shown the human periodontium or, jaw bone **44** with an implant placement location area **14** together with adjacent teeth. The dental drill **16** with mounted drill bit **36** is positionable over the intended implant site. The ultrasonic probe head **48** is located in front of the intended implant site **14**, and operates to generate a beam of ultrasound propagating towards the prepositioned fiducial markers **28***a*,**28***b*,**28***c*,**30***a*,**30***b*. During drilling operation, the real-time position of the drill bit **36** is relative to the jaw bone **44**, is thus sensed, and output graphically as the secondary graphic image **70** on the display **20** superimposed with the image **14**. If the angulation and position of the drill bit **36** deviates from a planned axis A_P-A_{P1} the system **10** will inform the surgeon on either the display **20** and/or as well as acoustically using a built-in speaker **54** (FIG. **3**). By pre-selecting degrees of freedom of drill **16** movement (FIG. **3**) it is possible to allow the practitioner to readjust the drill bit **36** trajectory as necessary, while the ultrasonic sensor assembly **26** continuously operates to obtain updated images and calculate current drill bit **36** position.

The placed reference fiducial markers **28***a*,**28***b*,**28***c* further preferably appear in both displayed images. As a result, the surgeon may electronically align the reference fiducial markers **28** on the x-ray image with those of the live ultrasonic feed. Once this alignment (or near alignment) has been achieved, a software function may be used to electronically lock the input x-ray image **14'** to the live ultrasonic feed image by digitally keeping the reference fiducial markers **28** aligned image-to-image, creating a single scale and reference frame for the two images being viewed one on top of the other as one continuous image. While the drill bit **36** is advanced into the bone **44**, the area **14** is preferably continuously scanned and a detected ultrasonic image showing drill bit **36** placement appears on screen in real-time. By aligning the drill bit **36** so that its image **70** is moved into alignment with the preselected center line trajectory plotted or modelled on the screen **20**, the practitioner may maintain optimum desired drill bit **36** alignment, correcting as required based on the planned line of trajectory.

In the event that the ultrasonic sensor assembly **26** moves during the procedure, the displayed image **14'** may change slightly as the images stay synchronized. The alignment of the drill bit **36** to the reference fiducial markers **28** and/or modelled image **42** will, however, maintain the desired reference basis.

In an alternate embodiment, the drill bit **36** may be provided with a number of markers around the shank to ultrasonically visualize the drill bit orientation, length, diameter, and depth. In another possible embodiment, dental implant drill **16** may be provided with ring feature near the chucked end of the drill head **34**. The ring feature is chosen from a known distance from the tip of the drill and is visible in the real-time as part of the generated ultrasonic image. When the drill bit **36** is at the proper depth in the formed bore **12**, the depth ring will be at a predetermined position along the drill angle trajectory, and may be sensed by the system **10** to provide the surgeon both a visual and audible signal to stop drilling.

The system **10** of the present invention preferably is programmed to include a number of non-limiting operational features, and which may for example include:

1. Dental implant drill guidance programme instructions that use x-ray images; developed procedure plan data; and live ultrasonic imaging layered and aligned with placed marker spheres to provide critical drill entry, alignment, and drill depth information in real-time to

US 9,986,968 B2

9

the surgeon for the optimum placement of the dental implant mounting screw(s).

2. Software and analytics which, from a limited number of patient x-rays or, extrapolate data to provide adequate 3D interpolation for the development of a procedure plan and drill guidance measurements for entry location; 3D drilling angle; and drilling depth.

3. Software which is operable to accurately merge data from x-ray; procedure development drawings; and real-time ultrasonic imaging into one image using marker spheres to assure the accuracy of this alignment. Further, once aligned imaging coordination software maintains the alignment and merger of these images in real-time by actively keeping the marker spheres on all images aligned with, the marker spheres on the real-time sonic image. In this way the sonic probe may be moved and re-orientated for a better viewing angle and image without having to rebuild the image merger.

4. A CMUT based multi micro transducer probe head **48** which is provided for better imaging; higher resolution; with little or no heat generation allowing for extended real-time imaging without the need to cool the probe to accommodate patient comfort and safety,

5. The system **10** may operate to capture a real image with the ultrasonic probe head **48** and generates a virtual image of the tissue and bone from x-ray data for areas not visible to the ultrasonic probe.

6. Use of fiducial markers **28,30** allows for the alignment of produced images from several sources; as well as 2D images virtually transformed into 3D images to provide full data to the surgeon.

7. Use of spherical fiducial markers to assure image scaling is coordinated with the scale of the real-time ultrasonic image.

It is recognized that in a preferred embodiment, the system **10** contemplates the construction of a three-dimensional virtual image **14'** built from multiple 2D scan or x-ray images, whereby

1. The surgeon views each x-ray on the screen and assigns a unique identifier to each reference fiducial marker **28** on the first image.

2. The surgeon then assigns the same identifier to the corresponding marker **28** in every x-ray image.

3. The system then scales and overlays all of the fiducial markers as per identifier, thus making each x-ray a cross section through a virtual 3D image as per the alignment of that x-ray.

4. The system processing software is configured to allow the system to use this information to create a virtual 3D image **14'** over these sections.

5. The surgeon can now use the generated virtual 3D image **14'** upon which to plot and develop his implant screw placement

In a possible operating mode, the virtual image **14'** is merged with the real-time ultrasonic image. On a first ultrasonic image appearing on a display screen **40**, the processor **32** or surgeon again assigns the same identifiers to the fiducial markers **28** in the image, as was done for the fiducial markers in the virtual image, and then aligns both images on the display screen **40**. Once alignment has been completed, the system **10** electronically locks the x-ray based model **14'** in constant re-alignment with the real-time ultrasonic image. As a result, even if the ultrasonic probe head **48** is moved, the images will remain properly aligned and to scale with the real-time ultrasonic image.

While the detailed description describes the implant placement system **10** as used in the positioning of a dental

10

implant in a patient's jaw bone **44**, the invention is not so limited. It is to be appreciated that the system **10** may equally be used in the positioning of other types of implants in other loci in patient's bone and/or soft tissues.

Similarly, while the detailed description describes the ultrasonic sensor assembly **26** as sensing and indicating the orientation of a drill bit relative to an intended installation location, the system may also be used to detect and display in real-time, the relative positioning of a variety of medical tours and/or appliances relative to a selected biological area of interest.

While the detailed description describes the fiducial spatial coordinate system as including three reference fiducial markers **28a,28b,28c** and two fiducial markers **30a,30b**, the invention is not so limited. It is to be appreciated that fewer or greater numbers of fiducial markers may be provided, depending upon the imaging and sensor capabilities.

Although FIG. **1** illustrates the CBCT apparatus **24** as being electronically connected directly to the signal processing unit **18**, the invention is not so limited. It is to be appreciated that in a more economical construction, the CBCT apparatus **24** could be provided at a remote location and where for example, a single CBCT apparatus **24** may be used to produce and transmit scanned images of different patient implant placement areas for use on separate signal processing units **18** and displays **20** at different locations.

Although the delated description describes and illustrates various preferred embodiments, the invention is not so limited. Many variations and modifications will now occur to persons skilled in the art. For a definition of the invention, reference may be had to the appended claims.

We claim:

1. A dental implant placement system comprising:

at least one fiducial marker adapted for placement in an intended implant area of a patient's mouth; an ultrasonic sensor assembly, said ultrasonic assembly comprising an ultrasonic sensor sized for positioning in said patient's mouth generally adjacent said intended implant area;

an imaging apparatus selected from the group consisting of an x-ray apparatus and a cone-beam computed tomography (CBCT) apparatus;

said fiducial marker being detectable by both the ultrasonic sensor and the imaging apparatus;

an output assembly having a display electronically coupled to said ultrasonic sensor assembly and said imaging apparatus, the imaging apparatus being operable to produce and output on said display a three-dimensional image of said intended implant area;

a drill assembly comprising:

a drill bit actuable to form a bore in the patient's jaw at the intended implant area; and

positional markers being detectable by said ultrasonic sensor to provide an indication of an orientation of said drill bit in said patient's mouth, wherein the output assembly is operable to correlate the positional markers detected by said ultrasonic sensor to said fiducial markers, and to output on said display a visual representation of said drill bit position relative to said three dimensional image.

2. The implant placement system as claimed in claim **1**, wherein said output assembly is operable to receive data representative of a modelled preferred implant placement orientation at said intended implant area, and to output on said display with said three-dimensional image placement orientation data representative of said preferred implant placement orientation.

US 9,986,968 B2

11   **12**

3. The implant placement system as claimed in claim **2**, wherein said data representative of said preferred implant placement orientation comprises a visual representation of a preferred bore position and depth relative to said patent's jaw.

4. The implant placement system as claimed in claim **3**, wherein said visual representation is superimposed on said three dimensional image.

5. The implant placement system as claimed in claim **1**, wherein the drill assembly comprises a dental drill having a drill head, said drill bit being mounted in said drill head for selective journaling in rotation about a drill axis, said positional markers comprising a plurality of markers mounted to said dental drill relative to said drill axis.

6. The implant placement system as claimed in claim **1**, wherein said fiducial markers are imageable by at least one of said ultrasonic sensor assembly and said imaging apparatus for output on said display with said output three-dimensional image.

7. The implant placement system as claimed in claim **1**, wherein said output assembly is operable to effect correlation of said positional markers and said fiducial markers substantially in real-time.

8. The implant placement system as claimed in claim **1**, wherein the output assembly is operable to display with said three-dimensional image a modelled bore image, said modelled bore image representative of an optimum bore orientation, depth and/or configuration sized to receive a dental implant seated therein in a screw-fit, press-fit or compression-fit manner.

9. The implant placement system of claim **1**, wherein the output assembly includes a processor having data management software stored thereon, said data management software being operable in substantially real-time to correlate fiducial marker position detected by said ultrasonic sensor assembly with a fiducial marker position detected by said imaging apparatus.

10. An implant placement system comprising:

at least one fiducial marker adapted for placement in an intended implant area of a patient's mouth;

an ultrasonic sensor assembly, the said ultrasonic sensor assembly comprising an ultrasonic sensor for positioning adjacent said intended implant area in said patient's mouth;

an imaging apparatus selected from the group consisting of an x-ray apparatus, a magnetic resonance imaging apparatus and a cone-beam computed tomography (CBCT) apparatus;

said at least one fiducial marker being detectable by both the ultrasonic sensor and the imaging apparatus; and

an output assembly electronically coupled to said ultrasonic sensor assembly and said imaging apparatus, the output assembly including a display, and wherein the imaging apparatus is operable to produce and output to said display a three-dimensional visual image of said intended implant area,

a drill assembly comprising:

a drill bit actuable to form a bore in the patient's bone at the intended implant area;

positional markers being detectable by said ultrasonic sensor to provide the position and orientation of said drill bit relative to the intended implant area; and

wherein in use, the output assembly is operable to correlate the positional markers detected by said ultrasonic sensor to detected ones of said fiducial markers, and to display on said display a visual representation of said drill bit position relative to said visual image based on said correlation.

11. The implant placement system as claimed in claim **10**, wherein said output assembly is operable to receive data representative of a modelled preferred implant placement orientation at said intended implant area, and to output on said display with said visual image, placement orientation data representative of said preferred implant placement orientation.

12. The implant placement system as claimed in claim **11**, wherein said data representative of said preferred implant placement orientation comprises a visual representation of a preferred bore placement and depth relative to said patent's bone.

13. The implant placement system as claimed in claim **12**, wherein the implant comprises a dental implant and wherein the visual representation of a preferred bore placement and depth comprise a virtual computer generated bore sized to receive the dental implant seated therein in a screw-fit, press-fit or compression-fit manner.

14. The implant placement system of claim **12**, wherein the output assembly includes a processor having data management software stored thereon, said data management software being operable in substantially real-time to correlate fiducial marker position detected by said ultrasonic sensor assembly with a fiducial marker position detected by said imaging apparatus.

15. The implant placement system as claimed in claim **10**, wherein the intended implant area is an area of a patient's jaw bone, and wherein the drill assembly comprises a dental drill having a drill head, said drill bit being mounted in said drill head for selective journaling in rotation about a drill bit axis, said positional markers comprising a plurality of fiducial markers mounted to drill relative to said drill bit axis.

16. The implant placement system as claimed in claim **10**, wherein said fiducial markers are imageable by at least one of said ultrasonic sensor assembly and said imaging apparatus for output on said display with said output three-dimensional image.

17. The implant placement system as claimed in claim **10**, wherein said output assembly is operable to effect a correlation of said positional markers with said fiducial markers substantially in real-time.

18. A dental implant placement system comprising:

a plurality of fiducial markers adapted for placement in an intended implant area within a patient's mouth;

an ultrasonic sensor assembly, said ultrasonic assembly comprising an ultrasonic sensor sized for positioning in said patient's mouth generally adjacent said intended implant area;

an imaging apparatus selected from the group consisting of an x-ray apparatus and a cone-beam computed tomography (CBCT) apparatus;

said fiducial markers being detectable by both the ultrasonic sensor and the imaging apparatus;

an output assembly having a display electronically coupled to said ultrasonic sensor assembly and said imaging apparatus, the imaging apparatus being operable to produce and output on said display a three-dimensional image of said intended implant area;

a drill assembly comprising:

a drill head mounting a drill bit actuable to form a bore in the patient's jaw at the intended implant area; and

said ultrasonic sensor being operable to detect said drill head to provide an indication of an orientation of said drill bit in said patient's mouth, wherein the output assembly is operable to correlate the position

US 9,986,968 B2

13

of the drill head detected by said ultrasonic sensor to said fiducial markers, and to output on said display a visual representation of said drill bit position relative to said three dimensional image.

19. The implant placement system as claimed in claim **18**, wherein the output assembly is operable to display with said three-dimensional image a modelled bore image, said modelled bore image representative of an optimum bore orientation, depth and/or configuration sized to receive a dental implant seated therein in a screw-fit, press-fit or compression-fit manner.

20. The implant placement system of claim **19**, wherein the output assembly includes a processor having data management software stored thereon, said data management software being operable in substantially real-time to correlate fiducial marker position detected by said ultrasonic sensor assembly with a fiducial marker position detected by said imaging apparatus.

* * * * *

14

REFERENCES

[1] B. Slak, A. Daabous, W. Bednarz, E. Strumban, and R. G. Maev, "Assessment of gingival thickness using an ultrasonic dental system prototype: A comparison to traditional methods," *Ann. Anat.*, vol. 199, 2015.

[2] B. Ślak, A. Ambroziak, E. Strumban, and R. G. Maev, "Enamel thickness measurement with a high frequency ultrasonic transducer-based hand-held probe for potential application in the dental veneer placing procedure," *Acta Bioeng. Biomech.*, vol. 13, no. 1, 2011.

[3] N. Shah, "Recent advances in imaging technologies in dentistry," *World J. Radiol.*, vol. 6, no. 10, p. 794, 2014.

[4] H. Ahman, L. Thompson, A. Swarbrick, and J. Woodward, "Understanding the advanced signal processing technique of real-time adaptive filters," *J. Diagnostic Med. Sonogr.*, vol. 25, no. 3, pp. 145–160, 2009.

[5] M. L. Oelze and J. Mamou, "Review of quantitative ultrasound: envelope statistics and backscatter coefficient imaging and contributions to diagnostic ultrasound," *IEEE Trans Ultrason Ferroelectr Freq Control.*, vol. 63, no. 2, pp. 336–351, 2016.

[6] S. Ronald, "Focused ultrasound in ophthalmology," pp. 1865–1875, 2016.

[7] C. E. Solarte and A. Shaikh, *Ultrasound techniques in ophthalmology*, Second Edi., no. March. Elsevier Ltd, 2007.

[8] R. K. Mlosek, S. Malinowska, Z. D. Obrazowej, and S. Kluczowe, "Ultrasound image of the skin, apparatus and imaging basics," *J. Ultrason.*, vol. 13, no. 1, pp. 212–221, 2013.

[9] R. Kleinerman, T. B. Whang, R. L. Bard, and E. S. Marmur, "Ultrasound in dermatology: Principles and applications," *J. Am. Acad. Dermatol.*, vol. 67, no. 3, pp. 478–487, 2012.

[10] C. Hernández-Ibáñez, N. Blazquez-Sánchez, M. Aguilar-Bernier, R. Fúnez-Liébana, F. Rivas-Ruiz, and M. de Troya-Martín, "Usefulness of High-Frequency

Ultrasound in the Classification of Histologic Subtypes of Primary Basal Cell Carcinoma," *Actas Dermosifiliogr.*, vol. 108, no. 1, pp. 42–51, 2017.

[11] R. Baum, Gilbert; Greenwood, Ivan; Slawski, Stan; Smirnow, "Observation of Internal Structures of Teeth by Ultrasonography," *Am. Assoc. Adv. Sci.*, vol. 98, no. 3634, pp. 448–450, 1963.

[12] J. Marotti *et al.*, "Recent advances of ultrasound imaging in dentistry-a review of the literature," *Oral Surg. Oral Med. Oral Pathol. Oral Radiol.*, vol. 115, no. 6, pp. 819–832, 2013.

[13] A. A. Alok, S. Singh, M. Kishore, and A. Shukla, "Ultrasonography - A boon in dentistry," 2019.

[14] "The intraoral ultrasonography in dentistry," *Niger. J. Clin. Pract.*, vol. 21, no. 2, pp. 125–133, 2018.

[15] G. M. Zhang and D. M. Harvey, "Contemporary ultrasonic signal processing approaches for nondestructive evaluation of multilayered structures," *Nondestruct. Test. Eval.*, vol. 27, no. 1, pp. 1–27, 2012.

[16] F. S. Foster, C. J. Pavlin, K. A. Harasiewicz, D. A. Christopher, and D. H. Turnbull, "Advances in ultrasound biomicroscopy. [Review] [154 refs]," *Ultrasound Med. Biol.*, vol. 26, no. 1, pp. 1–27, 2000.

[17] G. Gurun, J. S. Zahorian, A. Sisman, M. Karaman, P. E. Hasler, and F. Levent Degertekin, "An analog integrated circuit beamformer for high-frequency medical ultrasound imaging," *IEEE Trans. Biomed. Circuits Syst.*, vol. 6, no. 5, pp. 454–467, 2012.

[18] FDA, "Ultrasound Imaging." [Online]. Available: https://www.fda.gov/radiation-emitting-products/medical-imaging/ultrasound-imaging.

[19] B. Strozeski, "Reflection and transmission of acoustic wideband plane waves by layered viscoelastic media," *J. Acoust. Soc. Am.*, vol. 71, no. 1, pp. 9–21, 1982.

[20] Y. Labyed and T. A. Bigelow, "Estimating the total ultrasound attenuation along the propagation path by using a reference phantom," *J. Acoust. Soc. Am.*, vol. 128, no. 5, pp. 3232–3238, 2010.

[21] D. O. A. C. Hristopher and D. A. H. T. Urnbull, "Advances in Ultrasound

Biomicroscopy," vol. 26, no. 1, pp. 1–27, 2000.

[22] E. Bossy, M. Talmant, and P. Laugier, "Three-dimensional simulations of ultrasonic axial transmission velocity measurement on cortical bone models," *J. Acoust. Soc. Am.*, vol. 115, no. 5, pp. 2314–2324, 2004.

[23] M. Wang, D. Han, and S. Li, "The application and research of high-frequency ultrasonic reflection technique used in the measurement of small diameter's tube cavity size," *Meas. J. Int. Meas. Confed.*, vol. 46, no. 1, pp. 521–526, 2013.

[24] I. Cespedes, "Methods for Estiamtion of Subsample Time Delays of Digitized Echo Signals," *Ultrason. Imaging*, vol. 17, pp. 142–171, 1995.

[25] L. Svilainis, K. Lukoseviciute, and D. Liaukonis, "Reiterative deconvolution: New technique for time of flight estimation errors reduction in case of close proximity of two reflections," *Ultrasonics*, vol. 76, pp. 154–165, 2017.

[26] C. Li, L. Huang, N. Duric, H. Zhang, and C. Rowe, "An improved automatic time-of-flight picker for medical ultrasound tomography," *Ultrasonics*, vol. 49, no. 1, pp. 61–72, 2009.

[27] L. Svilainis, K. Lukoseviciute, V. Dumbrava, and A. Chaziachmetovas, "Subsample interpolation bias error in time of flight estimation by direct correlation in digital domain," *Meas. J. Int. Meas. Confed.*, vol. 46, no. 10, pp. 3950–3958, 2013.

[28] C.-H. C. Sa-Kit Sin, "A comparison of deconvolution techniques for the ultrasonic nondestrutive evaluation of materilas," *IEEE Trans. Image Process.*, vol. 1, no. 1, pp. 3–10, 1992.

[29] F. Honarvar, H. Sheikhzadeh, M. Moles, and A. N. Sinclair, "Improving the time-resolution and signal-to-noise ratio of ultrasonic NDE signals," *Ultrasonics*, vol. 41, no. 9, pp. 755–763, 2004.

[30] M. Hajian, F. Honarvar, and H. Abrishami-Moghaddam, "Reflectivity estimation using expectation maximization algorithm in ultrasonic nondestructive evaluation," *2009 16th Int. Conf. Syst. Signals Image Process. IWSSIP 2009*, no. 1, pp. 1–4, 2009.

[31] S. Dasgupta and R. L. Nowack, "Frequency extrapolation to enhance the

deconvolution of transmitted seismic waves," *J. Geophys. Eng.*, vol. 5, no. 1, pp. 118–127, 2008.

[32]   S. Wan, B. I. Raju, and M. A. Srinivasan, "Robust deconvolution of high-frequency ultrasound images using higher-order spectral analysis and wavelets," *IEEE Trans. Ultrason. Ferroelectr. Freq. Control*, vol. 50, no. 10, pp. 1286–1295, 2003.

[33]   H. Jin, K. Yang, S. Wu, H. Wu, and J. Chen, "Sparse deconvolution method for ultrasound images based on automatic estimation of reference signals," *Ultrasonics*, vol. 67, pp. 1–8, 2016.

[34]   T. Olofsson and E. Wennerström, "Sparse deconvolution of B-scan images," *IEEE Trans. Ultrason. Ferroelectr. Freq. Control*, vol. 54, no. 8, pp. 1634–1641, 2007.

[35]   T. Olofsson, "Semi-sparse deconvolution robust to uncertainties in the impulse responses," *Ultrasonics*, vol. 42, no. 1–9, pp. 969–975, 2004.

[36]   M. F. Insana, R. F. Wagner, D. G. Brown, and T. J. Hall, "Describing small-scale structure in random media using pulse-echo ultrasound," *J. Acoust. Soc. Am.*, vol. 87, no. 1, pp. 179–192, 1990.

[37]   J. A. Jensen, "A model for the propagation and scattering of ultrasound in tissue," *J. Acoust. Soc. Am.*, vol. 89, no. 1, pp. 182–190, 1991.

[38]   U. R. Abeyratne, S. Member, A. P. Petropulu, J. M. Reid, and L. Fellow, "er Order Spectra ased Deconvolution trasound Images," vol. 42, no. 6, pp. 1064–1075, 1995.

[39]   M. A. Almualimi, S. Al-Qahtani, M. L. Wille, and C. M. Langton, "Improvement of B-scan spatial resolution by pulse-echo ultrasound transit time spectroscopy," *Appl. Acoust.*, vol. 145, pp. 193–204, 2019.

[40]   W. Vollmann, "Resolution Enhancement of Ultrasonic B-Scan Images by Deconvolution," *IEEE Trans. Sonics Ultrason.*, vol. 29, no. 2, pp. 78–82, 1982.

[41]   S. P. Neal, P. L. Speckman, and M. A. Enright, "Flaw signature estimation in ultrasonic nondestructive evaluation using the Wiener filter with limited prior information," *IEEE Trans. Ultrason. Ferroelectr. Freq. Control*, vol. 40, no. 4, pp. 347–353, 1993.

[42] C. A. Zala, "High-Resolution Inversion of Ultrasonic Traces," *IEEE Trans. Ultrason. Ferroelectr. Freq. Control*, vol. 39, no. 4, pp. 458–463, 1992.

[43] E. Thiébaut, "Introduction To Image Reconstruction and Inverse Problems," *Opt. Astrophys.*, vol. 198, pp. 1–26, 2005.

[44] R. Tibshirani, "Regression Shrinkage and Selection via the Lasso," *J. R. Stat. Soc.*, vol. 58, no. 1, pp. 267–288, 1996.

[45] V. Fonti, "Feature Selection using LASSO," *VU Amsterdam*, pp. 1–26, 2017.

[46] M. A. T. Figueiredo, J. M. Bioucas-Dias, and R. D. Nowak, "Majorization-minimization algorithms for wavelet-based image restoration," *IEEE Trans. Image Process.*, vol. 16, no. 12, pp. 2980–2991, 2007.

[47] I. Selesnick, "Total variation denoising (an MM algorithm) Majorization-Minimization," vol. 2012, no. 0, pp. 1–13, 2013.

[48] M. A. T. Figueiredo, J. B. Dias, J. P. Oliveira, and R. D. Nowak, "On total variation denoising: A new majorization-minimization algorithm and an experimental comparison with wavalet denoising," *Proc. - Int. Conf. Image Process. ICIP*, no. 5, pp. 2633–2636, 2006.

[49] Y. Sun, P. Babu, and D. P. Palomar, "Majorization-Minimization Algorithms in Signal Processing, Communications, and Machine Learning," *IEEE Trans. Signal Process.*, vol. 65, no. 3, pp. 794–816, 2017.

[50] I. Selesnick, "Sparse deconvolution (an MM algorithm)," *Connexions Website, 2012*, pp. 1–17, 2012.

[51] H. Endo and R. B. Randall, "Enhancement of autoregressive model based gear tooth fault detection technique by the use of minimum entropy deconvolution filter," *Mech. Syst. Signal Process.*, vol. 21, no. 2, pp. 906–919, 2007.

[52] D. Dolmatov and V. Abramets, "Application of frequency-domain algorithms in ultrasound imaging of composite materials," *MATEC Web Conf.*, vol. 48, no. 1, pp. 1–7, 2016.

[53] J. R. Thornbury, "Eugene W. Caldwell Lecture. Clinical efficacy of diagnostic imaging: love it or leave it.," *Am. J. Roentgenol.*, vol. 162, no. 1, pp. 1–8, 2013.

[54] E. A. Omari and T. Varghese, "Signal to noise ratio comparisons for ultrasound

attenuation slope estimation algorithms," *Med. Phys.*, vol. 41, no. 3, pp. 1–9, 2014.

[55] F. A. Duck, "The Meaning of Thermal Index (TI) and Mechanical Index (MI) Values," *BMUS Bull.*, vol. 5, no. 4, p. 36, 1997.

[56] S. Kudrle, M. Proulx, P. Carrières, and M. Lopez, "Fingerprinting for Solving A/V Synchronization Issues within Broadcast Environments," *SMPTE Motion Imaging J.*, vol. 120, no. 5, pp. 36–46, 2011.

[57] H. E. Schroeder and M. A. Listgarten, "The gingival tissues: the architecture of periodontal protection," *Periodontol. 2000*, vol. 13, no. 1, pp. 91–120, 1997.

[58] K. L. Vandana and B. Savitha, "Thickness of gingiva in association with age, gender and dental arch location," *J. Clin. Periodontol.*, vol. 32, no. 7, pp. 828–830, 2005.

[59] J. L. Ackerman, W. R. Proffit, and D. M. Sarver, "The emerging soft tissue paradigm in orthodontic diagnosis and treatment planning," *Clin. Orthod. Res.*, vol. 2, no. 2, pp. 49–52, 1999.

[60] C. Baldi *et al.*, "Coronally Advanced Flap Procedure for Root Coverage. Is Flap Thickness a Relevant Predictor to Achieve Root Coverage? A 19-Case Series," *J. Periodontol.*, vol. 70, no. 9, pp. 1077–1084, 1999.

[61] R. Pontoriero and G. Carnevale, "Surgical Crown Lengthening: A 12-Month Clinical Wound Healing Study," *J. Periodontol.*, vol. 72, no. 7, pp. 841–848, 2001.

[62] T. Linkevicius, A. Puisys, L. Linkeviciene, V. Peciuliene, and M. Schlee, "Crestal Bone Stability around Implants with Horizontally Matching Connection after Soft Tissue Thickening: A Prospective Clinical Trial," *Clin. Implant Dent. Relat. Res.*, vol. 17, no. 3, pp. 497–508, 2013.

[63] D. Hwang and H.-L. Wang, "Flap Thickness as a Predictor of Root Coverage: A Systematic Review," *J. Periodontol.*, vol. 77, no. 10, pp. 1625–1634, 2006.

[64] M. Olsson and J. Lindhe, "Periodontal characteristics in individuals with varying form of the upper central incisors," *J. Clin. Periodontol.*, vol. 18, no. 1, pp. 78–82, 1991.

[65] A. Eghbali, T. De Rouck, H. De Bruyn, and J. Cosyn, "The gingival biotype assessed by experienced and inexperienced clinicians," *J. Clin. Periodontol.*, vol.

36, no. 11, pp. 958–963, 2009.

[66] T. De Rouck, R. Eghbali, K. Collys, H. De Bruyn, and J. Cosyn, "The gingival biotype revisited: transparency of the periodontal probe through the gingival margin as a method to discriminate thin from thick gingiva," *J. Clin. Periodontol.*, vol. 36, no. 5, pp. 428–433, 2009.

[67] N. A. Frost, B. L. Mealey, A. A. Jones, and G. Huynh-Ba, "Periodontal Biotype: Gingival Thickness as It Relates to Probe Visibility and Buccal Plate Thickness," *J. Periodontol.*, vol. 86, no. 10, pp. 1141–1149, 2015.

[68] M. Paolantonio, "Treatment of Gingival Recessions by Combined Periodontal Regenerative Technique, Guided Tissue Regeneration, and Subpedicle Connective Tissue Graft. A Comparative Clinical Study," *J. Periodontol.*, vol. 73, no. 1, pp. 53–62, 2002.

[69] W. Bednarz, A. Furtak, E. Leszczyńska, and A. Sender-Janeczek, "The repeatability and reproducibility of gingival thickness measurement with an ultrasonic device," *Dent. Med. Probl.*, vol. 55, no. 3, pp. 281–288, 2018.

[70] H. Uchida, K. Kobayashi, and M. Nagao, "Measurement in vivo of Masticatory Mucosal Thickness with 20 MHz B-Mode Ultrasonic Diagnostic Equipment," *J. Dent. Res.*, vol. 68, no. 2, pp. 95–100, 1989.

[71] H.-P. Müller, N. Schaller, T. Eger, and A. Heinecke, "Thickness of masticatory mucosa," *J. Clin. Periodontol.*, vol. 27, no. 6, pp. 431–436, 2000.

[72] X. Xiang *et al.*, "An Update on Novel Non-Invasive Approaches for Periodontal Diagnosis," *J. Periodontol.*, vol. 81, no. 2, pp. 186–198, 2010.

[73] C. C. B. O. Mota, L. O. Fernandes, R. Cimões, and A. S. L. Gomes, "Non-Invasive Periodontal Probing Through Fourier-Domain Optical Coherence Tomography," *J. Periodontol.*, vol. 86, no. 9, pp. 1087–1094, 2015.

[74] J.-Y. Park, J.-H. Chung, J.-S. Lee, H.-J. Kim, S.-H. Choi, and U.-W. Jung, "Comparisons of the diagnostic accuracies of optical coherence tomography, micro-computed tomography, and histology in periodontal disease: anex vivostudy," *J. Periodontal Implant Sci.*, vol. 47, no. 1, p. 30, 2017.

[75] K. Al-Azri *et al.*, "Optical coherence tomography use in the diagnosis of enamel

defects," *J. Biomed. Opt.*, vol. 21, no. 3, p. 036004, 2016.

[76] L. L. Otis, M. J. Everett, U. S. Sathyam, and B. W. Colston, "Optical Coherence Tomography: A New Imaging," *J. Am. Dent. Assoc.*, vol. 131, no. 4, pp. 511–514, 2000.

[77] M. Diagnostics, "Vivosight." [Online]. Available: https://vivosight.com/researcher/vivosight-scanner/. [Accessed: 20-Jan-2019].

[78] J. R. Landis and G. G. Koch, "The Measurement of Observer Agreement for Categorical Data," *Biometrics*, vol. 33, no. 1, p. 159, 1977.

[79] D. Kloukos, G. Koukos, I. Doulis, A. Sculean, A. Stavropoulos, and C. Katsaros, "Gingival thickness assessment at the mandibular incisors with four methods: A cross-sectional study," *J. Periodontol.*, vol. 89, no. 11, pp. 1300–1309, 2018.

[80] J. M. Stein, N. Lintel-Höping, C. Hammächer, A. Kasaj, M. Tamm, and O. Hanisch, "The gingival biotype: measurement of soft and hard tissue dimensions - a radiographic morphometric study," *J. Clin. Periodontol.*, vol. 40, no. 12, pp. 1132–1139, 2013.

[81] A. L. Januario, M. Barrivierra, and W. R. Duarte, "Soft Tissue Cone-Beam Computed Tomography: A Novel Method for the Measurement of Gingival Tissue and the Dimensions of the Dentogingival Unit," *J. Esthet. Restor. Dent.*, vol. 20, no. 6, pp. 366–373, 2008.

[82] V. Bhaskar, H.-L. Chan, M. MacEachern, and O. D. Kripfgans, "Updates on ultrasound research in implant dentistry: a systematic review of potential clinical indications," *Dentomaxillofacial Radiol.*, vol. 47, no. 6, p. 20180076, 2018.

[83] M. Cassetta, A. A. A. Sofan, F. Altieri, and E. Barbato, "Evaluation of alveolar cortical bone thickness and density for orthodontic mini-implant placement," *J. Clin. Exp. Dent.*, pp. e245-52, 2013.

[84] W. Zhang, J. Tullis, and R. Weltman, "Cone Beam Computerized Tomography Measurement of Alveolar Ridge at Posterior Mandible for Implant Graft Estimation," *J. Oral Implantol.*, vol. 41, no. 6, pp. e231–e237, 2015.

[85] S. Desai, I. Karthikeyan, and R. Singh, "An in-office, cost effective technique for measuring width of bone using intra-oral periapical radiographs in occlusal

projection," *J. Indian Soc. Periodontol.*, vol. 17, no. 1, p. 82, 2013.

[86] L.-C. Chen, T. Lundgren, H. Hallström, and F. Cherel, "Comparison of Different Methods of Assessing Alveolar Ridge Dimensions Prior to Dental Implant Placement," *J. Periodontol.*, vol. 79, no. 3, pp. 401–405, 2008.

[87] L. A. Perez, S. L. Brooks, H.-L. Wang, and R. M. Eber, "Comparison of linear tomography and direct ridge mapping for the determination of edentulous ridge dimensions in human cadavers," *Oral Surgery, Oral Med. Oral Pathol. Oral Radiol. Endodontology*, vol. 99, no. 6, pp. 748–754, 2005.

[88] A. M. Timock *et al.*, "Accuracy and reliability of buccal bone height and thickness measurements from cone-beam computed tomography imaging," *Am. J. Orthod. Dentofac. Orthop.*, vol. 140, no. 5, pp. 734–744, 2011.

[89] R. A. Vacarescu, B. Slak, A. Maeva, and R. G. Maev, "Portable high-frequency device for cosmetic and clinical fingernail assessment," in *Canadian Conference on Electrical and Computer Engineering*, 2017.

[90] R. A. Vacarescu *et al.*, "Investigation of a correlation between taxane-based chemotherapy and the ultrasonic time-of-flight of human fingernails," *Ski. Res. Technol.*, vol. 24, no. 1, 2018.

VITA AUCTORIS

NAME:	Bartosz Slak
PLACE OF BIRTH:	Sycow, Lower Silesia, Poland
YEAR OF BIRTH:	1985
EDUCATION:	The University of Windsor, Faculty of Science
	Department of Physics, M.Sc.
	Windsor, Ontario, Canada, 2014
	The University of Technology in Wroclaw, Faculty of Fundamental Problems of Technology, Department of Technical Physics, B.Sc. Eng. & M.Sc.
	Wroclaw, Lower Silesia, Poland, 2009